

Cell morphogenesis in Brassicaceae:

Analysis of myosin functions and the BEACH domain protein SPIRRIG



Inaugural-Dissertation

zur

Erlangung des Doktorgrades

der Mathematisch-Naturwissenschaftlichen Fakultät

der Universität zu Köln

vorgelegt von

Lisa Marie Stephan

aus Bensberg

Köln, 2018

Berichterstatter/in: Prof. Dr. Martin Hülskamp

Prof. Dr. Ute Höcker

Prüfungsvorsitzender: Prof. Dr. Kay Hofmann

Tag der mündlichen Prüfung: Donnerstag, 13. September 2018

Table of Contents

List of Figures	IV
List of Tables	VI
List of Abbreviations	VII
Zusammenfassung	X
Abstract	XII
1 Introduction	1
2 Material and Methods	13
2.1 Plasmids and organisms.....	13
2.2 Biomolecular methods.....	14
2.2.1 <i>Polymerase chain reaction (PCR)</i>	14
2.2.2 <i>Restriction digest</i>	16
2.2.3 <i>Cloning</i>	17
2.2.4 <i>Production of competent E.coli cells</i>	18
2.2.5 <i>Transformation of competent cells</i>	18
2.2.6 <i>Plasmid preparation</i>	19
2.2.7 <i>Sequencing</i>	19
2.3 Biochemical methods.....	19
2.3.1 <i>Protein expression in E.coli</i>	19
2.3.2 <i>Protein detection</i>	20
2.3.3 <i>Protein purification</i>	20
2.3.4 <i>Co-Immunoprecipitation (Co-IP)</i>	20
2.4 Plant techniques	21
2.4.1 <i>Plant growth conditions</i>	21
2.4.2 <i>Seed sterilization</i>	22
2.4.3 <i>RNA extraction</i>	23
2.4.4 <i>DNase treatment</i>	23

2.4.5	<i>cDNA synthesis</i>	23
2.4.6	<i>Production of plant extracts for genotyping</i>	24
2.4.7	<i>Particle bombardment</i>	24
2.4.8	<i>Tobacco leaf infiltration</i>	24
2.4.9	<i>Floral dip</i>	25
2.4.10	<i>Crossing</i>	25
2.4.11	<i>Selection of transformed plants</i>	25
2.4.12	<i>Fluorescein diacetate (FDA) staining</i>	25
2.4.13	<i>Latrunculin B treatment</i>	25
2.4.14	<i>Fixation of cells</i>	26
2.5	<i>Yeast techniques</i>	26
2.5.1	<i>Co-transformation of competent yeast cells</i>	26
2.5.2	<i>Yeast two-hybrid</i>	26
2.6	<i>Microscopical methods</i>	27
2.6.1	<i>Stereo microscopy</i>	27
2.6.2	<i>Fluorescence microscopy</i>	27
2.6.3	<i>Confocal laser scanning microscopy</i>	27
2.6.4	<i>Analysis of organelle movement</i>	27
2.7	<i>In silico methods</i>	29
2.7.1	<i>Sequence analysis</i>	29
2.7.2	<i>Tracking of organelles</i>	29
2.7.3	<i>Plant measurements</i>	29
2.7.4	<i>Statistical analysis</i>	29
2.7.5	<i>Analysis of qPCR data</i>	29
3	Results	32
	I. Cytoplasmic streaming.....	32
3.1	Effects of myosin loss.....	32
3.1.1	<i>Novel phenotypes</i>	33

3.1.2	<i>Myosin loss and P-body movement</i>	37
3.2	Overexpression of truncated myosins – a dominant negative effect.....	40
3.3	Myosin full length constructs – from functional to function?	55
3.4	Stirring and passive flow of cytoplasm	60
3.4.1	<i>Is stirring sufficient for movement?</i>	60
II.	SPIRRIG	65
3.5	The SPIRRIG protein.....	65
3.6	<i>spi</i> mutants in <i>Arabis alpina</i>	69
3.6.1	<i>Common phenotypes in Arabis and Arabidopsis</i>	70
3.6.2	<i>Unique phenotypes in Arabis spi mutants</i>	74
3.6.3	<i>spi and salt stress responses</i>	76
4	Conclusions	94
I.	Cytoplasmic streaming	94
II.	SPIRRIG	97
	Appendix	103
	References	116
	Declaration of academic integrity	122
	Lebenslauf	123

List of Figures

Figure 1: The plant cytoskeleton consists of filamentous actin and microtubules.	1
Figure 2: Actin and myosin.....	3
Figure 3: P-body function and composition.....	5
Figure 5: Protein structure of SPIRRIG in <i>Arabidopsis thaliana</i>	10
Figure 6: Parameters for leaf morphology.....	34
Figure 7: Calculations on leaf morphology.	35
Figure 8: Morphology of Col-0 and myosin mutants at 21°C and 28°C.	36
Figure 9: Hypocotyl length in dark grown seedlings.....	37
Figure 10: Significance of P-body speed in different myosin mutants.	38
Figure 11: Movement classes of P-bodies in myosin mutants.....	40
Figure 12: Myosin domains and structure.	41
Figure 13: Phylogenetic tree of class XI myosins.	42
Figure 14: Analysis of Col-0 T1 plants expressing YFP:XI-1-coiled coil.....	44
Figure 15: Trichome phenotypes in Col-0 and GTD overexpression lines.	45
Figure 16: P-body movement in Col-0 and transgenic lines.	47
Figure 17: Peroxisome movement in Col-0 and transgenic lines.....	48
Figure 18: Peroxisome movement in Col-0 and <i>xi-2</i>	49
Figure 19: The actin cytoskeleton in Col-0 _{35S::YFP:XI-K-GTD} transgenic lines.	50
Figure 20: Myosin Va activity regulation (Hammer and Sellers, 2011).	51
Figure 21: Schematic representation of organelle binding by myosins and myosin fragments.	52
Figure 22: Bridging of cargo blocking by GTDs.....	53
Figure 23: Localisation of myosin full length constructs in Arabidopsis leaf cells.	56
Figure 24: Localisation of myosin full length constructs and 35S::LifeAct-CFP in Col-0 leaf cells.....	57
Figure 25: Co-localisation of myosin full length constructs.	58
Figure 26: Rescue of peroxisome movement in the <i>12k</i> mutant with 35S::XI-K:YFP.	59
Figure 27: Actin organisation in Arabidopsis leaf epidermal cells.	60
Figure 28: Effect of molecular stirrer on peroxisome movement.	61
Figure 29: FRAP series in Col-0 epidermal pavement cell.....	62

Figure 29: FRAP series in Col-0 epidermal pavement cell.....	62
Figure 30: Fluorescence Recovery after Photobleaching.....	63
Figure 31: Phylogram of the BEACH domains in the plant kingdom.	67
Figure 32: The SPIRRIG protein in <i>Arabidopsis thaliana</i> and <i>Arabis alpina</i>	68
Figure 33: SPIRRIG expression in different tissues of <i>Arabis alpina</i>	68
Figure 34: Schematic representation of the <i>SPIRRIG</i> gene in three EMS <i>spi</i> mutants.	69
Figure 35: Complementation assay of <i>spi</i> EMS mutants.	69
Figure 36: Expression of SPIRRIG in <i>pep1</i> and <i>spi</i> mutants.....	70
Figure 37: Complexity of 10 day old cotyledon cells in <i>pep1</i> and <i>Aaspi</i> mutants.	71
Figure 38: Root hairs of seven day old seedlings in <i>pep1</i> and <i>Aaspi</i> mutants.....	71
Figure 39: Trichome shapes in <i>pep1</i> and <i>Aaspi</i> mutants.	72
Figure 40: Dark grown hypocotyls of <i>pep1</i> and <i>Aaspi</i> mutants.	75
Figure 41: FDA staining of <i>Arabis</i> root hairs.....	76
Figure 42: Germination of <i>pep1</i> and <i>spi</i> mutants under salt stress.....	77
Figure 43: Cotyledon whitening of <i>Aaspi</i> mutants.....	79
Figure 44: Primary root growth of <i>pep1</i> and <i>Aaspi</i> on different concentrations of NaCl after four days.....	80
Figure 45: Seedling growth of <i>Arabis alpina</i> lines on stone wool under salt stress.	81
Figure 46: Seedling growth of <i>Arabis alpina</i> lines on soil under salt stress.....	82
Figure 47: Localisation of 35S::YFP-SPI-PBW in tobacco leaves cells.....	83
Figure 48: Localisation of SPI-PBW under salt stress.	84
Figure 49: Quantity values of reference gene expression under control and salt stress conditions.....	85
Figure 50: Determination of the optimal number of control genes for normalization.	87
Figure 51: Transcript levels of AaESE1 under salt stress.....	88
Figure 52: Relative transcript levels of TSPO-related protein in response to salt stress.....	89
Figure 53: Relative transcript levels of NTF2 family protein in response to salt stress.....	90
Figure 54: Relative transcript levels of lipid transfer protein 4 in response to salt stress.	91
Figure 55: Relative transcript levels of an integrase-type DNA-binding superfamily protein in response to salt stress.....	92
Figure 56: Relative transcript levels of FAMT in response to salt stress.	93
Figure 57: Graphs of qPCR primer efficiency tests.....	115

List of Tables

Table 1: Myosin XI functions in <i>Arabidopsis thaliana</i>	7
Table 2: Plasmids used in this work.	13
Table 3: Organisms used in this work.	14
Table 4: Phusion polymerase reaction and program.	14
Table 5: Taq Polymerase and Green Taq Mix reaction and program.	15
Table 6: Site-directed mutagenesis reaction and program.	15
Table 7: qPCR reaction and program.	16
Table 8: Transformation of competent cells.	19
Table 9: Specifications for protein purification buffers and beads.	20
Table 10: Specifications and short names of myosin mutants.	32
Table 11: P-body speed in myosin mutants.	38
Table 12: Yeast 2-hybrid results of interactions of myosin tails and coils.	54
Table 13: The BEACH domain protein family in the plant kingdom.	66
Table 14: Trichome measurements in <i>Arabidopsis alpina</i>	72
Table 15: Classes of different trichomes in <i>pep1</i> , Col-0 and <i>spi</i> mutants.	73
Table 16: Hypocotyl length in <i>pep1</i> and <i>Aaspi</i> mutants.	74
Table 17: Fragmented root hair vacuoles in <i>pep1</i> and <i>Aaspi</i> mutants.	75
Table 18: Primer efficiencies and correlation of reference genes for <i>Arabidopsis alpina</i>	84
Table 19: Gene expression stability under salt stress.	85
Table 20: Ranking of stable reference genes under salt stress.	86
Table 21: List of primers, donor constructs and construct sources.	103
Table 22: List of destination vectors created using the gateway system.	106
Table 23: Detailed overview on genotyping and/or selfing of myosin mutants.	108
Table 24: Genotyping primer for SALK lines.	108
Table 25: List of qPCR primers.	109

List of Abbreviations

°C	degree Celsius
µl	micro litre
µm	micro meter
3-AT	3-Amino-1,2,4-triazole
Aa	<i>Arabidopsis alpina</i>
ABI1	ABL-INTERACTOR-1
ADP	Adenosine diphosphate
Amp	ampicillin
argF	ornithine carbamoyltransferase mutation blocks ability to use arginine
ARP2/3	actin-related protein 2/3
At	<i>Arabidopsis thaliana</i>
ATP	Adenosine triphosphate
BEACH	Beige and Chediak Higashi
BiFC	Bimolecular Fluorescence Complementation
bp	base pairs
BRK1	BRICK1
BSA	bovine serum albumin
Carb	carbenicillin
CC	coiled coil
ccdB	codes for a gene product that inhibits gyrases of commonly used bacterial strains
CCR4-NOT	CARBON CATABOLITE REPRESSOR PROTEIN 4-NEGATIVE ON TATA COMPLEX
cDNA	complementary DNA
CDS	coding sequence
CFP	cyan fluorescent protein
Chl	chloramphenicol
cm	centimetres
Co-IP	Co-Immunoprecipitation
Col-0	Columbia 0
ConA	Concanavalin A
conc.	concentrated
CRISPR/Cas	Clustered Regularly Interspaced Short Palindromic Repeats
CRK	CROOKED
Ct	Cycle threshold
DCP	Decapping protein
ddH ₂ O	double distilled water
DE3	lysogen that encodes T7 RNA polymerase used to induce expression in T7-driven expression systems
DMSO	dimethyl sulfoxide
DNA	deoxyribonucleic acid
dNTPs	deoxyribonucleotides
DTT	dithiothreitol
<i>E.coli</i>	<i>Escherichia coli</i>
EDTA	ethylenediaminetetraacetic acid
EMS	Ethyl methanesulfonate
endA	endA mutation in the non-specific endonuclease Endonuclease I; eliminates non-specific endonuclease activity, resulting in improved plasmid preps
ER	endoplasmic reticulum
et al.	et alii
EtOH	ethanol
FDA	Fluorescein diacetate
FLC	Flowering Locus C

FRAP	Fluorescence Recovery after Photobleaching
FRET AB	Förster Resonance Energy Transfer after Bleaching
FRET SE	Förster Resonance Energy Transfer Sensitized Emission
g	grams
GAL4-AD	GAL4 activation domain
GAL4-BD	GAL4 binding domain
galK	galactokinase mutation blocks catabolism of galactose—cells that are galK minus cannot grow in the presence of galactose as the sole carbon source
Gent	gentamycin
GFP	green fluorescent protein
GRL	GNARLED
GST	glutathione S-transferase
GTD	globular tail domain
gyrA96	DNA gyrase mutant produces resistance to nalidixic acid
h	hours
-H	without histidine
His	histidine
hsd	mutations in the system of methylation and restriction that allow <i>E.coli</i> to recognize DNA as foreign. The hsd genotype allows efficient transformation of DNA generated from PCR reactions
Hyg	hygromycin
Hz	hertz
IHF	integration host factor
INT	integrase
IPTG	isopropyl β -D-1-thiogalactopyranoside
Kan	kanamycin
kb	kilo base
kDa	kilo Dalton
KLK	KLUNKER
l	litre
-L	without leucine
lacY1	blocks use of lactose via β -D-galactosidase mutant
lacZ	β -D-galactosidase gene; mutations yield colourless (vs. blue) colonies in the presence of X-gal
lacZ Δ M15	element required for β -galactosidase complementation when plated on X-gal; used in blue/white screening of recombinants; usually carried on the lambdoid prophage ϕ 80 or F'
LatB	latrunculin B
LB	lysogeny broth
LBA1	left border primer for SALK lines
Leu	leucine
M	molar concentration
MBP	maltose binding protein
mcrBC, mrr	mutations that allow methylated DNA to not be recognized as foreign; this genotype is necessary when cloning genomic DNA or methylated cDNA
MES	2-(N-morpholino)ethanesulfonic acid
mg	milligrams
min	minutes
miRNA	microRNA
ml	millilitre
mM	millimolar
mm	millimetre
mRNA	messenger RNA
NASC	Nottingham Arabidopsis Stock Centre
NCBI	National Centre for Biotechnology Information

ng	nanogram
nm	nanometre
O/N	over night
OD	optical density
ompT	indicates that the <i>E.coli</i> lack an outer membrane protease
ORF	open reading frame
p	promoter
paj	pajares
PBS	phosphate buffered saline
PBW	PH-BEACH-WD40
PCR	polymerase chain reaction
<i>pep1</i>	<i>perpetual flowering 1</i>
PH	Pleckstrin-Homology
Pi	phosphate
pmol	picomol
PVDF	polyvinylidene fluoride
qPCR	quantitative PCR
recA	mutation in a gene responsible for general recombination of DNA; particularly desirable when cloning genes with direct repeats
relA	RNA is synthesized in absence of protein synthesis (relaxed phenotype) relA locus regulates the coupling between transcription and translation. In the wild type, limiting amino acid concentrations results in the shutdown of RNA synthesis
RFP	red fluorescent protein
RHA1	RAB HOMOLOG 1
RNA	ribonucleic acid
RNP	ribonucleoprotein
ROI	region of interest
rpm	rounds per minute
rpsL	confers resistance to streptomycin (this makes a mutant ribosomal protein, small subunit, the target of the drug)
RT	room temperature
SCAR/WAVE	SUPPRESSOR OF CYCLIC AMP RECEPTOR/WISKOTT-ALDRICH SYNDROME VERPROLIN-HOMOLOGOUS PROTEIN
SDS	sodium dodecyl sulphate
sec	seconds
SKL	serine-lysine-leucine
Spec	spectinomycin
SPI	SPIRRIG
SRA1	SPECIFICALLY RAC1-ASSOCIATED PROTEIN 1
ssDNA	single stranded DNA
Strep	streptomycin
supE,F	tRNA glutamine suppressor of amber (supE)(UAG) or tyrosine (supF)
T _A	annealing temperature
TB	Terrific Broth Medium
T-DNA	transfer DNA
thi-1	requires thiamine for growth on minimal media
Trp	tryptophan
VCS	VARICOSE
-W	without tryptophan
w/o	without
w/v	weight per volume
WRM	WORM
XRN	EXORIBONUCLEASE
xyl-5	blocks catabolism of xylose
YFP	yellow fluorescent protein

Zusammenfassung

Eine genaue Kontrolle des Zellwachstums und der Zellausdehnung ist für die Leistungsfähigkeit von Pflanzen und ihre Anpassung an die Umwelt von entscheidender Bedeutung. Während der Entwicklung differenzieren sich die Zellen morphologisch, um eine optimale Funktionalität zu gewährleisten. Es wird angenommen, dass diese spezialisierte Morphogenese hauptsächlich durch Endoreduplikation und Zytoskelettdynamik kontrolliert wird. Daher sind hoch spezialisierte Zellen wie Wurzelhaare oder Trichome beliebte Modellsysteme, um diese Prozesse zu untersuchen.

Im Jahr 1994 wurde eine Gruppe von *distorted* Trichom-Mutanten in einer EMS-Mutagenese in *Arabidopsis thaliana* identifiziert. Abgesehen von der veränderten Trichom-Morphologie weisen alle Mitglieder dieser Gruppe unregelmäßige Formen von epidermalen Zellen des Blattes, des Hypocotyls und der Wurzeln auf. Die meisten der *distorted* Mutanten besitzen Defekte im Aktin-regulierenden ARP2/3- oder SCAR/WAVE Signalweg. Zwei der identifizierten Mutanten zeigten jedoch Veränderungen in ARP2/3 unabhängigen Proteinen: Myosin XI-K und das BEACH-Domänen Protein SPIRRIG.

XI-K ist ein Motor-Protein, das mit dem Aktin-Zytoskelett interagiert. Abgesehen von seiner Funktion beim Transport von Organellen erwies es sich als wesentlich für die Aktinorganisation. In dieser Arbeit wurde die Funktion des XI-K Proteins zusammen mit den redundanten Myosinen XI-1, XI-2 und XI-I analysiert. Zusätzlich wurden der passive Strom und das *Stirring* (engl. für Rühren) des Zytoplasmas analysiert. Hierdurch wurde die Unterscheidung von Effekten ermöglicht, die durch aktiven Transport von Organellen und passive Beschleunigung des Zytoplasmas verursacht werden.

Diese Studie zeigte, dass das *Stirring* nicht ausreicht, um die Organellbewegung oder den passiven Zytoplasmastrom in Arabidopsis-Blattzellen zu erhöhen. Tatsächlich unterscheidet sich der passive Strom im Wildtyp nicht von der Dreifach-Mutante *xi-1 xi-2 xi-k*. Dies lässt den Schluss zu, dass eine Verlangsamung des passiven Zytoplasmastroms nicht der Grund für den *distorted* Phänotyp in *xi-k* Mutanten ist. Es wurde jedoch gezeigt, dass der Langstreckentransport von P-bodies und Peroxisomen ausschließlich durch Myosin K vermittelt wird, und dass die Blockierung dessen Cargos zu *distorted* Phänotypen führen kann. Diese Ergebnisse zeigen, dass Prozesse, die mit diesen Cargos assoziiert sind, den beobachteten Phänotyp beeinflussen könnten. Es wurde festgestellt, dass die Entwicklung der

xi-k Mutante in Langzeit-Hitze und -Dunkelheit unverändert blieb. Die verringerte Anpassungsfähigkeit von *xi-k* Dreifach- und Vierfachmutanten bestätigte jedoch eine Beteiligung des XI-K Proteins an diesen morphologischen Prozessen.

SPIRRIG, ein weiteres Protein, das an der Zellmorphogenese beteiligt ist, gehört zur Familie der BEACH-Domänen Proteine. Mitglieder dieser Familie sind bekannte Vermittler von Membrandynamik und -transport. In Arabidopsis wurde gezeigt, dass *spi* Mutanten ein intaktes Aktin-Zytoskelett aufweisen und somit das SPI Protein nicht an der Aktin-Organisation beteiligt ist. Darüber hinaus wurde festgestellt, dass das SPI Protein in Arabidopsis essentiell für Reaktionen auf hohe Salinität ist und dass es eine Vielzahl von Transkripten in einer salzabhängigen Weise stabilisiert.

In dieser Arbeit wurde ein evolutionär-komparativer Ansatz gewählt, um die Funktion und Bedeutung von SPI in Pflanzen aufzuklären. Daher wurde eine detaillierte Analyse von SPI in einer eng verwandten Brassicaceae, *Arabis alpina*, durchgeführt. Es wurde festgestellt, dass der *distorted* Phänotyp in Arabis und Arabidopsis ähnlich ist und wahrscheinlich mit dem Verlust funktioneller WD40-Domänen im C-Terminus des Proteins einhergeht. Im Gegensatz zu Arabidopsis wurde festgestellt, dass *Aaspirrig* Mutanten keine fragmentierten Vakuolen in ihren Wurzelhaaren besitzen, was anzeigt, dass SPIRRIG für die Integrität der Vakuolen in diesen Zellen in Arabis nicht essentiell ist. Darüber hinaus wurde festgestellt, dass die Salzstressreaktion der untersuchten *Aaspi* Allele unterschiedlich ist, was auf eine Beteiligung der PH/BEACH-Domäne in diesem Prozess hinweist. Schließlich wurden neue Referenzgene für qPCR in *Arabis alpina* etabliert und verwendet, um differentiell regulierte Transkripte in *spirrig* Mutanten unter Normal- und Salzstressbedingungen zu identifizieren. Vier Kandidaten für zukünftige Analysen wurden gefunden, die die Funktion von SPIRRIG unter Salzstress aufklären und damit verbundene Signalwege aufzeigen könnten.

Abstract

Precise control of cell growth and expansion is essential for plant performance and adaptation to the environment. During development, cells differentiate into various shapes and sizes, allowing them to carry out specific functions. This specialized morphogenesis is thought to be controlled mostly through endoreduplication and cytoskeletal dynamics. Thus, highly specialised cells like root hairs or trichomes are popular model systems to study these processes.

In 1994, a group of distorted trichome mutants was identified in an EMS screen in *Arabidopsis thaliana*. Apart from altered trichome morphology, all members of this group showed irregular shapes of leaf pavement cells, epidermal hypocotyl cells and epidermal root cells. Most of these distorted mutants were found to be deficient in proteins of the actin regulating ARP2/3 or SCAR/WAVE complex. Strikingly, two of the identified distorted mutants lacked proteins independent of this pathway: myosin XI-K and the BEACH domain protein SPIRRIG.

XI-K is a motor protein interacting with the actin cytoskeleton. Aside from its function in transport of organelles, it was found to be essential for actin organisation. In this work, XI-K function was analysed alongside its redundant myosins XI-1, XI-2 and XI-I. In addition, the passive bulk flow and stirring of the cytoplasm were analysed, allowing the distinction of effects caused by active transport of organelles and passive acceleration of the cytoplasm.

This study showed that stirring is not sufficient to enhance organelle movement or bulk flow in *Arabidopsis* leaf cells. In fact, the bulk flow does not differ in wild type and the triple knockout mutant *xi-1 xi-2 xi-k*, indicating that a deceleration of passive flow of the cytoplasm is not the cause of the distorted phenotype in *xi-k* mutants. However, myosin XI-K was found to be the sole myosin mediating long range transport of P-bodies and peroxisomes, and that inhibition of XI-K cargos can produce distorted phenotypes. These results indicate that processes associated with these organelles might influence the observed phenotype. Development of the *xi-k* mutant was found to be unaltered in long term heat and darkness, however, reduced adaptability of *xi-k* triple and quadruple mutants indicated an involvement in these morphological processes.

SPIRRIG, another protein identified to be involved in cell morphogenesis, belongs to the family of BEACH domain containing proteins. Members of this family are known facilitators

of membrane dynamics and trafficking. In *Arabidopsis*, *spi* mutants were shown to have an intact actin cytoskeleton, indicating that the SPI protein is not involved in actin organisation. In addition, it was found that the *Arabidopsis* SPI protein is essential for plant salt stress responses, and that it stabilises a variety of transcripts in a salt dependent manner.

Here, an evolutionary comparative approach was chosen to elucidate SPI function and importance *in planta*. Thus, a detailed analysis of SPI in a closely related Brassicaceae, *Arabis alpina*, was carried out. It was found that the distorted phenotype is similar in *Arabis* and *Arabidopsis*, and is likely to be associated with the loss of functional WD40 repeats in the C-terminus of the protein. In contrast to *Arabidopsis*, it was found that *Aaspirrig* mutants do not possess fragmented vacuoles in their root hairs, indicating that SPIRRIG is not essential for vacuolar integrity in these cells in *Arabis*. Moreover, the salt stress response was found to differ in between *Aaspi* alleles, pointing towards an involvement of the PH/BEACH domain in this process. Finally, new reference genes for qPCR in *Arabis alpina* were established and utilized to identify differentially regulated transcripts in *spirrig* mutants under normal and salt stress conditions. Four candidates for future analyses were found which might elucidate the function of SPIRRIG in salt response and reveal associated pathways.

1 Introduction

The mechanisms of cell growth and morphogenesis are in the focus of plant science for decades. Due to fully sequenced model organisms like *Arabidopsis thaliana* and its excellent model systems like root hairs and trichomes, genetic and environmental factors regulating growth, size and shape of plant organs are better understood every day (Bögre et al., 2008; Mathur and Hülskamp, 2002). Still, there are multitudes of regulatory pathways to be investigated and dynamics to be studied. To date, the major players in specialized morphogenesis are thought to be endoreduplication and cytoskeletal dynamics, including vesicle transport and small GTPase signalling (Guimil and Dunand, 2007).

The plant cytoskeleton

In planta, the cytoskeleton consists of two different types of linear protein polymers: actin filaments and microtubules (Figure 1). Due to large vacuoles in most plant cells, the cytoplasm is restricted to thin layers in the cell proximity and around the nucleus, which are connected by transvacuolar cytoplasmic strands (Kost and Chua, 2002). Both, actin and microtubules pervade the cytoplasm and build transport ways along which motor proteins move in a directional and energy-dependent manner to transport specific cargos.

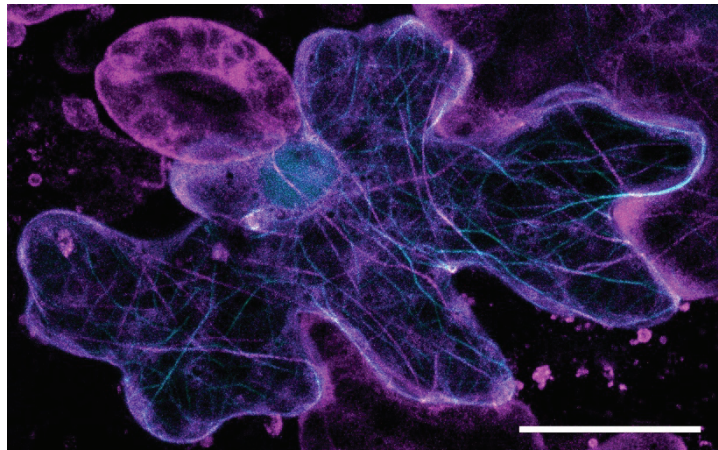


Figure 1: The plant cytoskeleton consists of filamentous actin and microtubules.

Arabidopsis thaliana leaf epidermal pavement cell labelled with the actin marker 35S::LifeAct-CFP (cyan) and the alpha tubulin marker 35S::GFP-TUA6 (magenta). Scale displays 20 μ m.

The directional movement and the consequential positioning of organelles and macromolecules via actin filaments are essential for the regulation and maintenance of cellular functions (Sellers, 2000), while microtubules also establish and maintain growth polarity (Mathur and Hülskamp, 2002) and ensure proper cell division by forming the mitotic spindle (Alberts et al., 2002).

The actomyosin system

Filamentous actin (F-Actin) is build up from globular actin (G-Actin). These actin filaments are polar structures with two structurally different ends, a fast growing + and a more inert – end (Figure 2A). Hydrolysis of ATP, which is bound to G-Actin, weakens the bonds within the polymers and thus increases depolymerisation. However, this hydrolysis is also the driving force behind the movement of myosins, the motor proteins moving along actin filaments (Figure 2C): the myosin binds to ATP and is thereby released from the actin filament. ATP hydrolysis causes the myosin to undergo a conformational change and the subsequent release of the phosphate reconnects the myosin with actin.

In *Arabidopsis thaliana*, the existing 17 myosins are grouped into two classes (Peremyslov et al., 2011): myosin class VIII, whose 4 members are involved in endocytosis, cell wall formation and plasmodesmata-mediated transport; and myosin class XI, whose 13 members (XI-1, XI-2 and XI-A to XI-K) are functioning in organelle trafficking (Tominaga and Nakano, 2012). The protein domain organization of myosin class XI in plants is highly similar to that of myosin class V in vertebrates and yeast (Figure 2B; Tominaga et al., 2003): The N-terminal motor domain mediates ATP hydrolysis and is followed by several copies of calmodulin-binding IQ motifs. The C-terminal tail region comprises an α -helical coiled-coil region (CC) for dimerisation between myosins, and the globular tail domain (GTD) for cargo-binding (Figure 2B and C).

While the motor domain is highly conserved in myosin class V/XI members, the tail domain is strongly diverse and therefore essential for differences in dimerisation and cargo transport characteristics. To date, class XI myosins were only found to function as homodimers (Li and Nebenführ, 2008a). However, heterodimerisation of several myosins was detected to low extents in mammalian cells (Singh and Bandman, 2006) and might be present in plants as well.

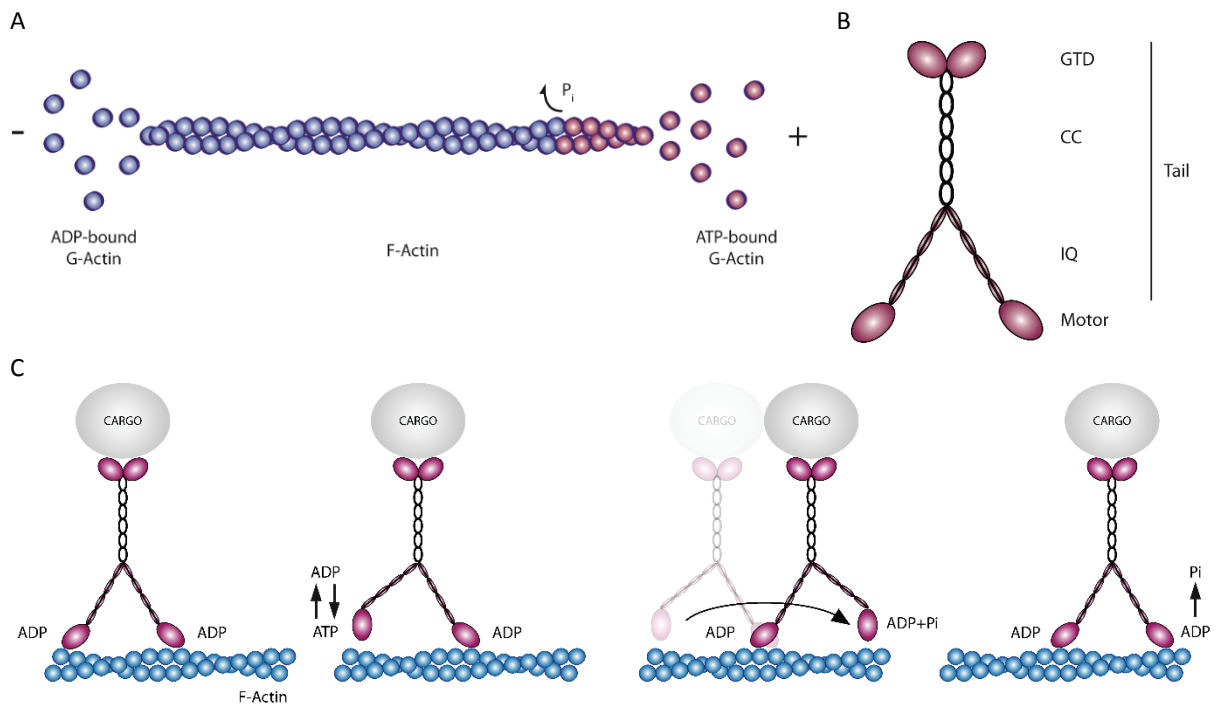


Figure 2: Actin and myosin.

A – Filamentous actin. B - Predicted structure of a myosin class V/XI dimer, modified (Spudich, 2001). IQ – calmodulin-binding IQ motif, CC – coiled-coil domain, GTD – globular tail domain. C - Myosin dependent transport of cargos along actin filaments, driven by ATP hydrolysis.

Cargos of class XI myosins

In plants, the cargos of class XI myosins include the endoplasmic reticulum, chloroplasts, Golgi stacks, peroxisomes, mitochondria, vacuoles, pre-vacuolar/endosomal vesicles (Li and Nebenführ, 2008b) as well as processing bodies (P-bodies; Steffens et al., 2014a). Of these, Golgi stacks, peroxisomes, mitochondria, and P-bodies are of specific interest in this work.

The Golgi apparatus is a hub between secretory, lysosomal, and endocytic pathways. There, proteins are processed, packed into vesicles and sent for their specific destinations. While in yeast multiple Golgi complexes are distributed within the cytoplasm, mammals possess only one Golgi apparatus whose integrity and localization depends on microtubules. In contrast, the plant Golgi complexes are exclusively moved by actin and myosins within the cytoplasm (Nakano and Luini, 2010). During pathogen attacks, Golgi bodies accumulate at infection sites together with ER, mitochondria and peroxisomes. These accumulations, together with aggregations of the cytoplasm, build-up of actin filaments, as well as cell, endomembrane and cell wall components, are essential to mediate penetration resistance (Hardham et al., 2008; Takemoto et al., 2003).

Mitochondria, amongst other functions, produce energy for eukaryotic cells. Consequently, their movement is essential to bring them in contact with energy-consuming structures like the ER or the plasma membrane to balance energy levels. Additionally, mitochondria were found to be essential for calcium signalling and the control of apoptosis, which again emphasizes the need for directed transport of these organelles to their place of activity. Although mitochondrial movement is mainly carried out by actin and myosins, there is data pointing to a role of microtubules in medium and fast movements as well (Zheng et al., 2009).

Peroxisomes are membrane-enclosed organelles which contain a multitude of enzymes. They are sites of fatty acid β -oxidation and are involved in biosynthesis of phytohormones, essential compounds like biotin or salicylic acid, as well as signalling molecules. They are important for the glyoxylate cycle and immune responses, and, together with mitochondria and chloroplasts, function in photorespiration (reviewed in Hu et al., 2012). Consequently, peroxisomes have many sites of function. In mammalian cells, peroxisome movement was found to rely on microtubules, however, plant peroxisome movement is solely dependent on the actomyosin system.

P-bodies are ribonucleoprotein complexes (RNPs) that function in deadenylation, decapping, storage and degradation of mRNAs. Moreover, they contain components of the miRNA-dependent gene silencing machinery and mRNA quality control. Though well described in yeast, the detailed composition and molecular function of several P-body components in *Arabidopsis* remain poorly understood. However, the core components of mRNA degradation seem to be conserved between plants, yeast and mammals (Figure 3). The first and rate-limiting step in mRNA degradation is the deadenylation, which is carried out by the CCR4-NOT complex (CARBON CATABOLITE REPRESSOR PROTEIN 4-NEGATIVE ON TATA COMPLEX). This deadenylase complex was found to accumulate in P-bodies of mammalian cells (Andrei et al., 2005; Cougot et al., 2004) and in yeast (Muhlrad and Parker, 2005), where it catalyses the shortening of the 3'-poly(A) tail. Subsequently, mRNAs are either degraded in 3' to 5' direction by the exosome, or via decapping and 5' to 3' decay.

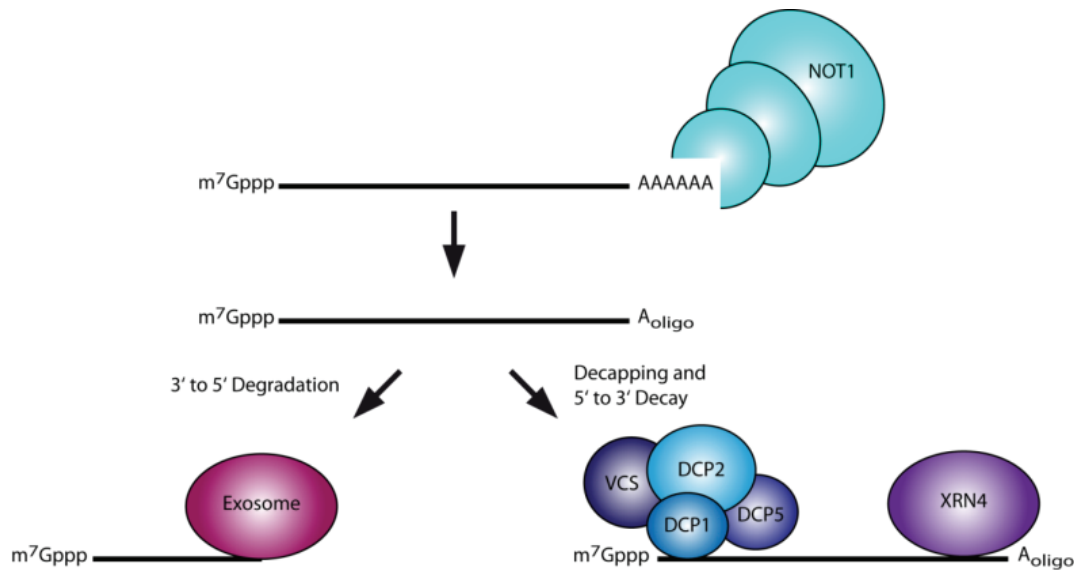


Figure 3: P-body function and composition.

First step – Deadenylation, shortening of the 3'-poly(A) tail. Second step – mRNAs are either degraded in 3' to 5' direction by the exosome, or via decapping and 5' to 3' decay. NOT1 – CCR4-NOT complex, DCP1, 2 and 5-DECAPPING PROTEIN 1, 2 and 5, VCS- VARICOSE, XRN4- 5'-3' exoribonuclease 4.

The mRNA decapping complex in yeast and mammals includes the decapping enzymes DCP1 (DECAPPING 1) and DCP2 (DECAPPING 2). The Arabidopsis homologues AtDCP1 and AtDCP2 were found to interact with the decapping enhancer protein VARICOSE (AtVCS). It was shown that binding to AtDCP1 and AtVCS enhances AtDCP2 function, suggesting that these three proteins form the decapping complex in Arabidopsis (Xu et al., 2006). Another decapping protein, AtDCP5 (DECAPPING 5), was also found to associate with this complex, and to act in translational repression, P-body formation and only indirectly in mRNA decapping (Xu and Chua, 2009). The 5' to 3' decay is carried out by XRN1 (5'-3' exoribonuclease 1) in mammals and yeast (Parker and Sheth, 2007). AtXRN4 (EXORIBONUCLEASE 4), the Arabidopsis homolog of yeast XRN1, was found to co-localize with P-bodies (Weber et al., 2008) and to be involved in the degradation of several unstable mRNAs (Eulalio et al., 2007).

Transport of organelles

In mammals and yeast, the directed transport of membrane-bound organelles was shown to be mediated via specific anchor proteins interacting with the myosin GTDs (Li and Nebenführ, 2008b). In yeast, extensive studies have been conducted to identify specific adapters for various organelles (Fagarasanu and Rachubinski, 2007). Two types of interactions have been characterized to date: direct binding of myosins to proteins within the respective membrane

(Fagarasanu et al., 2006) or indirect binding to the organelle via bridging proteins (Ishikawa et al., 2003). In Arabidopsis, anchoring of cargos to myosins is still poorly investigated (reviewed in Tominaga and Ito, 2015a). Recently, myosin-binding proteins were reported to bind to a new type of compartment called MyoB vesicles (Peremyslov, 2013). In addition, it was found via a yeast two-hybrid screening and an *in vitro* binding assay that the small GTPases RabD1 and RabC2a mediate binding of peroxisomes to XI-2 (Hashimoto et al., 2008). The last myosin adapter protein in *A. thaliana* was identified by mass spectrometry analysis of immunoprecipitated protein (Tamura et al., 2013). The authors could show that XI-I interacts with WIT1/20 (WPP DOMAIN-INTERACTING PROTEIN 1/20) from the outer-nuclear membrane, anchoring the myosin to the nucleus.

P-bodies are of special interest regarding directed movement, since - unlike Golgi stacks, mitochondria and peroxisomes - they are not enclosed by a membrane and underlie a highly dynamic assembly and disassembly. For P-bodies, an association with class XI myosins was first described in yeast (Chang et al., 2008). In Arabidopsis, P-body movement was found to be mediated via the direct interactions of the core component DCP1 with myosin class XI members (Steffens et al., 2014b).

Class XI myosin functions

The 13 members of the myosin class XI in Arabidopsis are both, highly redundant as well as specific for certain functions. For mutants of myosins G, H and J, no phenotypic differences to wild type plants are known so far. Myosins A, C, D and E were found to only show phenotypes in floral organs (reviewed in Duan and Tominaga, 2018). Table 1 shows an overview of known myosin functions of the other six members of class XI, the main players in growth and morphology.

Myosin *xi-b* single mutants show no obvious phenotype, however, if knocked out together with myosins XI-2 and XI-K, XI-B seems to have effects on leaf cell expansion/elongation and root hair elongation (Peremyslov et al., 2008). In this work, one focus is organelle movement, which is mostly carried out by myosins XI-1, XI-2, XI-F, XI-I and XI-K. However, since XI-F is plastid specific (Okamoto et al., 2015) it will not be discussed in detail.

Partially overlapping functions indicate a high level of redundancy between the four class XI myosins XI-1, XI-2, XI-I and XI-K. Indeed, most knockout mutants, including *xi-i* and

Introduction

Table 1: Myosin XI functions in *Arabidopsis thaliana*.

The table was modified from a review of Duan and Tominaga, 2018, and displays functions and phenotypes of myosin XI class members derived from their phenotypes.

Functions/phenotypes	Myosin XI	Notes
Leaf		
Organelle motility	XI-1, XI-2, XI-B, XI-I, XI-K	XI-2 and XI-K are major motor proteins for organelle trafficking.
Cell expansion	XI-1, XI-2, XI-B, XI-I, XI-K	Inhibition of diffuse growth in triple and quadruple myosin XI mutants.
F-actin organisation	XI-1, XI-2, XI-I, XI-K	Abnormal F-actin organization in <i>xi-2 xi-k</i> , <i>xi-1 xi-2 xi-k</i> , and <i>xi-1 xi-2 xi-i xi-k</i> .
Trichome shape	XI-1, XI-2, XI-K	Distorted trichome phenotype in <i>xi-k</i> , <i>xi-2 xi-k</i> , <i>xi-1 xi-k</i> , <i>xi-1 xi-2 xi-k</i> .
Nuclear shape	XI-2, XI-I, XI-K	Extremely elongated nuclear shape in the trichome of <i>xi-2</i> and <i>xi-k</i> . Spherical nuclear shape in <i>xi-i</i> .
Root		
Organelle motility	XI-2, XI-K	XI-2 and XI-K play major roles in organelle trafficking in root hairs.
Root growth	XI-1, XI-2, XI-K	Defect in root growth in <i>xi-1 xi-2 xi-k</i> mutants.
Root hair development	XI-1, XI-2, XI-B, XI-K	Inhibition of root hair growth in <i>xi-2</i> and <i>xi-k</i> mutants.
F-actin organisation in root epidermal cell	XI-1, XI-2, XI-K	Abnormal F-actin organization in <i>xi-1 xi-2 xi-k</i> .
F-actin organisation in root hair	XI-1, XI-2, XI-I, XI-K	Accumulation of thick F-actin bundles in root hair apices of triple and quadruple myosin XI mutants.
F-actin dynamics	XI-1, XI-2, XI-K	Less dense and more bundled cortical F-actin in the epidermal cells of <i>xi-1 xi-2 xi-k</i> mutants. A decrease in F-actin dynamics in root hairs of <i>xi-k</i> mutants.
Nuclear shape and movement	XI-I	<i>xi-i</i> mutants affect nuclear shape and movement in root hairs.
Stem		
Plant height	XI-1, XI-2, XI-B, XI-I, XI-K	Growth inhibition in triple and quadruple myosin XI mutants.
Bolting	XI-1, XI-2, XI-B, XI-I, XI-K	Late bolting in triple and quadruple myosin XI mutants.
Straightening	XI-1, XI-2, XI-F, XI-K	XI-F exhibits specific expression in the fiber cells of stem. Insufficient sedimentation of amyloplasts in <i>xi-1 xi-2 xi-k</i> mutants.
Reproduction		
Stigmatic papillae elongation	XI-1, XI-2, XI-K	Delayed stigmatic papillae elongation in <i>xi-1 xi-2 xi-k</i> .

several alleles of *xi-1* and *xi-2*, show no morphological differences to wild type plants under normal growth conditions (Hashimoto et al., 2005). In contrast, knockouts of *XI-K* and several

other alleles of *xi-2* mutants show defects in root hair elongation as well as in trafficking of Golgi stacks, peroxisomes, and mitochondria in root hairs and in leaf epidermal cells. These findings point to specific functions of the corresponding myosins, which cannot be adopted by other members of the class (Prokhnevsky et al., 2008).

Double mutants of the four myosins clearly show synergistic phenotypes, pointing to redundant functions as well: The *xi-1 xi-k* double mutants are shorter than wild type plants and show reduced leaf size, resulting from decreased cell size and number. In these mutants, as well as in the *xi-2 xi-k* double mutants, Golgi stacks, peroxisomes, and mitochondria move slower than in the single mutants and root hair length is strongly reduced (Peremyslov et al., 2008).

In triple and quadruple mutants, the effects on growth and organelle motility are even more increased (Tominaga and Ito, 2015b). In addition, the quadruple mutant exhibits a decreased antifungal immunity (Yang et al., 2014).

Distorted class of trichome mutants

In planta, there is a wide range of actin binding proteins which are no motor proteins, but specialized to regulate the dynamics and organization of the actin cytoskeleton (Ojangu et al., 2012). These include components of the ARP2/3 (ACTIN-RELATED PROTEIN 2/3) and SCAR/WAVE (SUPPRESSOR OF CYCLIC AMP RECEPTOR/WISKOTT-ALDRICH SYNDROME VERPROLIN-HOMOLOGOUS PROTEIN) pathway. The ARP2/3 complex mediates generation of new actin filaments by binding to the sides of already existing ones (Basu et al., 2005). It is formed by seven proteins: ARP2/WRM (WURM), ARP3/DIS1 (DISTORTED 1), ARPC1, ARPC2/DIS2 (DISTORTED 2), ARPC3, ARPC4 and ARPC5/CRK (CROOKED). The SCAR/WAVE complex functions as the activator for ARP2/3 and consists of five proteins: ABI1 (ABL-INTERACTOR-1), NAP1/GRL (NCK-ASSOCIATED PROTEIN 1/GNARLED), SRA1/KLK (SPECIFICALLY RAC1-ASSOCIATED PROTEIN 1/KLUNKER), BRK1 (BRICK1), and DIS3 (DISTORTED3), which is the actual SCAR/WAVE protein (Guimil and Dunand, 2007).

WRM, DIS1-3, CRK, GRL and KLK all belong to the *distorted* group of genes. Mutants of this group were initially found in an EMS screen in *Arabidopsis thaliana* (Hülkamp et al., 1994). They all share phenotypic characteristics like distorted trichomes and irregular shape of leaf pavement cells and epidermal cells of hypocotyl and root.

Introduction

In the course of this screen, two mutants were identified which resembled these phenotypes but were independent from the ARP2/3 and SCAR/WAVE pathways: the myosin class XI mutant *xi-k* and the WD40/BEACH domain mutant *spirrig* (*spi*). Both mutants show a weak distorted phenotype, with *xi-k* being the least severe. It was therefore hypothesized that both proteins, XI-K and SPI, are involved in similar processes as ARP2/3 and SCAR/WAVE complex proteins (Ojangu et al., 2007; Saedler et al., 2009).

Indeed, it was shown that *xi-2 xi-k* double mutants show a rather random actin organisation in Arabidopsis leaf mid vein cells, compared to the longitudinal organisation in Col-0 (Ueda et al., 2010). However, SPI seems to be not involved in actin organisation, since the corresponding mutants show an intact actin cytoskeleton (Schwab et al., 2003).

The WD40/BEACH domain protein SPIRRIG

BEACH domain proteins are known facilitators of membrane dynamics (De Lozanne, 2003). They are named after their corresponding mutations in mice and humans, the beige and Chediak Higashi syndromes. These proteins are involved in very distinct cellular processes like vesicle transport, membrane fusion, receptor signalling and autophagy (Cullinane et al., 2013). In agreement with these essential functions, the BEACH domain protein family is well conserved in mammals, plants and yeast, often exhibiting several members within one species. In Arabidopsis, only the BEACH domain protein SPIRRIG has been characterized so far (Saedler et al., 2009).

In the N-terminus, SPI carries tandemly repeated Armadillo repeats, each approximately 42 amino acids long. Armadillo domains share a conserved three-dimensional structure of three α helices, which fold together and interact to form a surface for protein–protein interactions

Introduction

(Coates, 2003). The Armadillo repeats are followed by a Concanavalin A (ConA)-like lectin domain, which is thought to be involved in oligosaccharide binding that mediates membrane fusion events (Burgess et al., 2009). In the C-terminus, SPI exhibits a Pleckstrin-Homology (PH) domain, followed by the name giving BEACH domain. The PH domain was found to interact with the BEACH domain to form a large groove, possibly serving as a ligand-binding site (Jogl et al., 2002). Similar to the majority of BEACH domain proteins, the BEACH domain of SPI is followed by several WD40 repeats, which can mediate protein-protein interactions. In total, this protein consists of 3602 amino acids.



Figure 5: Protein structure of SPIRRIG in *Arabidopsis thaliana*.

ARMADILLO - Armadillo repeat domain, ConA – Concanavalin A-like lectin domain, PH – Pleckstrin-Homology domain, BEACH – Beige and Chediak Higashi domain, WD40 – WD40 repeat domain.

The *spirrig* mutants in *A. thaliana* show the already mentioned defects in cell morphogenesis, like low complexity of epidermal pavement cells, weakly distorted and curled trichomes, disconnected and out-curved hypocotyl cells in dark grown seedlings, as well as defects in vacuolar integrity. In addition, recent findings point to a membrane-independent function for this BEACH domain protein as well (Steffens et al., 2015): It was shown that under salt stress conditions, SPI localizes to and facilitates the formation of P-bodies. Furthermore, it was revealed that several salt stress dependent mRNAs are stabilized and recruited to P-bodies by the SPI protein. Supported by the fact that the interaction between BEACH domain proteins and the P-body component DCP1 is evolutionarily conserved, the authors hypothesized that these functions are a general feature of BEACH domain proteins.

Aim of this work

This study aims to gain a deeper understanding of mechanisms involved in cell growth and morphogenesis, focussing on the actomyosin system and SPIRRIG, an actin independent factor for distortion of cell shapes.

(1) Cytoplasmic streaming

The analyses of *xi* mutants show a strong connection of myosin motive force and plant development. In addition, Tominaga et al. could show in 2013 that genetically modified high- and low-speed chimeric XI myosins altered cell size - and thereby overall plant size - by

changing the velocity of transport. In a subsequent review, these results were discussed and the authors concluded that the increase of myosin speed had improved the transport of nutrients, plant hormones, carbon dioxide, and cell wall precursors, which in turn led to increased cell growth (Tominaga and Ito, 2015b).

However, it is necessary to distinguish between active transport of cargos to specific sites by motor proteins, and the passive flow of the cytoplasm and its contents. Both, the active and inactive flow, result in cytoplasmic streaming and at this point have not been analysed coherently in *Arabidopsis thaliana*.

In this work, bulk flow was investigated to establish a base line for cytoplasmic streaming in *Arabidopsis*.

(2) Myosin function

Considering organelle movement, cell shape and trichome morphology, myosin XI-K seems to be the main player within the myosin class XI. However, due to high redundancy and synergistic/additive effects, it is neither promising nor advisable to investigate one myosin isolated from the others. Hence, the experiments in this study are designed to learn about the characteristics of myosins XI-1, XI-2, XI-I and XI-K, the major myosins mediating organelle movement and morphology of the plant.

A full set of single, double, triple and quadruple mutants of the four XI myosins was composed during this work. Novel phenotypes were investigated and organelle movement was characterized for all lines.

In recent years, few genomic fragments, for XI-I and XI-K, have been published. However, the choice of the coupled fluorophore was restricted to GFP and YFP, respectively, and no constructs for XI-1 and XI-2 were available. Since the detailed investigation of *Arabidopsis* myosins often fails, due to lack of functional full length constructs (Madison and Nebenführ, 2013), one focus point was to create a set of full length myosin constructs, to characterize their function.

Due to the lack of functional full length constructs, truncated myosin fragments lacking the motor domain were often used in former studies, although they cause a dominant negative effect on organelle movement. In this work, this effect was analysed in more detail and utilised to create new means to investigate myosin function.

Finally, the interaction behaviour of the four myosins was investigated, following indications from former studies that heterodimerisation occurs within these proteins.

(3) Spirrig

On a molecular level, the exact function of SPI remains unknown. It is proven to be a facilitator of membrane dynamics and new findings also indicate a membrane independent role in salt stress response/P-body dynamics. There are no findings which functionally connect SPIRRIG to trichome morphology. However, the *spirrig* mutants in *Arabidopsis thaliana* clearly show a weak distorted phenotype of their trichomes. To learn more about SPI function and importance *in planta*, an evolutionary comparative approach was chosen. Therefore, a detailed analysis of a closely related Brassicaceae, *Arabis alpina*, was carried out.

This newly established model organism is an arctic-alpine perennial plant. It is particularly suitable for laboratory use, since it is diploid, self-fertile, has a small and mostly sequenced genome and can be transformed with *Agrobacterium tumefaciens* (Wang et al., 2009). In addition, *Arabis alpina* was selected for this work, since it is sufficiently closely related to *Arabidopsis* to clearly identify orthologous genes and synteny, but also distant enough (26 to 40 million years; Beilstein et al., 2010; Koch et al., 2006) to expect phenotypic and molecular variations.

For this project, three putative *spirrig* mutants originated from an EMS screen (Wang et al., 2009) were verified and analysed. All mutant lines are in the *pep1* (*perpetual flowering 1*) background, which is a mutant of the ecotype Pajares (paj). *PEP1* is the orthologue of the *A. thaliana* gene *FLOWERING LOCUS C (FLC)* and is involved in perennial traits like duration of flowering, return to vegetative development, floral transition and flowering response to cold (Wang et al., 2009). As a consequence, handling of the *pep1* mutant is simplified compared to paj, since flowering does not require vernalisation in this line.

Apart from the phenotypic analyses of these mutant lines, *Arabis alpina* SPIRRIG was characterized regarding expression, localisation and behaviour under salt stress conditions. Finally, a set of novel reference genes for quantitative real-time PCR in *Arabis alpina* was established in the course of the expression analyses.

2 Material and Methods

2.1 Plasmids and organisms

A list of general vectors is provided in Table 2, a detailed list of all constructs used is attached to the appendix (Table 22).

Table 2: Plasmids used in this work.

Name	Resistance	Features	Origin
Donor Vectors			
pDONR201	Kan	Gateway donor vector	Invitrogen
pDONR207	Gent	Gateway donor vector	Invitrogen
Bacterial Expression Vectors			
pDest17-His	Amp/Carb	Gateway compatible, N-terminal His-tag	Invitrogen
pGEX2TMGW	Amp/Carb	Gateway compatible, N-terminal GST-tag, C-terminal His-Tag	(Imre Sommsich and Bekir Ülker)
pET40a	Amp/Carb	Gateway compatible, N-terminal MBP-tag	(EMBL, Heidelberg)
Yeast Expression Vectors			
pACT	Amp/Carb	Gateway compatible, Leu ORF	Clontech
pAS	Amp/Carb	Gateway compatible, Trp ORF	Clontech
Plant Expression Vectors			
pENSG:YFP	Amp/Carb	Gateway compatible, N-terminal YFP-tag	(Feys et al., 2005)
pENSG:CFP	Amp/Carb	Gateway compatible, N-terminal CFP-tag	(Feys et al., 2005)
pEXSG:YFP	Amp/Carb	Gateway compatible, C-terminal YFP-tag	(Feys et al., 2005)
pUBI::EXSG:YFP	Amp/Carb	Gateway compatible, C-terminal YFP-tag	(M. Jakoby)
pEXSG:CFP	Amp/Carb	Gateway compatible, C-terminal CFP-tag	(Feys et al., 2005)
pAUBERGINE	Amp/Carb	Gateway compatible, C-terminal mCherry-tag	(M. Jakoby)
pAMARENA	Amp/Carb	Gateway compatible, N-terminal mCherry-tag	(M. Jakoby)
pPACIFIC	Amp/Carb	Gateway compatible, C-terminal Turquoise-tag	(M. Jakoby)
pSYN	Amp/Carb	Gateway compatible, C-terminal YFP-N-tag	(Jakoby et al., 2006)
pSYC	Amp/Carb	Gateway compatible, C-terminal YFP-C-tag	(Jakoby et al., 2006)
pCL112	Spec	Gateway compatible, N-terminal YFP-N-tag	(J.F. Uhrig)
pCL113	Spec	Gateway compatible, N-terminal YFP-C-tag	(J.F. Uhrig)

The organisms used in this work are commercially available unless otherwise specified (Table 3).

Material and Methods

Table 3: Organisms used in this work.

Name	Genotype
Yeast	
AH109	MATa, trp1-901, leu2-3, 112, ura3-52, his3-200, gal4D, gal80D, LYS2::GAL1UAS-GAL1TATA-HIS3, GAL2UAS-GAL2TATA-ADE2, URA3::MEL1UAS-MEL1 TATA-lacZ
Agrobacterium tumefaciens	
GV31-01	pMP90 (Koncz et al., 1989), pMP90RK (Koncz et al., 1989)
RK19	LBA4404.pBBR1MCS.virGN54D (Hoekema et al., 1983)
Escherichia coli	
BL21DE3 RIL	F-ompThsdSB(rB-, mB-) gal dcm (DE3)
DB3.1	F-gyrA462 endA1 Δ(sr1-recA) mcrBmrr hsdS20(rB-, mB-) supE44 ara-14 galK2 lacY1 proA2 rpsL20(SmR) xyl-5 λ-leu mtl1
DH5α	F-Φ80lacZΔM15 Δ(lacZYA-argF) U169 recA1 endA1 hsdR17 (rK-, mK+) phoA supE44 λ-thi-1 gyrA96 relA1
NEB 5 alpha	fhuA2 Δ(argF-lacZ)U169 phoA glnV44 Φ80 Δ(lacZ)M15 gyrA96 recA1 relA1 endA1 thi-1 hsdR17
Arabidopsis thaliana	
Columbia	Col-0
spirrig	<i>spi-3, spi-4</i> (Steffens et al., 2015)
12k^R	Myosin 12k triple mutant, rescued with pMDC32:XI-K:YFP (Peremyslov et al., 2012)
GFP-TUA6	Col-0 expressing GFP-TUA6 (NASC stock number N6551, Takashi Hashimoto)
12k_{XI-KΔGTD-2xYFP}	Myosin 12k triple mutant expressing pMDC32:XI-KΔGTD-2xYFP (M. Jakoby)
Arabis alpina	
perpetual flowering 1	<i>pep1</i> (Wang et al., 2009)
spirrig	<i>spi-1, spi-2, spi-3</i>
Nicotiana benthamiana	

2.2 Biomolecular methods

2.2.1 Polymerase chain reaction (PCR)

Polymerase chain reactions were used to amplify DNA fragments of interest. Different techniques and polymerases were used dependent on the aim of the experiment.

Phusion PCR

Phusion polymerase is a fast, proof-reading polymerase which creates blunt ends. The standard reaction and program for Phusion High-Fidelity DNA polymerase (Thermo Fisher Scientific) is shown in Table 4.

Table 4: Phusion polymerase reaction and program.

Reaction			Program		
1	μl	DNA	98°C	2 min	
0.5	μl	Primer forward	98°C	20 sec	1
0.5	μl	Primer reverse	TA	20 sec	35x
0.5	μl	dNTPs 10 mM	72°C	15-30 sec/kb	J
5	μl	5x HF buffer	72°C	3 min	
0.3	μl	Phusion	4°C	Pause	
17.2	μl	ddH ₂ O			

Material and Methods

For Alignment PCRs, which connect two fragments with an overlapping region, variants of the Phusion PCR were used. In the first variant, 1 µl of each fragment was added to the Phusion reaction and primers at the start of the first fragment and the end of the second fragment were chosen. The program was run for 50 cycles. In the second variant, again 1 µl of each fragment was used but the primers were only added after the first 15 cycles. Subsequently, the PCR was run for another 35 cycles.

Genotyping PCR

For genotyping of plants, DreamTaq DNA Polymerase (Thermo Fisher Scientific) was used either in a reaction with separately added dNTPs and buffer or as a ready to use Green Taq Mix (Table 5).

Table 5: Taq Polymerase and Green Taq Mix reaction and program.

Reaction		Reaction		Program		
1 µl	DNA	1	µl DNA	96°C	2 min	
0.3 µl	Primer forward	0.3	µl Primer forward	96°C	30 sec	1
0.3 µl	Primer reverse	0.3	µl Primer reverse	TA	30 sec	35x
0.3 µl	dNTPs 10 mM	12.5	µl Green Taq Mix	72°C	60 sec /kb	↓
3 µl	10x buffer	10.9	µl ddH ₂ O	4°C	Pause	
0.2 µl	Taq					
26 µl	ddH ₂ O					

Site-directed mutagenesis

A site-directed mutagenesis is used to mutate single or few bases in a plasmid. To do so, primers are designed which extend approx. 10 to 15 bp left and right from the desired mutation, while the forward primer is the reverse complement version of the reverse primer. The reaction and program are displayed in Table 6.

Table 6: Site-directed mutagenesis reaction and program.

Reaction			Program		
0.5	µl	DNA	95°C	3 min	
2	µl	Primer forward	95°C	45 sec	1
2	µl	Primer reverse	42°C	45 sec	13x
1	µl	dNTPs 10 mM	72°C	1:50 min	↓
5	µl	High fidelity buffer with MgCl ₂	95°C	45 sec	
0.5	µl	High fidelity polymerase	60°C	45 sec	1 26x
39	µl	ddH ₂ O	72°C	7 min	↓
			72°C	10 min	
			12°C	pause	

After the PCR is completed, a DpnI digest is carried out by adding 1 µl DpnI to 50 µl PCR reaction (no other buffer or purification is needed). After an incubation for 1 ½ h on 37°C, the

Material and Methods

enzyme is deactivated on 80°C for 20 min. Subsequently, 1 µl of this reaction is used for transformation of competent cells.

Quantitative real-time PCR (qPCR)

Quantitative real-time PCR is a method to monitor the amplification of a fragment of interest in real-time by detection of a fluorescent dye, e.g. SYBR Green, which intercalates with double-stranded DNA. qPCRs were carried out in a QuantStudio 5 System (ABI/Life Technologies) equipped with a 96 well block. The qPCRs were performed using plates (96 well, 0.2 ml) and cover foil (Opti-Seal Optical Disposable Adhesive) from BIOplastics and SYBR Green reagent from (Thermo Fisher Scientific). Analysis was carried out with the QuantStudio TM Design and Analysis Software version 1.4.1. Reactions and program are displayed in the following table:

Table 7: qPCR reaction and program.
Asterisks indicate points of data collection.

Reaction			Program		
5	µl	SYBR Green	50°C	2 min	
0.2	µl	Primer I	95°C	10min	
0.2	µl	Primer II	95°C	15 sec	1 40x
1	µl	ddH ₂ O	60°C	1 min	* ↓
1	µl	cDNA	95°C	15 sec	
			60°C	1 min	
			95°C	1 sec	*

The primers were designed using GenScript Real-time PCR Primer Design (www.genscript.com) at an optimum T_m of 60±2°C. For each sample, at least three biological and three technical replicates were analysed.

Visualization of PCR fragments

10x XO loading buffer (1ml 0.5 M EDTA pH 8, 5.81 ml 86% glycerol, 10mg xylene cyanol, 100 µl 1M Tris/HCl pH 8, 25-50 mg Orange G, ad. 10 ml ddH₂O) and the 1 kb (plus) ladder or 100 bp ladder (Thermo Fisher Scientific) were used for gel electrophoresis. The documentation was carried out with the BioRad Universal Hood II and Quantity One Software version 4.5.0.

2.2.2 Restriction digest

All plasmids were digested with suitable restriction enzymes (single digest: 2.0 µl DNA, 2.0 µl buffer, 0.3 µl enzyme, 15.7 µl ddH₂O; double digest: according to the Double Digest

Calculator of Thermo Fisher Scientific, FastAP treatment was carried out if necessary for ligation). The reactions were incubated at 37°C for 1 h and subsequently checked on agarose gels for expected size and possible contaminations.

2.2.3 Cloning

Gateway cloning

The Gateway system (Invitrogen) was developed according to a recombination pathway of the lambda phage. The phage recombines a specific sequence of its DNA (attP) with a corresponding sequence of a bacterium (attB) via phage-coded integrase (INT) and the bacterium-coded integration host factor (IHF). This recombination results in an integration of phage DNA into the genome of the bacterium, which is flanked by the attB and attP sequences, which are then referred to as attL and attR sequences (L and R for left and right). The reverse reaction removes these sequences and restores the primary attB and attP sequences. The gateway donor and destination vectors contain the ccdB gene in between these flanking sequences, which codes for a gene product that inhibits the gyrase of commonly used bacterial strains. This gene is substituted by DNA of interest during BP-/LR-reactions, allowing a selection of successfully transformed bacteria.

For BP-reactions, genes of interest were amplified with primers containing attB sites via PCR and recombined with a donor vector (1.75 µl PCR product (150 ng/µl), 0.25 µl donor (10 ng/µl), 0.5 µl BP Clonase (Thermo Fisher Scientific)). For LR-reactions, entry clones with the genes of interest were recombined with desired destination vectors (0.5 µl (10-40 ng) donor vector, 0.25 µl destination vector (150 ng/µl), 0.5 µl LR Enzyme Mix (Thermo Fisher Scientific), 1.25 µl ddH₂O). The reactions were incubated at room temperature (RT) for 1-16 h and subsequently used for transformation of competent cells.

Blunt-end cloning

Blunt-end cloning was carried out with the pJET system (Thermo Fisher Scientific). The reactions were performed with purified or non-purified PCR products (1 µl non-purified PCR product or 0.15 pmol (5 ng/100 bp) purified PCR product, 10 µl 2x reaction buffer, 1 µl pJET cloning vector, ad. 20 µl ddH₂O, 1 µl T4 DNA ligase). The reaction was briefly vortexed and centrifuged for 3-5 sec. After an incubation at RT for 5 min, up to 5 µl of the reaction were used for the transformation of 50 µl competent cells.

Material and Methods

T4 DNA ligation

Fragments of interest were created by PCR and/or restriction digest and ligated using T4 DNA ligase (Thermo Fisher Scientific). The reactions (20-100 ng linear vector DNA, 1:1-5:1 insert DNA, 2 µl 10x T4 DNA ligase buffer, 2 µl 50% PEG 4000, 1 µl (5U) T4 DNA ligase, ad. 20 µl ddH₂O) were incubated at 22°C for 1 h or 12°C O/N. Up to 5 µl of the reaction were used for transformation of competent cells.

Assembly of large DNA fragments

Large DNA fragments are often hard to assemble and common cloning strategies fail. In order to assemble full length SPIRRIG and its domains, the Gibson Assembly and NEBuilder systems were used (New England Biolabs). Both systems are exonuclease-based methods, in which an exonuclease creates overhangs, a polymerase fills in the gaps of the single strand regions and a DNA ligase seals the nicks. Reactions were carried out according to the provided manuals.

2.2.4 Production of competent *E.coli* cells

A pre-culture was prepared (25 ml of selective LB medium (Bertani, 1951), 37°C, O/N, shaking) and used to inoculate 250 ml main culture (37°C, shaking, until OD₆₀₀ is 0.55). The culture was transferred to an ice-water bath for 10 min, then the cells were harvested by centrifugation at 2500g for 10 min at 4°C. The medium was poured off and the cells were washed two times with 80 ml/20 ml of ice-cold Inoue transformation buffer (800 ml ddH₂O, 10.88 g MnCl₂ x 4 H₂O, 2.2 g CaCl₂ x 2 H₂O, 18.65 g KCl, 10 ml sterile PIPES solution (0.5 M, pH 6.7); ad 1 l with ddH₂O; sterilise by filtration; Inoue et al., 1990). Subsequently, 1.5 ml of DMSO were added and the bacterial suspension was mixed by swirling and placed on ice for 10 min, aliquoted and stored at -80°C.

2.2.5 Transformation of competent cells

Competent cells were transformed with plasmids of interest according to table 8. For standard transformations (e.g. to produce plasmids), DH5α cells were used. For transformations of empty donor or destination vectors, DB3.1 cells were used, since this strain exhibits a gyrase which is insensitive to the protein encoded by the *ccdB* gene. For protein expression, competent cells of *E.coli* BL21DE3 RIL lines were used. RIL lines are more suitable for expression of Arabidopsis proteins, since they have a higher amount of arginine (R)-, isoleucine (I)- and leucine (L)-tRNAs, matching the codon usage of Arabidopsis. Agrobacteria were used for plant transformation.

Table 8: Transformation of competent cells.

	<i>DH5α</i>	<i>DB3.1</i>	<i>RIL</i>	<i>Agrobacteria</i>
<i>Plasmid</i>	0.5 µl (or complete LR/BP)	Max. 0.5 µl	0.5 µl	2 µl
<i>Comp. cells</i>	25-50 µl	25-50 µl	25-50 µl	25-50 µl
<i>Incubation on ice</i>	20-30 min	20-30 min	20-30 min	20-30 min
<i>Heat shock</i>	42°C for 1½ min	42°C for 1½ min	42°C for 1½ min	42°C for 1½ min
<i>Add medium</i>	300 µl LB	300 µl LB	300 µl LB	700 µl YEB
<i>Incubation</i>	Shake for 30 min at 37°C	Shake for 30 min at 37°C	Shake for 30 min at 37°C	Shake for 1 ½ h at 28°C
<i>Selection</i>	OPTIONAL: pellet cells, pour off media, resuspend in backflow and plate cells			Plate 100 µl
<i>Incubation</i>	O/N at 37°C	O/N at 37°C	O/N at 37°C	2-4 days at 28°C

2.2.6 Plasmid preparation

Plasmids were prepared from selective overnight LB cultures of recombinant *E.coli* cells with the GeneJet Plasmid Miniprep Kit (Thermo Fisher Scientific) according to the provided manual. The plasmids were eluted in 50 µl elution buffer.

2.2.7 Sequencing

Sequencing was carried out by the GATC Biotech AG using LightRun.

2.3 Biochemical methods

2.3.1 Protein expression in *E.coli*

The vectors used for protein expression contain a tac promoter, which has an analogous function to the lac operon, in which Isopropyl β-D-1-thiogalactopyranoside (IPTG) is used to trigger transcription of a protein of interest by binding to the lac repressor and releasing it from the lac operator.

Colonies of transformed RIL lines were used to generate O/N cultures which were used to inoculate 50-100 ml selective TB (Terrific Broth Medium: 12 g tryptone, 24 g yeast extract, 4 ml glycerol, add 900 ml ddH₂O, autoclave, add 100 ml phosphate buffer pH 7.5, sterilized by filtration). Cells were incubated at 37°C under constant shaking. Induction with IPTG (1 mM final concentration) was performed after the OD600 values reached 0.6-0.8. Induction was carried out with variable conditions. For protein purification, the cultures were pelleted (4000 rpm, 15 min, 4°C) and stored at -20°C.

2.3.2 Protein detection

Protein samples were boiled with 2x loading dye (50 mM Tris/HCl (pH 6.8); 2% SDS; 10% glycerol; 0.1% bromophenol blue; 100 mM DTT) at 95°C for 5 min. Subsequently, proteins were separated on acrylamide gels (separation gel (5 ml, 10%): 1.9 ml ddH₂O, 1.7 ml Rotiphorese Gel 30 (37.5:1, Roth), 1.3 ml Tris/HCl (1.5 M, pH 8.8), 0.05 ml SDS (10%), 0.05 ml ammonium persulphate (10%), 2 µl tetramethylethylenediamine; stacking gel (1 ml): 0.68 ml ddH₂O, 0.17 ml Rotiphorese Gel 30 (37.5:1, Roth), 0.13 ml Tris/HCl (1.5 M, pH 6.8), 0.01 ml SDS (10%), 0.01 ml ammonium persulphate (10%), 1 µl Tetramethylethylenediamine). The PageRuler Prestained Protein Ladder (Thermo Scientific) was used as marker. To visualize the proteins, gels were stained with Coomassie (80 mg Coomassie Brilliant Blue G250, ad 1 l ddH₂O; mix for 2 h; add 3 ml conc. HCl).

2.3.3 Protein purification

All steps were performed at 4°C. The pellets of 100 ml cultures were resuspended in 10 ml binding buffer with (EDTA-free) Protease Inhibitor Cocktail (Roche; 1 tablet/50 ml buffer). Afterwards, 100 µg/ml lysozyme were added and samples were incubated on ice for 20-40 min. The samples were sonicated twice at 60% for 1 min (Sonopuls, Bandolin) and centrifuged at 3220 rpm for 15 min. The lysates were added to 100 µl equilibrated beads and incubated for 30 min under constant rotation. Samples were washed three times with 15 ml binding buffer. Elution of the tagged proteins was performed with elution buffer, which was added at a ratio of 1:1 to the beads, followed by incubation on ice for 15 min. Subsequently, the samples were centrifuged at 500g for 3 min and the supernatants were saved. Three elution fractions were prepared according to this method, additionally 50 µl of the beads were boiled with 2x protein loading dye to release proteins which are still attached to the beads.

Table 9: Specifications for protein purification buffers and beads.

	<i>GST purification</i>	<i>MBP purification</i>	<i>His purification</i>
<i>Elution buffer</i>	Buffer+40 mM Glutathione red.	Buffer+10 mM Maltose	Buffer+10 mM Imidazole
<i>Beads</i>	GSH	Amylose	NiNTA

2.3.4 Co-Immunoprecipitation (Co-IP)

Co-IPs were prepared with beads, labelled with a protein of interest, and the lysates of the putative interactors. Lysates and beads were prepared according to the protocol for protein purification (2.3.3). After incubation for 1-1.5 h at 4°C under constant rotation, the mixtures were washed and eluted again according to the protein purification protocol.

2.4 Plant techniques

2.4.1 Plant growth conditions

Seeds were either put out on soil or were sterilized and put out on MS (Murashige and Skoog, 1962) containing plates. For Arabidopsis, ½ MS plates were used, Arabis plants were grown on full MS plates. The seeds were stratified for at least three days (Arabidopsis) or for five days (Arabis). Subsequently, plants were grown under long day conditions at $21\pm 1^\circ\text{C}$ and $100\pm 20 \mu\text{mol/m}^2\text{s}$ light intensity.

Rosette size measurement of transgenic T1 lines

Transgenic lines were grown on soil, selected with BASTA and transferred to single pots. Pictures were taken when the plants reached an approximate diameter of 1.5 cm and again 7 days later.

Heat treatment

For heat treatment the plants were germinated on soil and grown for eight days under standard conditions. They were then transferred to $28\pm 0.5^\circ\text{C}$ and $100\pm 20 \mu\text{mol/m}^2\text{s}$ light intensity. After 17 days, leaves were dissected and pictures were taken.

Dark growth

To analyse plant growth in the dark, seeds were put out on plates, stratified and transferred to $21\pm 1^\circ\text{C}$ and $100\pm 20 \mu\text{mol/m}^2\text{s}$ light intensity for 4 h. Next, the plates were wrapped light-tight and vertically grown for seven days. Pictures were taken with the stereo microscope.

Salt treatment

For germination assays, seeds were grown on MS plates and MS plates supplemented with 125 mM NaCl. From day one to 20, seeds were checked for breakthrough of either root or cotyledons every day under a stereo microscope.

For cotyledon whitening assays, three different approaches were chosen: I) seeds were directly put out on MS plates supplemented with 125 mM NaCl, grown horizontally and maximum cotyledon whitening was noted after 20-28 days; II) seeds were planted on MS plates, grown horizontally, and transferred to MS plates and MS plates supplemented with 125 mM NaCl after five; III) seeds were planted on MS plates, grown horizontally, and transferred to MS plates and MS plates supplemented with 125 mM NaCl after 10 days. Cotyledon whitening was checked visually every day for 10 days.

Material and Methods

For primary root growth assays, seeds were planted on MS plates, grown vertically, and transferred to MS plates and MS plates supplemented with different concentrations of NaCl after ten days. Growth was then documented for four or eight days.

Seedling growth under transpiring conditions was tested on soil/sand, stone wool, agarose and soil. Growth on sand/soil was attempted as described before (Steffens et al., 2015). For cultivation on stone wool, pots with a diameter of 6 cm were supplied with stone wool cubes of 4x4x4 cm or 150 well trays supplied with fitting stone wool pieces were used. The stone wool was soaked in $\frac{1}{2}$ MS before planting. Plants were watered by dipping every three to four days with $\frac{1}{2}$ MS until day 20 and subsequently with either $\frac{1}{2}$ MS or $\frac{1}{2}$ MS supplemented with 125mM NaCl until day 30. The growth on agarose was carried out in PCR tubes, filled with MS and agarose. The tubes were placed into a tip box and cut open at the bottom to allow growth of the roots into the liquid medium supplied below. After growing the seedlings to a diameter of approx. 1 cm, the PCR tubes were transferred to individual 15 ml Falcon tubes. The tubes were placed into an exactly fitting hole in the lid. The growth on soil was carried out under standard conditions, plants were watered by dipping every three to four days with water until day 20 and subsequently with either water or water supplemented with 125 mM NaCl until day 30.

For transcript measurements, two to three 5-7 day old seedlings were transferred from plates to liquid $\frac{1}{2}$ MS or liquid $\frac{1}{2}$ MS with 125 mM NaCl for 4 h under constant shaking. Afterwards, samples were immediately snap frozen with liquid nitrogen.

For short term salt stress of leaves, samples were transferred to $\frac{1}{2}$ MS with 125 mM NaCl for 60-80 min.

2.4.2 Seed sterilization

Sterilisation with ethanol and sodium hypo chloride

Seeds were transferred to a 1.5 ml or 2 ml reaction tube. 500 μ l 70% ethanol was added and the seeds were incubated under constant shaking for 5 min. This step was repeated with 100% ethanol and subsequently with 2% sodium hypo chloride. Here, the shaking was carried out for 8 min. The seeds were washed two times with 500 μ l ddH₂O and either immediately transferred to plates or stratified in ddH₂O.

Material and Methods

Sterilisation with ethanol

Seeds were transferred to a 1.5 ml or 2 ml reaction tube. 500 μ l 70% ethanol was added and the seeds were incubated under constant shaking for 15-20 min. This step was repeated with 100% ethanol. Seeds were transferred to sterile Whatman paper and after drying re-transferred into a clean 1.5 ml reaction tube.

2.4.3 RNA extraction

RNA extraction with Tri-Reagent

For the extraction of RNA, approximately 100 mg plant material and 4-5 sterile glass beads (2.7 mm) were added to a safe lock tube and frozen in liquid nitrogen. Samples were grinded in a tissue lyser at 30 Hz for 1 min and again frozen in liquid nitrogen. Afterwards, 300 μ l cold TRI Reagent (Ambion by Life Technologies) was added and samples were again grinded in the tissue lyser at 30 Hz for 2 min. After the addition of 700 μ l cold TRI Reagent, samples were vortexed for 15 sec and incubated at RT for 3 min. To create a phase separation, 200 μ l chloroform was added, the reaction tubes were vortexed briefly and centrifuged at full speed for 15 min at 4°C. The upper phase was transferred into a new tube and 550 μ l isopropanol was added. The samples were vortex briefly, incubated at RT for 10 min and centrifuged at full speed for 20 min at 15°C to pellet the RNA. The supernatant was discarded and the pellet was washed twice with 500 μ l ethanol (70% and absolute, respectively). Subsequently, the pellet was dried for 30 min at 37°C, resuspended in 50 μ l ddH₂O and incubated at 37°C for ten min.

RNA extraction with RNeasy Kit

RNA extraction with the RNeasy Kit (Qiagen) was carried out according to the provided manual.

2.4.4 DNase treatment

In order to get rid of residual DNA, a DNase treatment was performed by adding 0.66 μ l 10x DNaseI buffer and 0.33 μ l DNaseI per μ l RNA. The samples were incubated at 37°C for 1 h, EDTA was added (0.083 μ l of a 25 mM EDTA solution per μ l RNA) and the reaction was deactivated at 65°C for 10 min.

2.4.5 cDNA synthesis

For cDNA synthesis with oligodT primers, either the RevertAid First Strand cDNA Synthesis Kit (Thermo Fisher Scientific) or the SuperScript™ III First-Strand Synthesis Kit (Thermo

Fisher Scientific) were used according to the provided protocol. The cDNA was tested for DNA contamination and integrity using an adequate reference gene.

2.4.6 Production of plant extracts for genotyping

Small leaves or parts of leaves were harvested and added to a 2 ml safe lock reaction tube together with 3-4 glass beads (2.7 mm) and 300 µl magic buffer (50 mM Tris/HCl pH 7.2, 300 mM NaCl, 10% Sucrose). Samples were shook in the tissue-lyser at 30 Hz for 1.5 minutes. Of this solution, 1 µl was used as a template for PCR.

2.4.7 Particle bombardment

Plasmids of interest (300-1500 ng per shot) were bound to equilibrated microcarriers (gold, BioRad) with CaCl₂ (2.5 M) and spermidine (0.1 M) under vigorous shaking. Microcarriers were washed with increasing concentrations of EtOH (70%, 100%), subsequently resuspended in 100% EtOH, and spotted onto macrocarriers. After complete evaporation of EtOH, bombardment was carried out with the Biolistic Particle Delivery System (Model PDS-1000/He, BioRad) using a rupture disk for 900 PSI pressure. Young rosette leaves from *Arabidopsis* seedlings were used for bombardment.

2.4.8 Tobacco leaf infiltration

Selective YEB medium was inoculated with transformed *Agrobacterium tumefaciens* colonies and incubated at 28°C for approx. 36 h under constant shaking. The cultures were centrifuged for 15 min at 4000 rpm and the pellets were resuspended in 5 ml 1x Agromix (90 ml 10x Agromix (100 mM MgCl₂ x 6 H₂O, 100 mM MES, set pH on 5.6), 10 ml 3,5-Dimethoxy-4-hydroxyacetophenon (3 mg/ml in 100% EtOH), 900 ml ddH₂O). The OD₆₀₀ was set to 0.8 with 1x Agromix for all cultures. Desired combinations of constructs and RK19 culture were mixed in equal parts. After an incubation of 20 min to 4 h at RT, the mixtures were injected into the bottom side of young tobacco leaves.

Bimolecular fluorescence complementation (BiFC)

In vivo interaction of proteins was investigated using tobacco leaf infiltration with agrobacteria transformed with BiFC constructs. These vectors contain the N-terminal and C-terminal part of the gene encoding YFP, respectively. When in very close proximity, the parts assemble to a functional YFP protein and fluorescence is visible.

2.4.9 Floral dip

Transformed *Agrobacteria* were incubated in 5 ml LB in a reaction tube O/N or in a 25 ml flask for approx. eight hours. A 200 ml main culture was inoculated and incubated at 37°C at least O/N, until it was non-transparent. Next, 10 g sucrose and 40 µl Silwet were added to the culture. After 10 min, the culture was filled into a 200 ml beaker and the plants of interest were dipped into the liquid until all flowers were covered with *Agrobacteria*. Subsequently, the plants were grown under normal conditions and the seeds of the next generation were selected for BASTA or hygromycin resistance, respectively.

2.4.10 Crossing

Crossing in both Brassicaceae species used in this work was carried out similarly. Using sharp forceps, the receiving flower was emasculated through removal of the anthers under the binocular microscope. The stigma is then pollinated by mechanically applying pollen of the designated crossing partner.

2.4.11 Selection of transformed plants

BASTA selection

Seeds were put out on soil and grown under normal conditions. BASTA solution (0.1% BASTA (Aventis), 0.001% Tween20, ad. 1 l ddH₂O) was sprayed as soon as seedlings were visible and cotyledons started to open. After 5-10 days, trays were checked for survivors.

Hygromycin selection

Seeds were sterilized and put out on hygromycin selection plates (ddH₂O + Phytoagar + 1 mM KNO₃, autoclave, add 20 µg/ml Hyg). After a few days, plates were checked for survivors (only plants with true roots).

2.4.12 Fluorescein diacetate (FDA) staining

Fluorescein diacetate labels the cytoplasm but does not enter the vacuole. Hence it can be used as a negative stain. Plants were treated with a 0.05% w/v solution of FDA (Sigma) in ddH₂O for 15-20 min.

2.4.13 Latrunculin B treatment

Latrunculins are able to disrupt the actin cytoskeleton. Latrunculin B sequesters G-actin and prevents F-actin assembly. Plants were treated with a 20 µM solution of Latrunculin B (Sigma) in ½ MS or ½ MS with 125 mM NaCl for 5 to 20 minutes, until organelle movement was completely inhibited.

2.4.14 Fixation of cells

Cells were fixed with glutaraldehyde (2.5%) and paraformaldehyde (2%) in 0.08 M HEPES buffer (11.92 g HEPES, 24.22 g NaCl, ad. 1 l ddH₂O) pH 7 for 4 h.

2.5 Yeast techniques

2.5.1 Co-transformation of competent yeast cells

For transformation of competent yeast cells, genes of interest were integrated into yeast expression vectors pAS and pACT, bearing the genes encoding the GAL4-Binding Domain (GAL4-BD) and the GAL4-Activation Domain (GAL4-AD), respectively. Subsequently, overnight YPAD cultures (8 g Difco peptone, 4 g yeast extract, 40 mg adenine, 380 ml ddH₂O; adjust pH to 5.8 with HCl; autoclave; add 20 ml 40% Glucose) of yeast AH109 cells were used to inoculate transformation cultures (10-15 transformations: 0.5-1 ml overnight culture in 50 ml YPAD). The cultures were incubated at 30°C under constant shaking until the OD₆₀₀ reached 0.6 and then spun down for 5 min at 4000 rpm. Cells were resuspended in 10 ml LiAc (0.1 M) per 50 ml culture and again centrifuged for 5 min at 4000 rpm. The supernatant was decanted and the yeast cells were resuspended in the remaining liquid. Afterwards, 240 µl PEG (50% PEG 3350), 36 µl 1 M LiAc, 10 µl ssDNA (10 mg/ml, boiled at 95°C for 10 min) and 65 µl ddH₂O per transformation were added and the resulting mixture was vortexed for 30 sec. Subsequently, 1 µl of plasmid (600-1000 ng/µl) was filled into a 1.5 ml reaction tube and 350 µl of the yeast mixture were added. The tube was vortexed shortly and then incubated for 40 min at 42°C. After incubation, the mixtures were spun down for 30 sec at 6000 rpm, the pellets were resuspended in 60 µl ddH₂O and plated on SD-LW plates (0.68 g Yeast Nitrogen Base w/o Amino Acids w/o (NH₄)₃SO₄, 2 g ammonium sulphate, 0.24 g DO Supplement -LWH, 8 mg histidine, 40 mg Adenine, 7.2 g Agar, 380 ml ddH₂O, adjust pH to 5.8 with 1 M NaOH, autoclave; add 20 ml 40% Glucose). The plates were incubated at 30°C for three to four days.

2.5.2 Yeast two-hybrid

For yeast two-hybrid assays, yeast cells were co-transformed with two plasmids (pACT and pAS backbones), containing genes encoding putatively interacting proteins. Clones were picked from SD-LW plates, resuspended in 60 µl ddH₂O and stamped on SD-LWH plates (0.68 g Yeast Nitrogen Base w/o Amino Acids w/o (NH₄)₃SO₄, 2 g ammonium sulphate, 0.24 g DO Supplement -LWH, 40 mg adenine, 7.2 g agar, 380 ml ddH₂O, adjust pH to 5.8 with 1 M NaOH, autoclave; add 20 ml 40% glucose) containing 3-AT (42.04 g 3-Amino-

1,2,4-Triazole, ad. 500 ml ddH₂O, sterile). Interaction of the proteins was indicated by growth of colonies, since a physical connection of the GAL4 domains, mediated by an interaction of the fused proteins, is necessary for expressing histidine, an essential amino acid. As negative control, pACT-GFP constructs were co-transformed and tested with all pAS constructs, to exclude auto-activation of GAL4-BD fused proteins.

2.6 Microscopical methods

2.6.1 Stereo microscopy

Stereo microscopy was carried out with the Leica MZ 16F stereo microscope and the LAS AF software.

2.6.2 Fluorescence microscopy

Fluorescence microscopy was carried out with the Leica DMRB microscope equipped with a Sony Alpha 6000 camera or with the Leica DMRE microscope and equipped with the Leica DFC 7000 T camera using the LAS X software.

2.6.3 Confocal laser scanning microscopy

Confocal laser scanning microscopy was carried out with the Leica DMRE, DM5500 and DM6000 CS Microscopes and documented with the TCS-SP2, TCS-SPE and TCS-SP8 imaging systems, respectively (Leica Microsystems, Heidelberg, Germany).

2.6.4 Analysis of organelle movement

The movement of organelles was analysed in transiently transformed Arabidopsis rosette leaf cells along the central vein. A particular plane was scanned 50 times at given intervals of 1.29-1.6 sec with a confocal laser scanning microscope.

Fluorescence Recovery after Photobleaching (FRAP)

FRAP was performed with the TCS-SP8 software FRAP Wizard, using the DM6000 CS microscope equipped with a 63x objective (HC APO 63x/0.90 W). The pre-bleach and post bleach images were acquired using a resolution of 128 x 128 pixels, a scan speed of 1800 Hz and a detection range of 597-623 nm. An area of 2.5 μ m x 2.5 μ m was determined as the region of interest (ROI) and bleaching was performed at 80% laser power and 100% laser intensity at 561 nm of an Argon laser. The FRAP experiment was carried out with 2 pre-bleach steps (0.04 sec), 5 bleach steps (0.04 sec) and 118 post-bleach steps (0.04 sec), resulting in a total measuring time of 5 sec.

Material and Methods

Förster Resonance Energy Transfer (FRET)

FRET was carried out with the TCS-SP8 software, using the DMDM6000 CS microscope equipped with a 10x (HC PL FLUOTAR 10x/0.03) or 20x objective (HC PL APO 20x/0.75). Three different FRET techniques were performed using the corresponding wizards of the software. All samples analysed were CFP/YFP pairs.

FRET Acceptor Bleaching (AB)

FRET AB pre-bleach and post bleach images were acquired using a resolution of 512 x 512 pixels and a scan speed of 400 Hz. Entire cells were determined as the region of interest (ROI) for bleaching. The Argon laser was set to 80% laser power and 30% laser intensity at 514 nm. 5 bleach steps were carried out. FRET efficiency was measured for single loci instead of the whole cell.

FRET Sensitized Emission (SE)

FRET SE correction images were acquired using a resolution of 512x512 pixels and a scan speed of 400 Hz. The Argon laser was set to 20% laser power and a specific intensity for each set. FRET efficiency was measured for single loci at defined planes.

Fluorescence lifetime imaging microscopy (FLIM) with FRET

FLIM with FRET was carried out using the Picoquant Symphotime software, following the Leica Confocal Application Letter for FRET with FLIM. The acquisition was performed at a resolution of 512 x 512 pixels with the 440 nm pulsed laser at 10 to 40 MHz. The donor only lifetimes τ_{int_1} and τ_{int_2} were determined with a 3-exponential fit, the third lifetime being the fixed Raman time of 0.3 ns. The two measured lifetimes were used to calculate the average of the intensity lifetime of the donor samples

$$\tau_{int_{donor}} = \frac{amp_1 \times \tau_{int_1}^2 + amp_2 \times \tau_{int_2}^2}{amp_1 \times \tau_{int_1} + amp_2 \times \tau_{int_2}}$$

The FRET samples were calculated with a 3-exponential fit as well, with one lifetime being the fixed Raman time of 0.3 ns and the other lifetime being fixed to the average of the intensity lifetime of the donor samples. Efficiencies were calculated according to the formula

$$E = 1 - \frac{\tau_{int_{donor},FRET}}{\tau_{int_{donor},no\ FRET}}$$

2.7 *In silico* methods

2.7.1 Sequence analysis

Sequences were taken from TAIR (Berardini et al., 2015a), NCBI (National Centre for Biotechnology Information, www.ncbi.nlm.nih.gov) and the Genomic resources for *Arabidopsis thaliana* website (www.arabidopsis.org).

In silico sequence analysis was carried out with CLC DNA Workbench version 5.6.1. Conserved domains were determined using CD-Search (Marchler-Bauer and Bryant, 2004) and/or PROSITE (Hulo et al., 2007).

Phylogenetic trees were created using the Neighbour Joining method with the Unipro UGENE software (version 1.16.0) and subsequently modified.

Schematic figures were generated using Adobe Illustrator CS4 version 14.0.0.

2.7.2 Tracking of organelles

Tracking was carried out using the Manual Tracking Plugin for ImageJ (Fabrice Cordelieres, Institut Curie, Orsay, France). Boxplots display the results of 10 cells, figures with progressive lines display the result of one representative cell from a set of ten.

2.7.3 Plant measurements

All measurements were carried out using ImageJ (Fabrice Cordelieres, Institut Curie, Orsay, France). Data was subsequently analysed with Microsoft Excel 2007.

Cell complexity was calculated using the formula

$$complexity = \frac{perimeter^2}{4 \times \pi \times area}$$

2.7.4 Statistical analysis

Statistical analysis was carried out with OriginPro 8.5 0G SR0, Microsoft Excel 2007 or R Studio. For normally distributed data sets, significance was tested using a student-t test, in all other cases a non-parametric test (Wilcoxon or ANOVA) was chosen. qPCR results were tested using Mann-Whitney U test due to the small number of samples.

2.7.5 Analysis of qPCR data

The qPCR data was analysed manually using Excel 2007. Extreme outliers were removed manually, a standard deviation of technical replicates was accepted below 0.5 Ct.

Material and Methods

Efficiency and correlation of primers

Efficiency of primers was calculated in cDNA dilution series of 1:10, 1:20, 1:40, 1:80, 1:160 and 1:320. Higher dilutions were not possible due to the concentration of RNA/cDNA. The average Ct values (y) plotted against the log₁₀ values of the dilutions (x) were used to calculate the slope of a regression line using

$$slope = \frac{\sum(x-\bar{x})(y-\bar{y})}{\sum(x-\bar{x})^2}.$$

The slope was then used in the formula

$$E[\%] = 100 \times (10^{\left(-\frac{1}{slope}\right)} - 1)$$

to calculate the efficiency in percent. The correlation of the values was calculated using the formula

$$\rho_{x,y} = \frac{Cov(X,Y)}{\sigma_x \times \sigma_y}.$$

Primers for reference genes were accepted with an efficiency of 90-110% and a correlation between -1 and -0.99. Primers for genes of interest were accepted with an efficiency of 80-120% and a correlation between -1 and -0.99.

Stability and number of reference genes

The stability of the reference genes within a given set of different treatments was calculated using the software NormFinder (Andersen et al., 2004), BestKeeper (Pfaffl et al., 2004) and geNorm (Vandesompele et al., 2002). The geNorm software was also used to define the number of reference genes necessary for normalisation.

Normalisation of qPCR data

Normalisation against one reference gene was carried out using the $\Delta\Delta Ct$ method. Here, the average Ct of the technical replicates is calculated. These values are then used to calculate

$$\Delta Ct = Ct(\text{gene of interest}) - Ct(\text{reference gene}).$$

In the next step $\Delta\Delta Ct$ is calculated using

$$\Delta\Delta Ct = \Delta Ct(\text{treated sample}) - \Delta Ct(\text{untreated sample}),$$

which is then used to calculate the fold change of the gene of interest by using the formula

$$\text{fold change} = 2^{-\Delta\Delta Ct}.$$

Normalisation against two or more reference genes was carried out using normalisation factors, according to the geNorm manual. Quantities of the reference genes and the genes of interest were determined with the formula

$$\text{quantity} = 2^{Ct - Ct_{min}},$$

with Ct being the average Ct of the technical replicates and Ct_{min} being the lowest Ct value of a reference gene over all samples/treatments tested for one biological replicate. In the next step, the normalisation factors (NF) for all reference genes within one sample/treatment were determined by calculating the geometric mean

$$NF = GM_{\bar{x}} = \sqrt[n]{x_1, x_2, x_3 \dots x_n}.$$

The quantities for the genes of interest are then divided by the normalisation factor for the given sample/treatment, resulting in the normalised fold change. Standard deviations between biological replicates were calculated over the means of the single replicates, rather than the raw data.

3 Results

The results obtained in this work are divided into two parts: the first part is focussing on the relevance of cytoplasmic streaming for cell morphology, including myosin XI function and passive flow (I); the second part concentrates on SPIRRIG in *Arabidopsis alpina*, an actin independent factor for cell morphology (II).

I. Cytoplasmic streaming

The factors involved in cytoplasmic streaming are highly dependent on each other, which is challenging for experimental design. Moreover, the high level of redundancy of the myosins impedes the analysis of directed movement of single organelles. Hence, the direct and indirect effects of alterations in cytoplasmic streaming are highly complex and it is necessary to consider multifocal views of the situation.

3.1 Effects of myosin loss

There are several phenotypes known for myosin single and multiple mutants (see Table 1), however, it is still challenging to find the intermediate steps connecting myosin loss and the changes in morphology. In order to build a base for a systematic analysis of myosin mutants, a set of double, triple and quadruple mutants was created by selfing, crossing and selection of candidates from existing heterozygous double mutants and single mutants. The triple knockout *12k* was kindly provided by Valera Peremyslov. Please find the chosen nomenclature in Table 10.

Table 10: Specifications and short names of myosin mutants.

SALK lines (Sessions et al., 2002) and GK lines (Gabi-Kat (Kleinboelting et al., 2012)) were obtained from NASC (Nottingham Arabidopsis Stock Centre).

mutant	short name	alleles
<i>xi-1</i>	1	SALK_022140, SALK_134363
<i>xi-2</i>	2	SALK_127984
<i>xi-i</i>	i	SALK_92443
<i>xi-k</i>	k	SALK_067972, GK_164_D12
<i>xi-1 xi-2</i>	12	SALK_022140, SALK_127984
<i>xi-1 xi-i</i>	1i	SALK_134363, SALK_92443
<i>xi-1 xi-k</i>	1k	SALK_134363, GK_164_D12
<i>xi-2 xi-i</i>	2i	GK_115_C01, SALK_92443
<i>xi-2 xi-k</i>	2k	GK_115_C01, GK_164_D12
<i>xi-i xi-k</i>	ik	SALK_92443, GK_164_D12
<i>xi-1 xi-2 xi-i</i>	12i	SALK_022140, SALK_127984, SALK_92443
<i>xi-1 xi-2 xi-k</i>	12k	SALK_022140, SAIL_632_D12, SALK_067972
<i>xi-1 xi-i xi-k</i>	1ik	SALK_022140, SALK_92443, GK_164_D12
<i>xi-2 xi-i xi-k</i>	2ik	SALK_127984, SALK_92443, GK_164_D12
<i>xi-1 xi-2 xi-i xi-k</i>	12ik	SALK_022140, SALK_127984, SALK_92443, GK_164_D12

Results

All mutant lines were genotyped and selected for homozygous plants. A detailed list of the lines, their sources and used primers is provided in the appendix (Table 23 and Table 24).

3.1.1 Novel phenotypes

It is known that cell expansion is negatively influenced by myosin loss. Consequently, the overall sizes of mutant plants, as well as certain shapes within the plant, are altered. These known phenotypes were analysed under normal greenhouse conditions, however, it is not yet known how resources are distributed under non-optimal conditions, while one or several myosins are knocked out. This is especially interesting, since scientists often point out the fact that directed movement – or the contribution of some myosins to it – does not seem essential for plants. Thus, phenotypes of single and multiple myosin mutants were investigated in two different non-optimal conditions: First, plant morphology was analysed under heat conditions, comparing growth at 28°C and 21°C. Here, not only the sheer growth rate matters, but also directed cell growth which is responsible for changes in the overall shape of leaves. Second, the growth of hypocotyls in the dark was investigated as an indicator for extreme cell enlargement.

3.1.1.1 *Mutant growth under heat conditions*

The comparison between plants grown in 21°C and 28°C revealed that all single mutants and double mutants, as well as the triple mutants *12i* and *1ik* evidently showed a heat response comparable to the wild type. The rosette leaves clearly showed an altered shape and elongated petioles (data not shown). However, for the triple mutants *12k* and *2ik*, as well as for the quadruple mutant, the phenotypes were not obvious and were analysed in more detail.

Setting up the experiment

To analyse the morphology of leaves under different temperature conditions, it was essential to find the parameters which best describe what was already obvious to the eye. Hence, different measurements were taken (Figure 6) and analysed: First, the length of the whole leaf was determined (yellow). The petiole was measured at the base (dark blue) and the crossover between petiole and leaf blade was defined as the position where the width of the petiole reaches 1.8 times its initial size from the base (purple). Using this crossover position, the petiole length was measured (orange) and a minimal ellipse was applied, which covers all of the leaf (light blue) and its area and perimeter were determined. Last, the exact shape of the leaf blade (within the ellipse) was recreated using a polygon tool (pink), and here as well, area and perimeter were determined.



Figure 6: Parameters for leaf morphology.

Left - Col-0 leaf 5 grown at 21°C for 17 days. Right - Col-0 leaf 5 grown at 28°C for 17 days. Yellow - length of the whole leaf; dark blue - petiole width at the base; purple - the crossover between petiole and leaf blade, which is defined as the position where the width of the petiole reaches 1.8 times its initial size from the base; orange - petiole length; light blue - a minimal ellipse, which covers all of the leaf; pink - the exact shape of the leaf blade within the ellipse. The scale displays 0.5 cm.

These values were then used to calculate different parameters, which could putatively describe the morphology (Figure 7): The relative length of the petiole compared to the whole leaf was determined by the ratio

$$relative\ length_{petiole} = \frac{length_{petiole}}{length_{leaf}}$$

This parameter was only significantly different between both conditions in leaf 3 and 4. Hence, it does not seem to capture the morphological difference very well. The complexity of the exact leaf shapes and the minimal ellipses were calculated using the formula

$$complexity = \frac{perimeter^2}{4 \times \pi \times area}$$

In contrast to the petiole length, the relative area ratio

$$relative\ area = \frac{area_{leaf\ shape}}{area_{ellipse}}$$

and the complexity ratio

$$relative\ complexity = \frac{complexity_{leaf\ shape}}{complexity_{ellipse}}$$

both showed significant effects from cultivation in higher temperatures.

Results

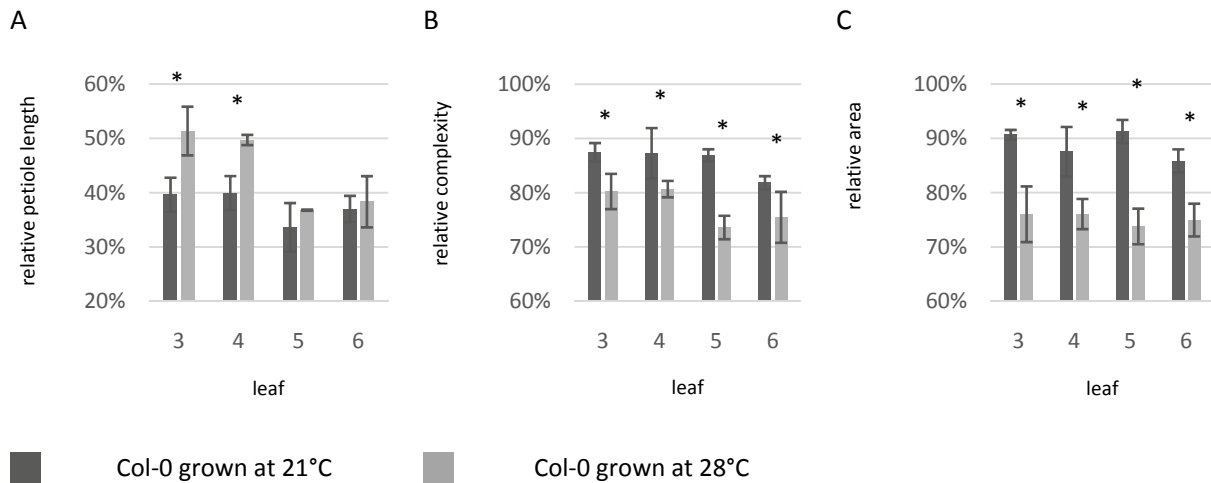


Figure 7: Calculations on leaf morphology.

16 leaves were analysed regarding relative petiole length, complexity ratio as well as area ratio. Significance was determined at levels of $p < 0.1$ (*) using a Mann-Whitney U test. Error bars depict the standard deviation.

However, later measurements with the triple and quadruple mutants were only constant and reliable when considering the relative area ratio (data not shown), so this parameter was chosen to determine if a heat phenotype occurred or not.

Heat phenotypes in myosin mutants

Heat phenotypes were analysed in leaves 5 and 6 of Col-0, the triple mutants *12k* and *2ik*, as well as the quadruple mutant *12ik* (Figure 8). In the representative pictures of the rosette morphologies, a clear tendency is visible: Col-0 shows a strong alteration in leaf morphology, which is also visible in the triple mutants to a lower extent. The quadruple mutant shows minimal to no heat reaction. These observations were also verified by the measurements, showing that *12ik* had no significant difference in morphology comparing plants grown at 28°C and 21°C. The triple mutants still showed significant alterations, however, they were strongly decreased compared to the wild type, which shows a reduction of the relative area ratio of 9% (leaf 5) to 11% (leaf 6) from 28°C to 21°C. While *2ik* still showed values altered 6-8% when grown at 28°C, the ratio of the *12k* mutant only differed 4% from plants grown at 21°C.

A



B

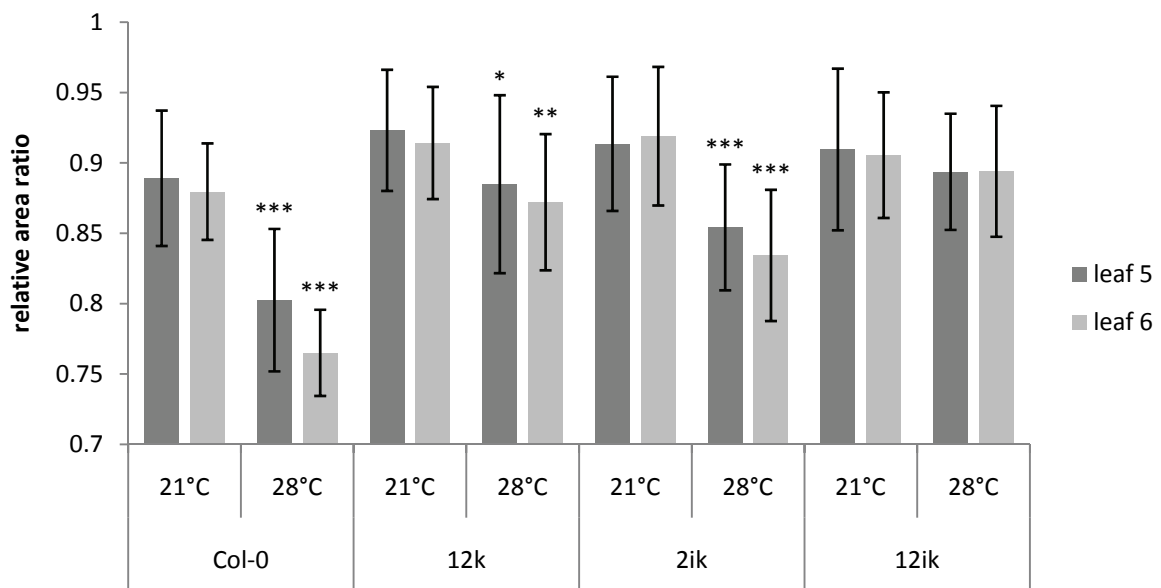


Figure 8: Morphology of Col-0 and myosin mutants at 21°C and 28°C.

A – Representative pictures of rosette growth under 21°C and 28°C. B – Relative area ratios of leaves 5 (N=19-23) and 6 (N=19-23) grown under 21°C and 28°C in three independent sets. Significance was determined at levels of $p < 0.001$ (***), $p < 0.01$ (**) and $p < 0.05$ (*) with an ANOVA test. Error bars depict the standard deviation.

Results

3.1.1.2 Mutant growth in the dark

In *Arabidopsis*, skotomorphogenesis leads to a strong phenotype, including the formation of an apical hook instead of open cotyledons and an elongated hypocotyl. In nature, these traits are necessary to ensure that the meristem is covered while the plant is empowered to grow out of the soil fast. The fast growth of the hypocotyl is mediated by elongation of the cells, rather than increased cell numbers. Hence, myosins might play a crucial role in this process. The lines which were found to be less adaptive to heat (*12k*, *2ik* and *12ik*) as well as two additional lines, which were likely to show only slightly weaker phenotypes (*2k*, *1ik*), were tested for this rapid growth process (Figure 9). It was found that *2ik* mutants as well as the quadruple mutant *12ik* have significantly shorter hypocotyls than Col-0 when grown in the dark for seven days. The *12k* line showed a tendency towards shorter hypocotyls as well, however, this change was not significant. The double mutant *2k* as well as the triple mutant *1ik* were indistinguishable from wild type.

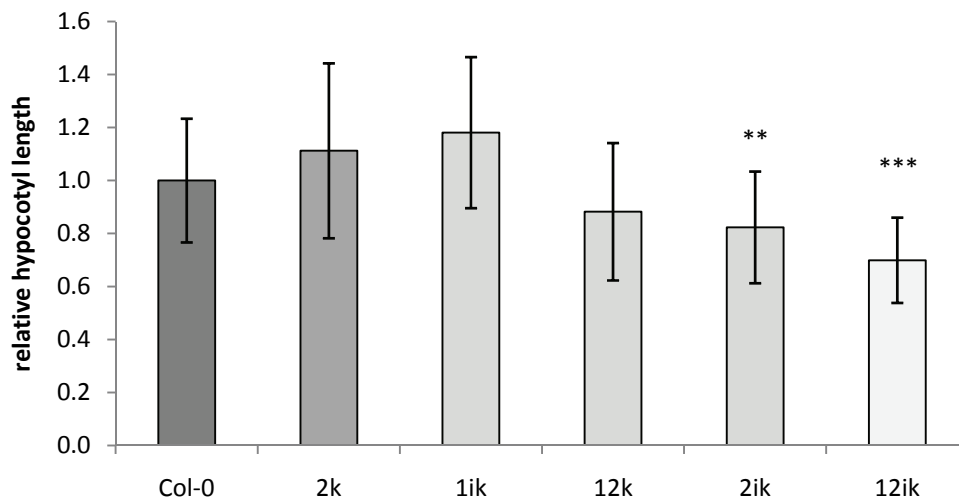


Figure 9: Hypocotyl length in dark grown seedlings.

Three independent sets of dark grown Col-0 (n=25), *2k* (n=11), *12k* (n=51), *1ik* (n=13), *2ik* (n=49) and *12ik* (n=42) hypocotyls were measured and normalized against Col-0. Significance was determined with ANOVA at levels of $p < 0.001$ (***), $p < 0.01$ (**) and $p < 0.05$ (*). Error bars depict the standard deviation.

3.1.2 Myosin loss and P-body movement

To date, myosin mediated P-body movement has not been analysed in detail. It was found that XI-K is the major player for long range transport in P-bodies. The transport of these ribonucleoprotein complexes is unique, since the myosins are directly anchored to a core component, rather than adaptor proteins (Steffens et al., 2014b). However, it is not clear to which extent the other three myosins are contributing to the movement.

Results

An extensive analysis of P-body movement in midvein cells of transiently transformed leaves of myosin mutants was carried out, to shed further light on the contribution of the four myosins and the role of XI-K in particular.

Table 11: P-body speed in myosin mutants.

Movement of P-bodies was analysed in transiently transformed Arabidopsis rosette leaf cells along the central vein. A particular plane was scanned 50 times at intervals of 1.6 sec with a confocal laser scanning microscope. P-body tracking was carried out using the Manual Tracking Plugin for ImageJ (Fabrice Cordelieres, Institut Curie, Orsay, France). *Mutants highlighted in gray were analysed by A. Steffens. The corresponding data might not be statistically relevant due to a lower amount of analysed cells (<10) and is therefore not discussed in detail.

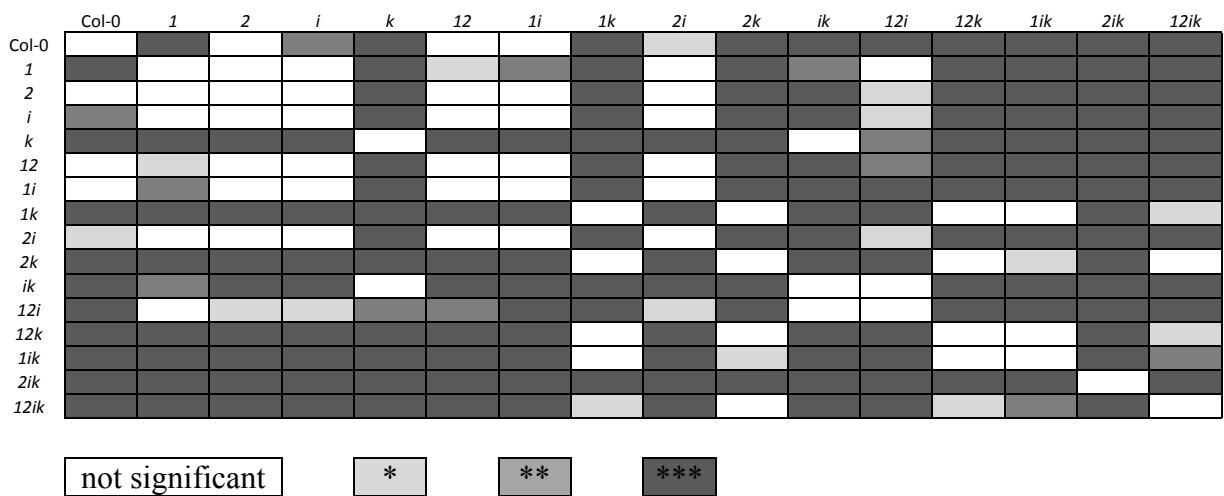
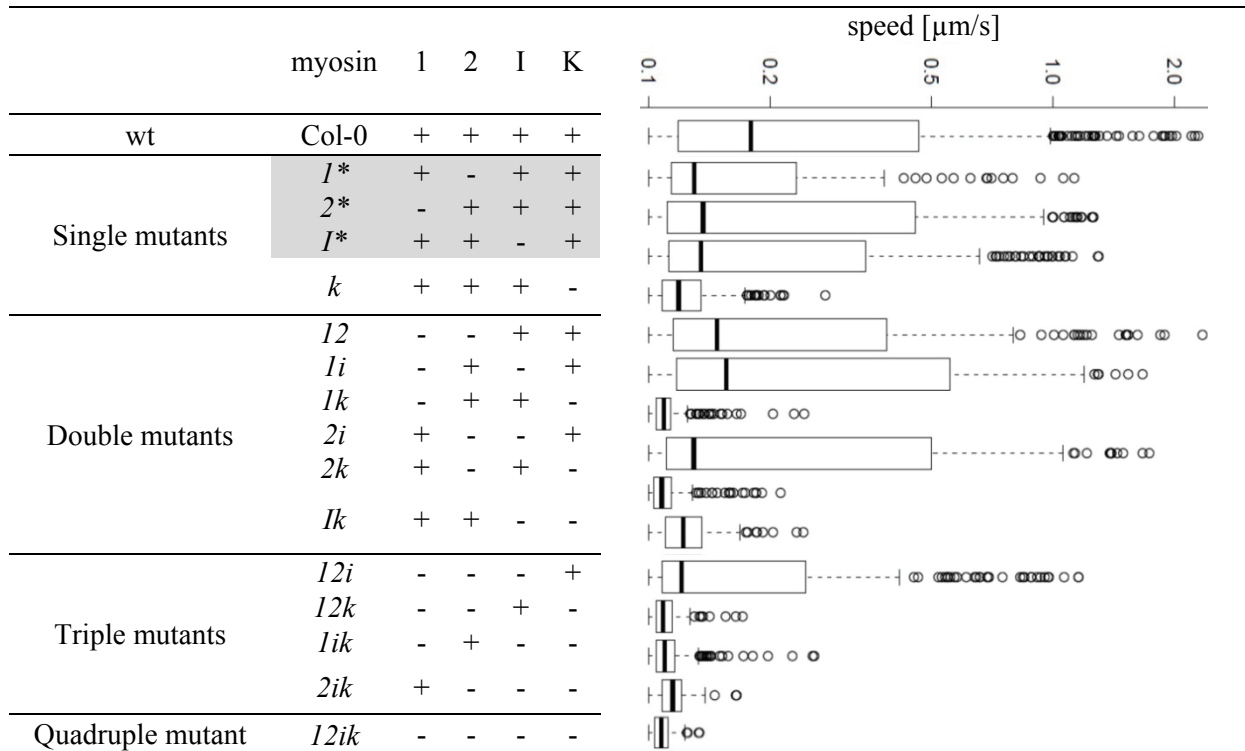


Figure 10: Significance of P-body speed in different myosin mutants.

Significance was determined by a two-sample Wilcoxon test, $p > 0.001$ (***), $p > 0.01$ (**), $p > 0.05$ (*).

Results

Table 11 and Figure 10 show that *xi-k* mutants have the strongest reduction in P-body movement, while *xi-2* shows no significant difference to the wild type (it is quite likely that *xi-1* and *xi-i* are not significantly different as well, considering that their double mutants *l2* and *li* show no difference to Col-0*). Myosin XI-I seems to have less redundant functions with XI-K than the other two myosins, since the corresponding double mutant does not show a significant difference to the *xi-k* single mutant, hence no synergistic effect. In contrast, the additional loss of *xi-1* or *xi-2* leads to a significant decrease in P-body speed. Furthermore, it is likely that XI-I shares more redundant functions with XI-1 and XI-K than XI-2, since 1IK shows a significantly stronger decrease in speed than 2IK. XI-2 proves to be the outsider in both, redundancy and importance, while XI-K seems to be most essential for P-body transport.

To analyse the data with regard to the different types of movement, four classes of P-body movement were defined (Arijit Das, AG Tresch). For this purpose, Col-0 P-bodies were divided into mobile and immobile groups by a one-sided t-test. The mobile group was further divided into three groups - slow, medium and fast moving - by k-means clustering and subsequent multivariate T^2 test based on distance, area, angle, displacement and speed of the movement. This new technique and the inclusion of all five parameters for clustering are extensions of the method described in Steffens et al., 2014, allowing for more accurate classification.

Figure 11 shows that the ratios of the four classes are similar in Col-0, *xi-1*, *xi-2* and *xi-i*. In contrast, *xi-k* is lacking all fast moving P-bodies and most medium moving ones. This shift is similar in all mutants lacking XI-K and gets more prominent the more myosins are knocked out. However, even with three myosins missing in the *l2i* triple mutant, long range transport is still functioning. In contrast to the former results (compare Table 11), the movement classes indicate no diverse characteristics of myosins 1, 2 and I regarding the quality of transport.

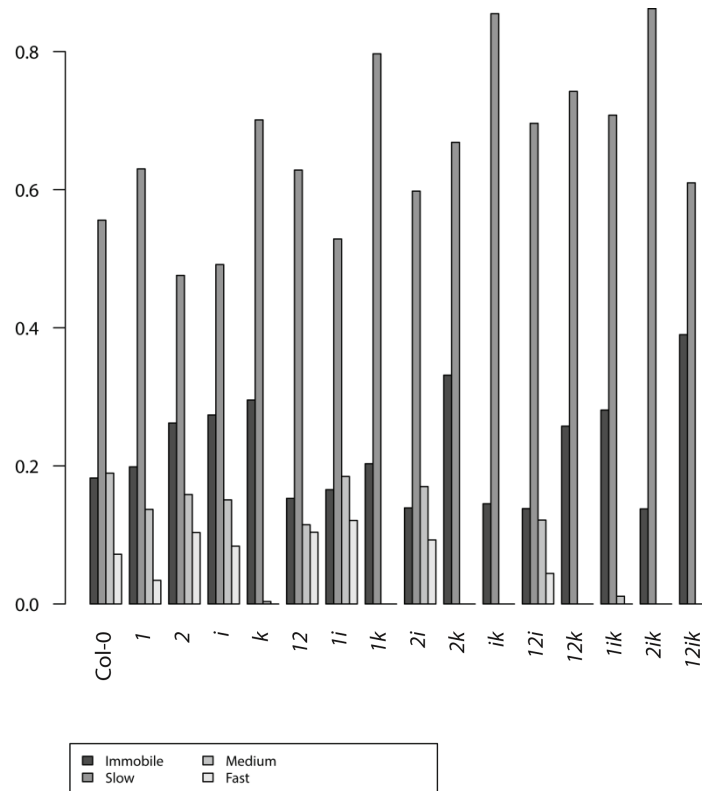


Figure 11: Movement classes of P-bodies in myosin mutants.

Four classes of P-body movement were defined (Arijit Das, AG Tresch). For this purpose, Col-0 P-bodies were divided into mobile and immobile groups by a one-sided t-test. The mobile group was further divided into three groups - slow, medium and fast moving - by k-means clustering and subsequent multivariate T^2 test based on distance, area, angle, displacement and speed of the movement.

3.2 Overexpression of truncated myosins – a dominant negative effect

It was shown that transiently expressed truncated myosin class XI tails, lacking the motor domain, have a dominant negative effect on organelle movement. This often occurs for proteins that function as dimers (Avisar et al., 2012). For respective constructs of XI-1, XI-2, XI-I and XI-K, it was found that they strongly decrease organelle motility. To date, no study found the underlying cause for this effect, however, various hypotheses are frequently discussed (Vick and Nebenführ, 2012). During my master's project, this effect was analysed by transient co-expression of myosin fragments and DCP1 in Arabidopsis leaves. The domains displayed in figure 12 were exactly recreated in the used myosin plasmids, following the two possible hypotheses that the dominant negative effect is either caused by inhibition of myosins through dimerisation with non-functional coiled-coils/tails, or by the GTD, e.g. through blocking of cargo binding sites.

Results

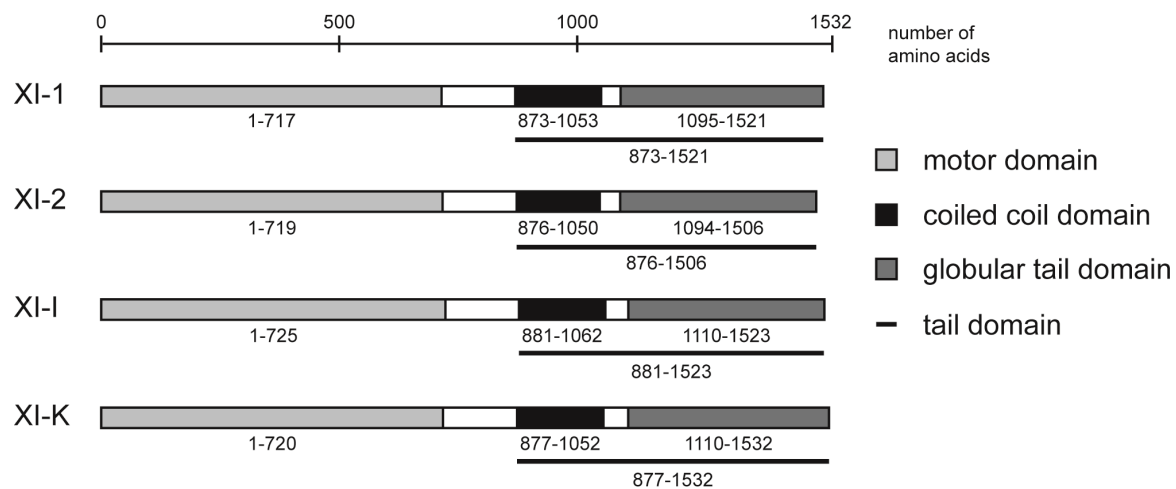


Figure 12: Myosin domains and structure.

Sequences were obtained from TAIR.de (Berardini et al., 2015a; Lamesch et al., 2012), the domains were determined with the NCBI CD-search (Marchler-Bauer et al., 2011, 2017). A detailed list of primers is attached to the appendix (Table 21).

All tested fragments (tail, coiled coil and GTD, under the control of the 35S promoter and N-terminally fused to YFP) showed a localisation to actin bundles as well as a localisation in dots, which partially overlapped with the DCP1-CFP signal, marking P-bodies (unpublished, data not shown).

The motility of P-bodies was determined, showing that the GTD domains cause a stronger reduction of movement than the coiled-coil domains. For all coiled-coil domains, a slight shift of medium and fast moving P-bodies to slow and immobile P-bodies was observed. This effect was much stronger for the GTD domains, resulting in a total loss of medium and fast moving P-bodies for XI-1-GTD, XI-I-GTD and XI-K-GTD. However, in XI-2-GTD expressing cells, the long range movement was still possible.

These findings suggest that, surprisingly, the dominant negative effect is mostly caused by the GTD domains. In contrast, the coiled coil fragments only have a minor effect.

As this effect is weakest for the XI-2 GTD, it is likely to have a minor role in P-body binding, hence, a different functional range than the other myosins. This might also be reflected by the phylogenetic relationship of the myosin class XI members (Figure 13), which indicates it to be the most distant to the other three myosins.

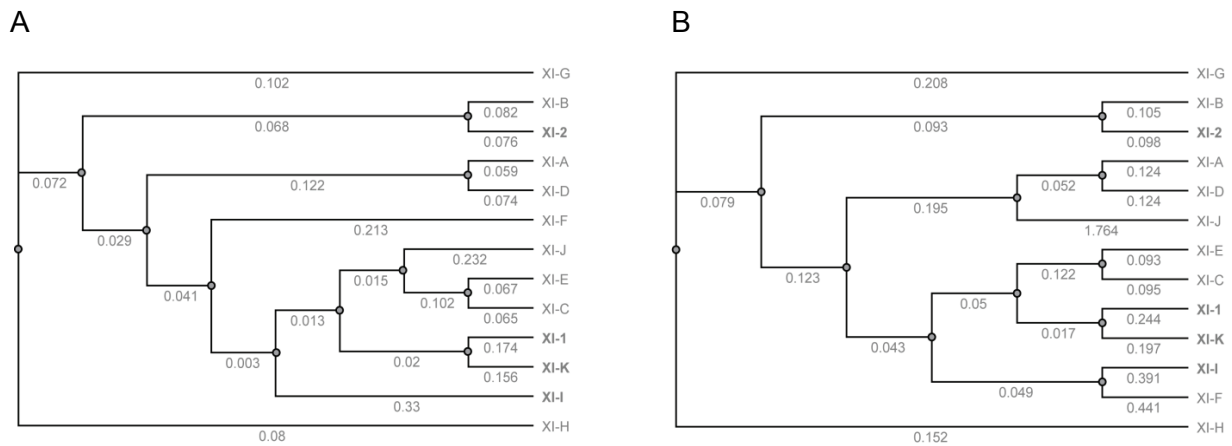


Figure 13: Phylogenetic tree of class XI myosins.

Tree of A) Motor domain and B) GTD domain created by PHYLIP Neighbour Joining method based on a CLUSTALO alignment of CDS sequences. Sequences were obtained from TAIR.de (Berardini et al., 2015a; Lamesch et al., 2012), the domains were determined with the NCBI CD-search (Marchler-Bauer et al., 2011, 2017).

The behaviour of the different constructs was rather unexpected and raised new questions:

(1) The fragments which were used to analyse the dominant negative effect showed differential behaviour. Is it possible to link these different characteristics to distinct phenotypes? (2) It was shown that myosin V members can change their conformation and thereby regulate their activity. To do so, the myosin bends down and creates a physical interaction between its GTD and motor domain (Hammer and Sellers, 2011). Does this also occur in plants and how is the activity of a myosin changed when GTDs are artificially added to the system? (3) The effect of the coiled coil fragments is minor, however, it is similarly strong for myosins 1, I and K. So how would a non-functional myosin dimer effect movement, if not even the loss of said myosin has an effect (in case of myosins 1 and I)?

(1) Phenotypic effects of myosin fragments

In order to link the different characteristics of the myosin fragments to distinct phenotypes stable lines were created expressing the GTDs and coiled-coils of the four myosins. For this purpose, the fragments of interest, under the control of the 35S promoter and N-terminally fused to YFP, were introduced into Col-0 plants via transformation with *Agrobacterium tumefaciens*.

In the T1 lines, fluorescence was visible. In addition to their expected localisation to actin, all fragments showed a strong localisation to the cytoplasm. These initial T1 lines were selfed and the resulting T2 lines were analysed by Hanna Bechtel during her Bachelor thesis under

Results

my supervision. She could detect what seemed to be a weak quadruple mutant phenotype for a multitude of lines. However, the observed phenotypes were finally found to rather be caused by co-silencing of the endogenous myosins than expression of the introduced fragments (data not shown).

After several analyses of 10 to 50 lines (which showed initial fluorescence in the T1 line) for each fragment (coiled coil and GTD of all four myosins, respectively), no stable line could be established. Thus, the phenotypic analyses had to be carried out with the T1 lines, where silencing did not occur yet.

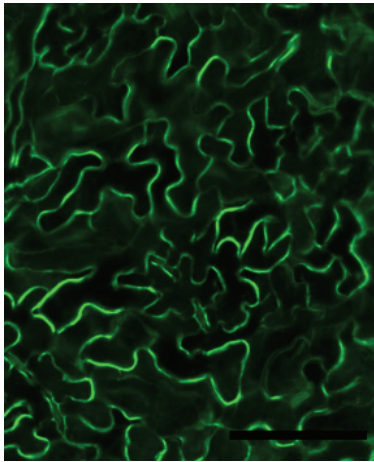
Coiled coil lines

On the basis of myosin mutant phenotypes and the results from transient experiments, the coiled coil lines were initially checked for their trichome phenotypes, organelle movement and expression of the myosin fragment. Despite their strong fluorescence, no obvious phenotype was detectable for any coiled coil line. In the transient experiments, the 35S::YFP:XI-1-coiled coil fragment was found to have the most severe effect on P-body movement of all myosin coiled coils. Hence, the lines expressing this fragment were chosen for a more detailed analysis of their trichome morphology and organelle movement.

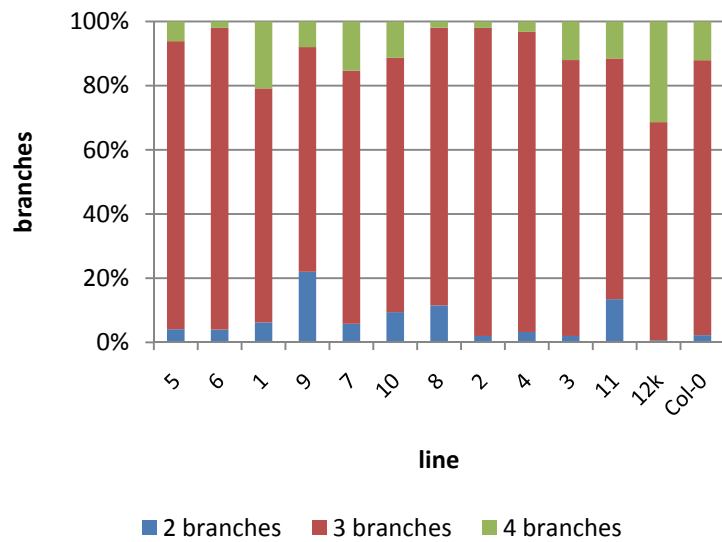
Figure 14 displays results gained from the analyses of 11 plants expressing 35S::YFP:XI-1-coiled coil. In these lines, the trichomes did not show a distorted phenotype. In addition, the data clearly show that no correlation exists between expression level (fluorescence intensity) and morphology of trichomes.

Results

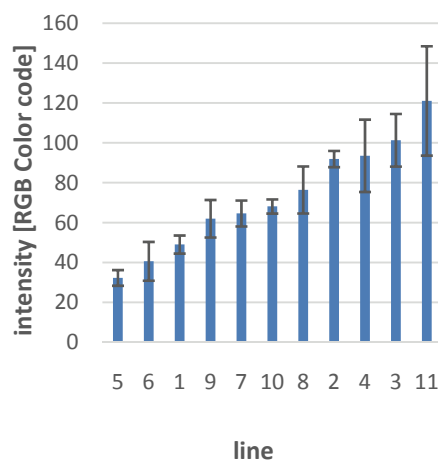
A



C



B



D

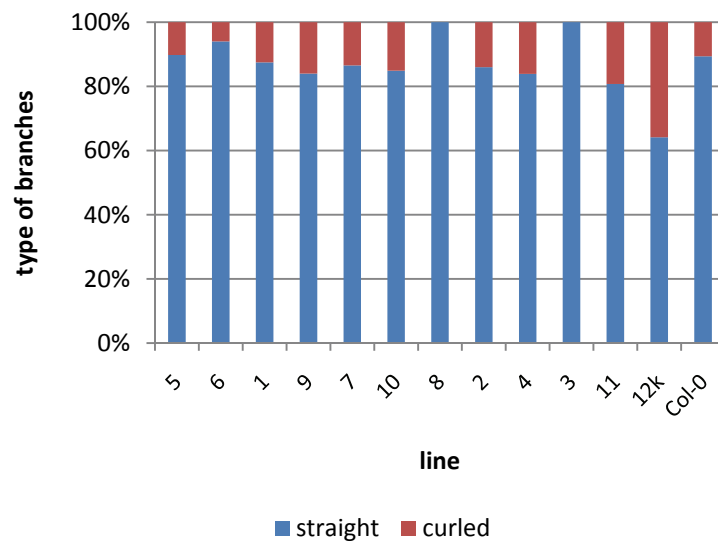


Figure 14: Analysis of Col-0 T1 plants expressing YFP:XI-1-coiled coil.

A - Fluorescence microscope image of Col-0 epidermal pavement cells expressing YFP:XI-1-coiled coil (line 7). Scale displays 100 μ m. B - Fluorescence intensity sorted by strength. C and D - Morphology of trichomes. Error bars depict standard deviations.

In addition, no alteration in the movement of P-bodies was visible (data not shown), thus it was not possible to gain any additional information on myosin function from these stable lines.

GTD lines

In accordance with the CC lines, the GTD lines were analysed for their expression, trichome morphology and organelle movement. The GTD lines of XI-2 and XI-K were chosen for a

Results

more detailed analysis, since XI-K is the major player in P-body movement and XI-2 is thought to be an important myosin for peroxisome transport (Peremyslov et al., 2008) or at least involved in the process (Prokhnevsky et al., 2008). In addition, these lines were of special interest, since they showed the strongest and weakest effect on P-body movement in the transient experiments, respectively.

The trichomes of all lines were analysed in more detail. For the lines expressing 35S::YFP:XI-2-GTD, no difference in trichome shape to Col-0 could be observed (Figure 15A, B). While the majority of trichomes in lines expressing 35S::YFP:XI-K-GTD was not obviously altered, all lines showed randomly occurring distorted trichomes (Figure 15C-G).

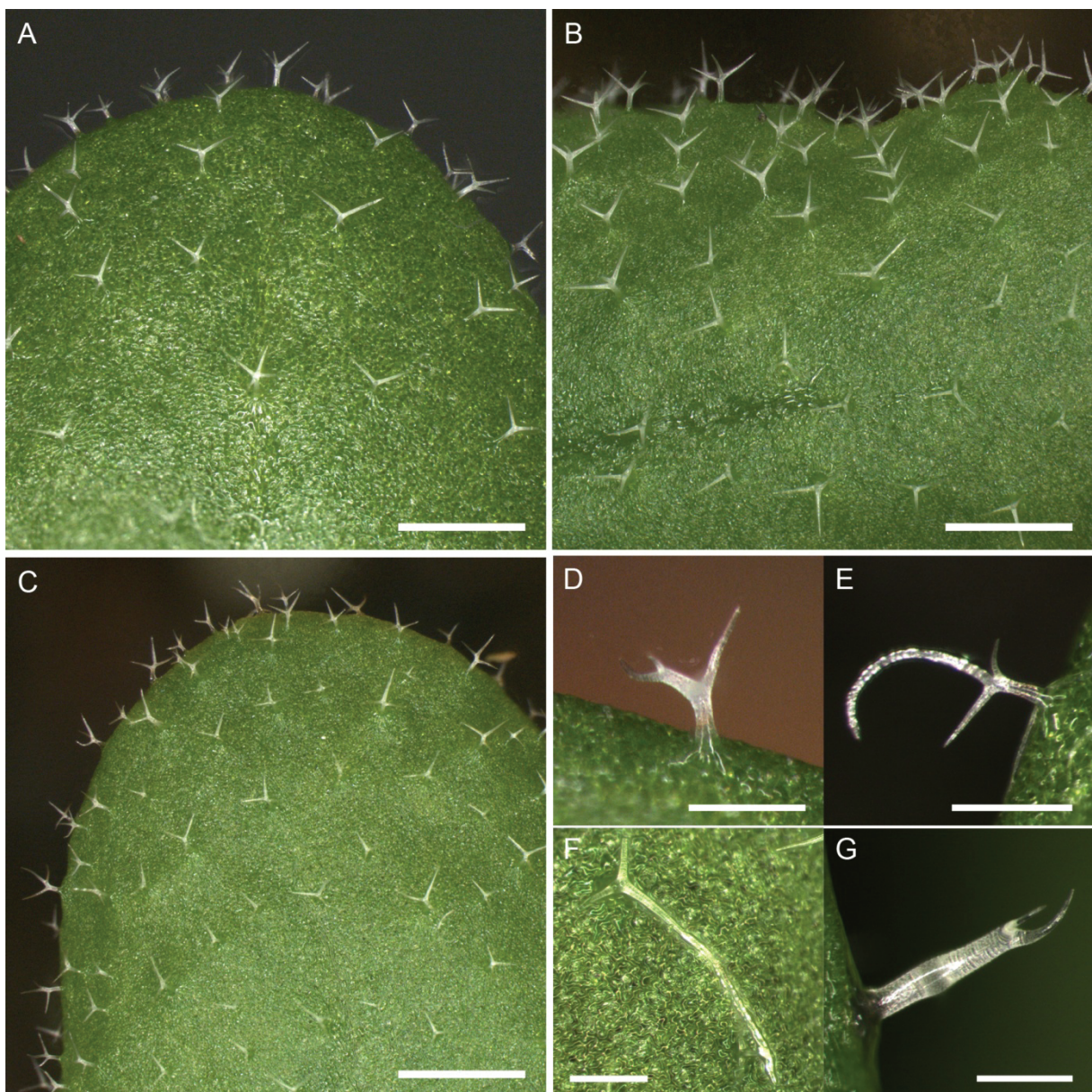


Figure 15: Trichome phenotypes in Col-0 and GTD overexpression lines. Overview of trichomes in A – Col-0, B – 35S::YFP:XI-2-GTD line 5, C – 35S::YFP:XI-K-GTD line 5. Scale displays 15 mm. D-G - Distorted trichomes in 35S::YFP:XI-K-GTD lines. Scale displays 250 μ m.

Results

Subsequently, these GTD lines were checked for movement of P-bodies and peroxisomes. XI-2 is supposed to be strongly involved in peroxisome movement, and XI-K was already found to be the major player in P-body transport. Hence, it was assumed that peroxisome speed would be reduced in the Col-0_{35S::YFP:XI-2-GTD} line, while P-bodies movement would be impaired in the Col-0_{35S::YFP:XI-K-GTD} line. However, this assumption proved to be wrong: the Col-0_{35S::YFP:XI-2-GTD} line showed no obvious alteration of organelle movement, while the Col-0_{35S::YFP:XI-K-GTD} line had decreased movement of both, P-bodies (Figure 16) and peroxisomes (Figure 17).

This result seemed to be rather contradictory to former studies, claiming that peroxisome movement is strongly decreased in *xi-2*. Consequently, the movement was tracked in this mutant (Figure 18). It was found, that the *xi-2* mutant has no obvious movement defect of peroxisomes. Since Peremyslov et al. used a different mutant allele in their studies, the exact reason for such contradicting results needs to be determined in the future. However, considering all data obtained for XI-2 so far, it is more likely that this protein is indeed not necessary for fast movement of peroxisomes.

Furthermore, the Col-0_{35S::YFP:XI-K-GTD} lines were analysed regarding their actin organisation (Figure 19). It was found that the actin cytoskeleton did not show any obvious defects.

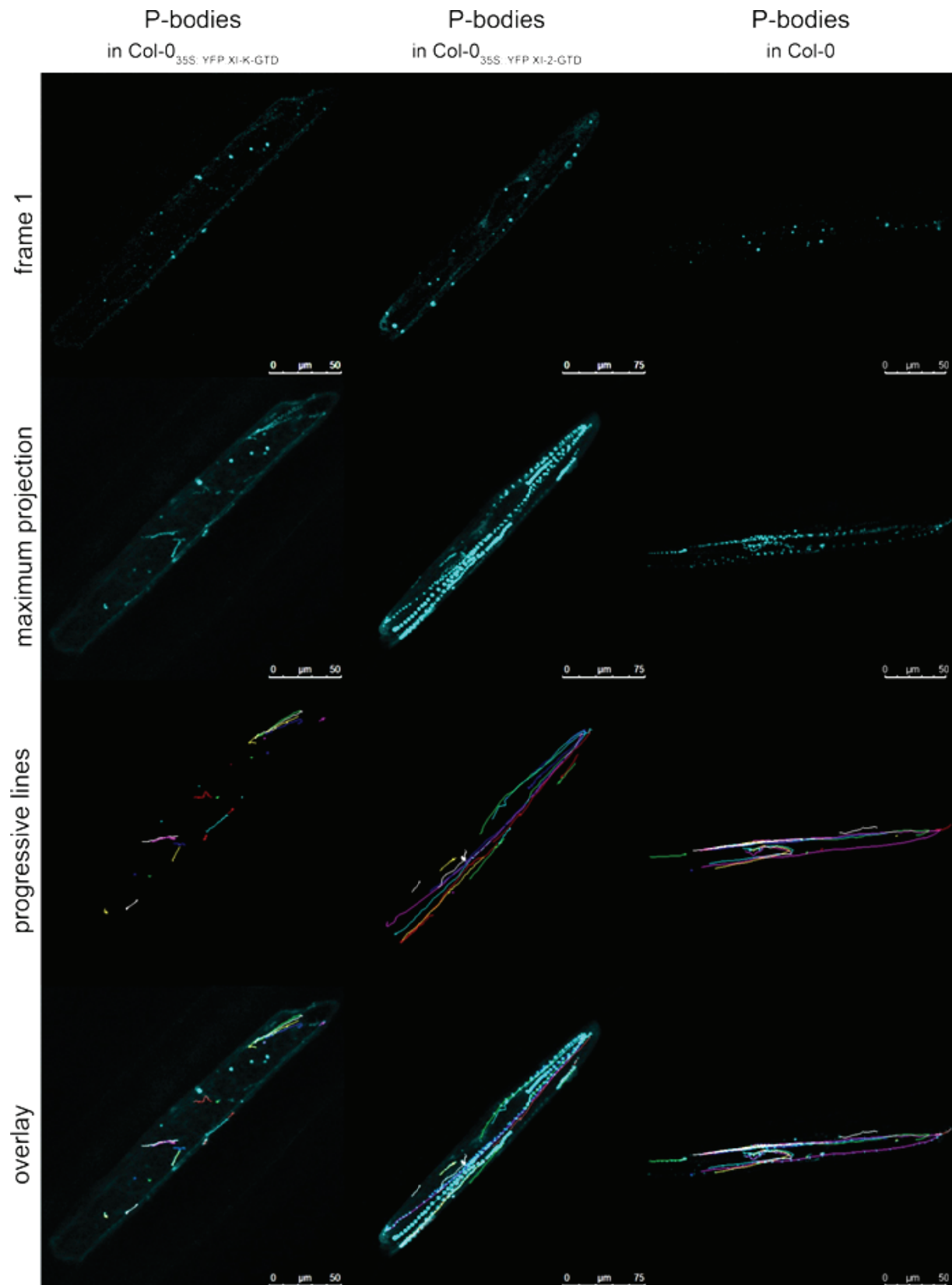


Figure 16: P-body movement in Col-0 and transgenic lines.

Col-0 as well as the Col-0^{35S::YFP:XI-2-GTD} line and Col-0^{35S::YFP:XI-K-GTD} line were transiently transformed by bombardment with 35S::DCP1::CFP. P-body movement was tracked manually over 50 frames (63.21 sec). Frame 1 displays the initial position of the P-bodies, in the maximum projection all frames of the video are stacked. Progressive lines indicate the trajectories of the P-bodies.

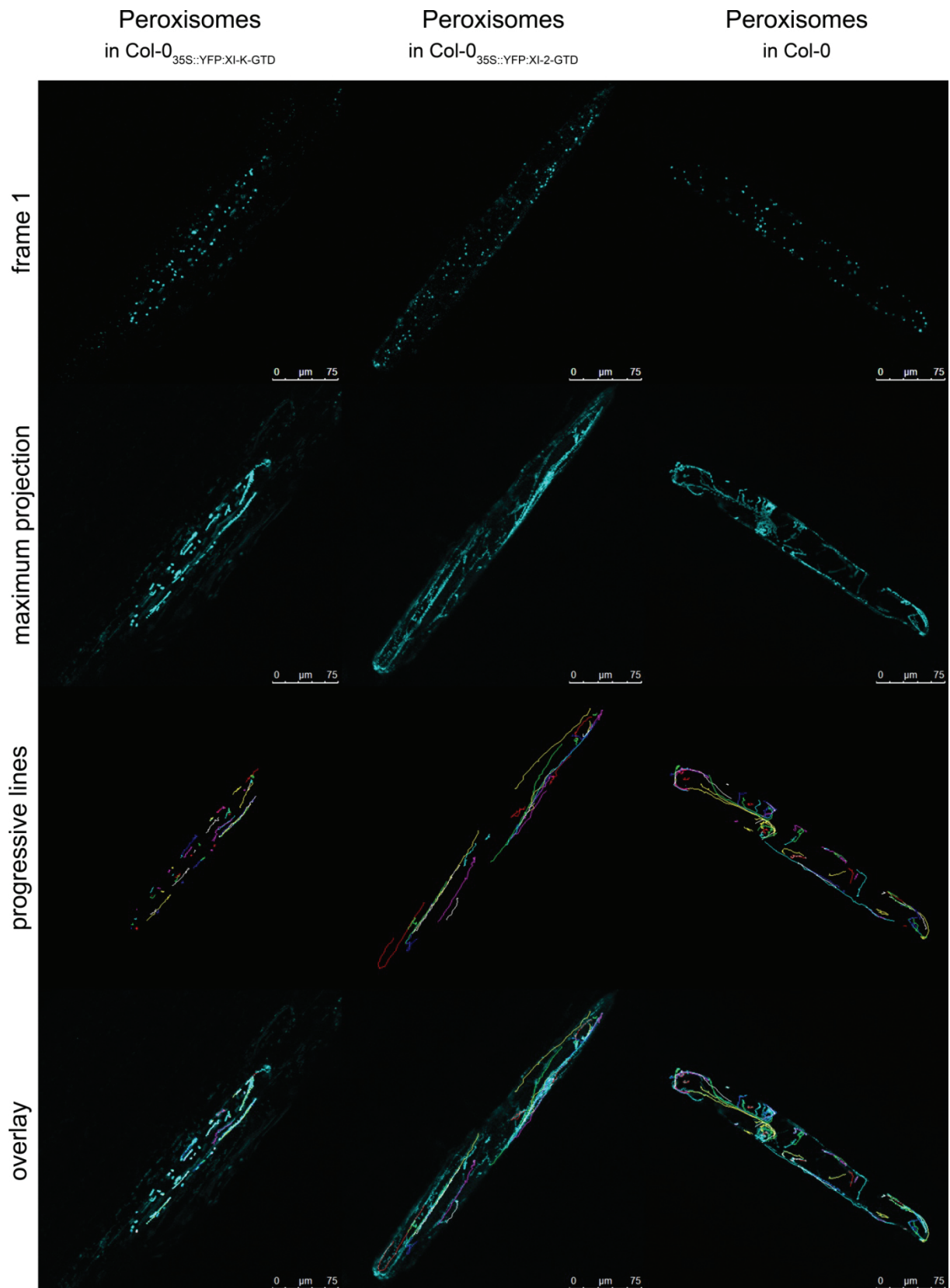


Figure 17: Peroxisome movement in Col-0 and transgenic lines.

Col-0 as well as the Col-0_{35S::YFP:XI-2-GTD} line and Col-0_{35S::YFP:XI-K-GTD} line were transiently transformed by bombardment with 35S::CFP:SKL. Peroxisome movement was tracked manually over 50 frames (63.21 sec). Frame 1 displays the initial position of the peroxisomes, in the maximum projection all frames of the video are stacked. Progressive lines indicate the trajectories of the peroxisomes.

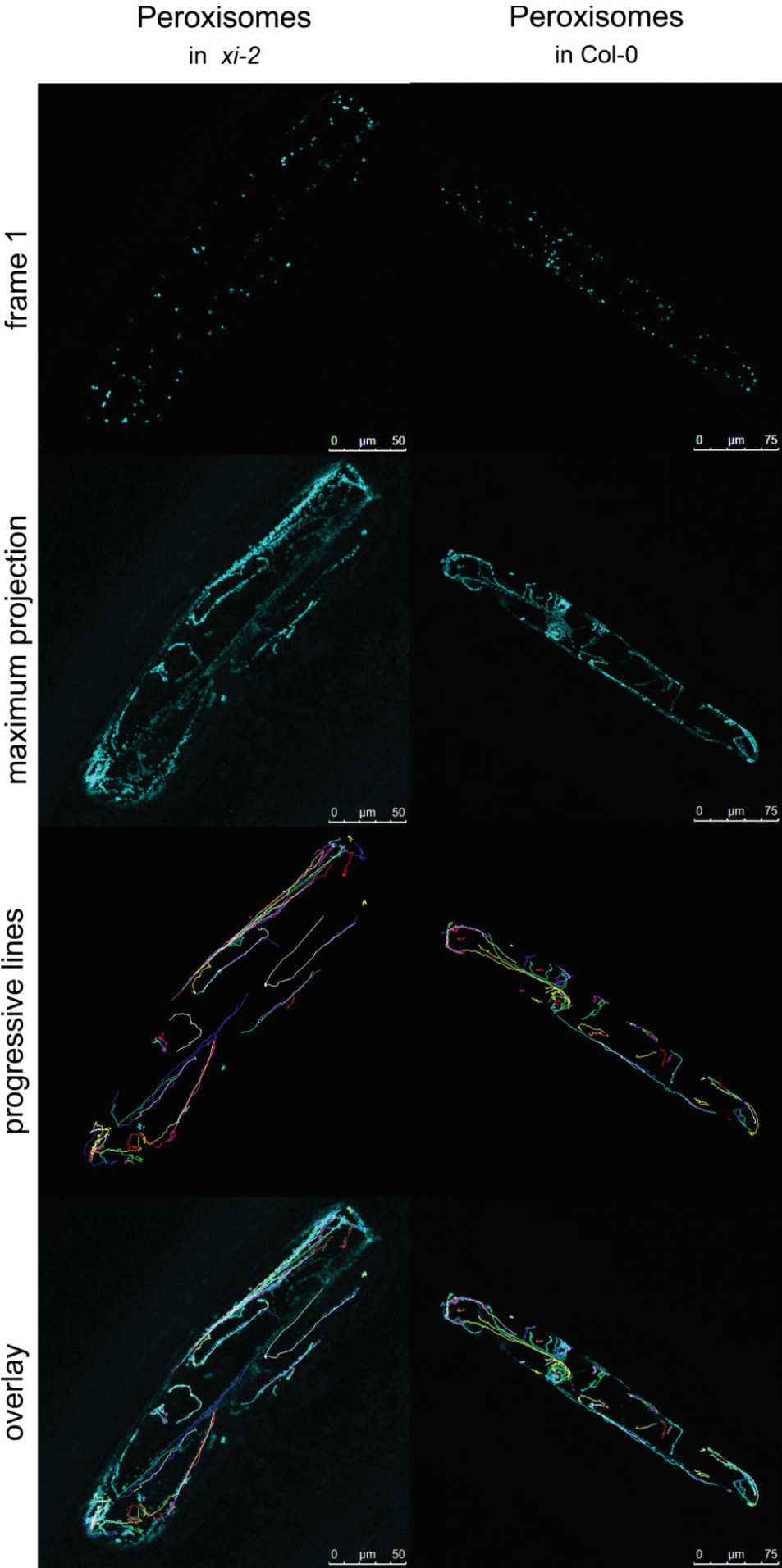


Figure 18: Peroxisome movement in Col-0 and xi-2. Col-0 as well as the myosin mutant xi-2 were transiently transformed by bombardment with 35S::CFP:SKL. Peroxisome movement was tracked manually over 50 frames (63.21 sec). Frame 1 displays the initial position of the peroxisomes, in the maximum projection all frames of the video are stacked. Progressive lines indicate the trajectories of the peroxisomes.

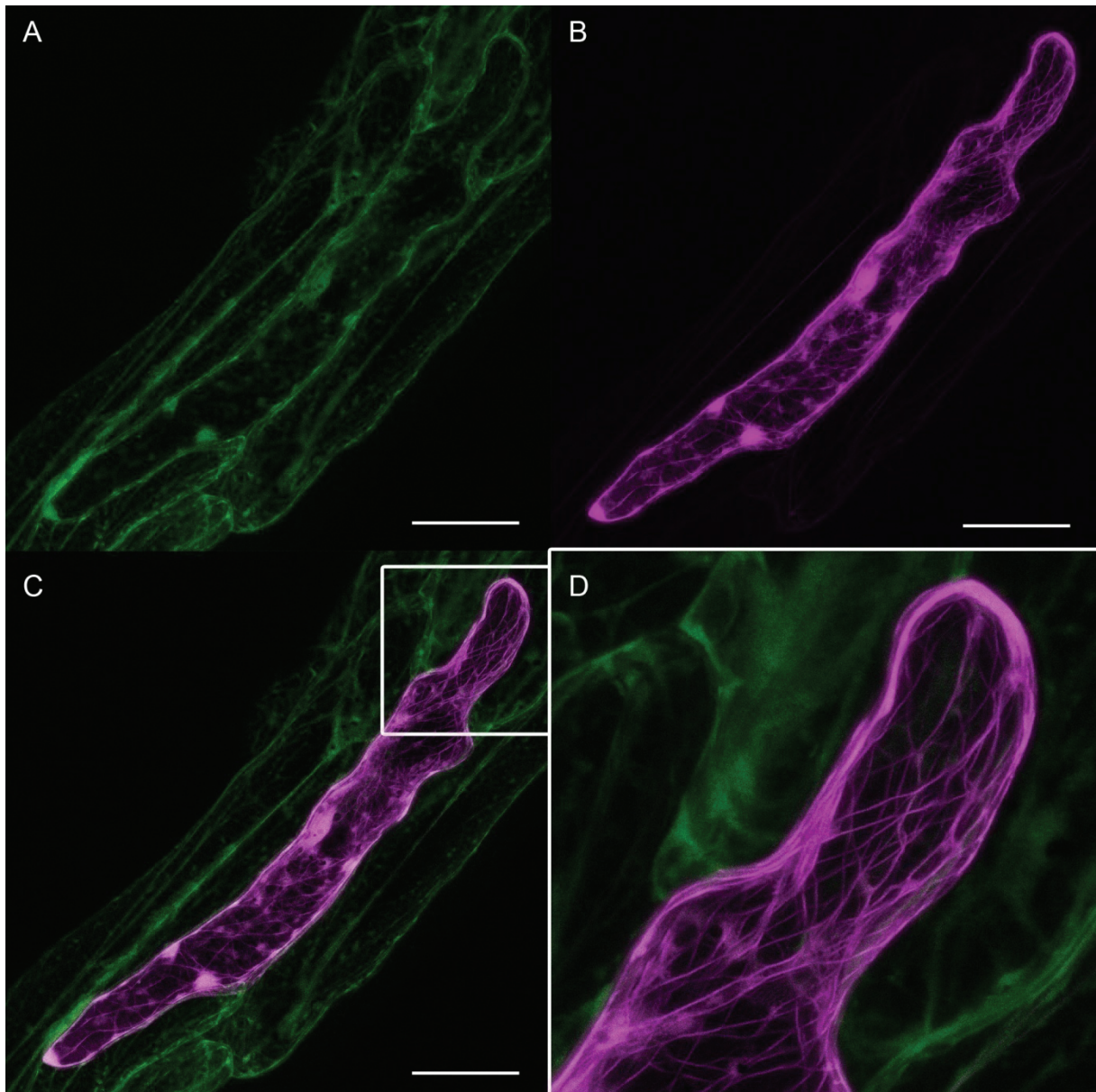


Figure 19: The actin cytoskeleton in Col-0_{35S::YFP:XI-K-GTD} transgenic lines.

The actin cytoskeleton was visualized by expressing 35S::LifeAct:CFP in Col-0_{35S::YFP:XI-K-GTD} epidermal midvein cells via particle bombardment. A – 35S::YFP:XI-K-GTD, B – 35S::LifeAct:CFP, C – Overlay, D – Actin filaments in higher magnification. The scale displays 50 μm .

(2) The effect of free GTDs on the plant cell

The GTDs of all four myosins cause a severe dominant negative effect on organelle movement. Although this is likely to be caused by blocking of cargo binding sites, it is necessary to investigate a possible regulatory effect of the GTDs.

For myosin Va, it was found that in the absence of both, a cargo molecule and calcium, a conformational change occurs which leads to a direct interaction of the GTD with the motor domain. In this form, the myosin is enzymatically and mechanically inactive. This bent conformation is changed by calcium, which causes the myosin to fold back in its upright,

Results

enzymatically active position. However, the mechanical and enzymatical activity, and thus the ability to move along actin, is only restored upon cargo binding (Figure 14, Hammer and Sellers, 2011). To date, it is not known if a similar regulation is present in the myosin XI class.

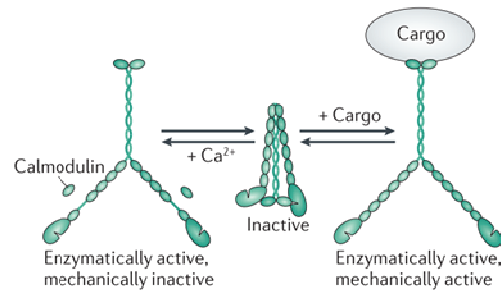


Figure 20: Myosin Va activity regulation (Hammer and Sellers, 2011).

To investigate this possible regulatory effect, constructs exclusively containing the motor domain were created and yeast 2-hybrid assays were carried out. The aim was to find out if the motor domains of the four XI myosins are capable of physically binding GTD domains, which would be a necessary requirement for the myosins to achieve an inactive conformation. It was found that none of the motor constructs showed an interaction with either of the GTD constructs (data not shown). NOT1, N-terminally fused to the GAL4-AD, was used as a positive control, which showed clear interactions with all GTD constructs. Thus, activation and deactivation of XI myosins by conformational change seems to be unlikely.

A molecular tool, newly developed in our group (Jakoby, unpublished) was used to further verify the hypothesis that the dominant negative effect of the GTDs is mediated by blockage of cargo binding sites. Figure 21A displays one possible mode of organelle binding in wild type. Here, the GTD domain binds an adaptor protein, which in turn binds a membrane or transmembrane protein of an organelle. Under the presence of free GTDs, the membrane proteins needed for binding, are thought to be blocked by adaptor proteins attached to free GTDs, hence, no movement is possible (Figure 21C). However, it is possible to bridge this blocking, using a conditional rescue line: First, the GTD domain of a genomic myosin XI-K construct under the endogenous promoter (pMDC32-XI-K:YFP, kindly provided by Valera Peremyslov) was replaced by a gateway cassette (XI-KΔGTD:YFP), and a tandem sequence of two YFPs was introduced (XI-KΔGTD-2xYFP). This construct was used to create stable lines in the *12k* background (*12k*_{XI-KΔGTD-2xYFP}). In the presence of a nanobody construct - LaG-16 (Fridy et al., 2014) fused with RHA1 (RAB HOMOLOG 1), pUBI::LaG-16-RHA1 - which is able to connect YFP and Golgi bodies, cargo binding of specific organelles can be restored (Figure 21B; Jakoby, unpublished). Following the hypothesis that the dominant negative effect of free GTDs is caused by blocking of cargo binding sites, free GTDs should not have an effect in this background, since its blockage is bridged through the nanobody construct (Figure 21D).

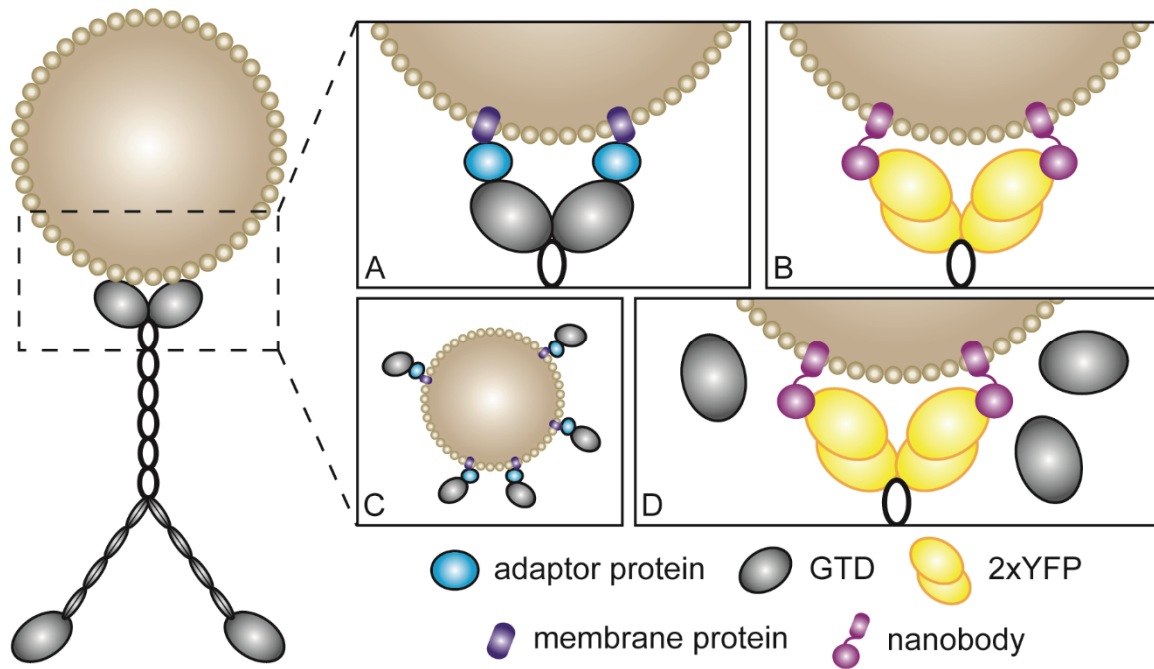


Figure 21: Schematic representation of organelle binding by myosins and myosin fragments.

A – Organelle binding in wild type, the GTD domain binds an adaptor protein which again binds a membrane protein of the organelle. B – Organelle binding in the $12k_{XI-K\Delta GTD-2xYFP}$ mutant in presence of a nanobody construct, the nanobody binds YFP on its one end, and is integrated into the membrane of the organelle on the other end. C – Organelle binding in wild type under the presence of free GTDs, the membrane proteins needed for binding are blocked by adaptor proteins attached to free GTDs. D - Organelle binding in the $12k_{XI-K\Delta GTD-2xYFP}$ mutant in presence of a nanobody construct and free GTDs, the nanobody binds YFP on its one end, and is integrated into the membrane of the organelle on the other end. The GTD does not have an effect since its blockage is bridged through the nanobody construct.

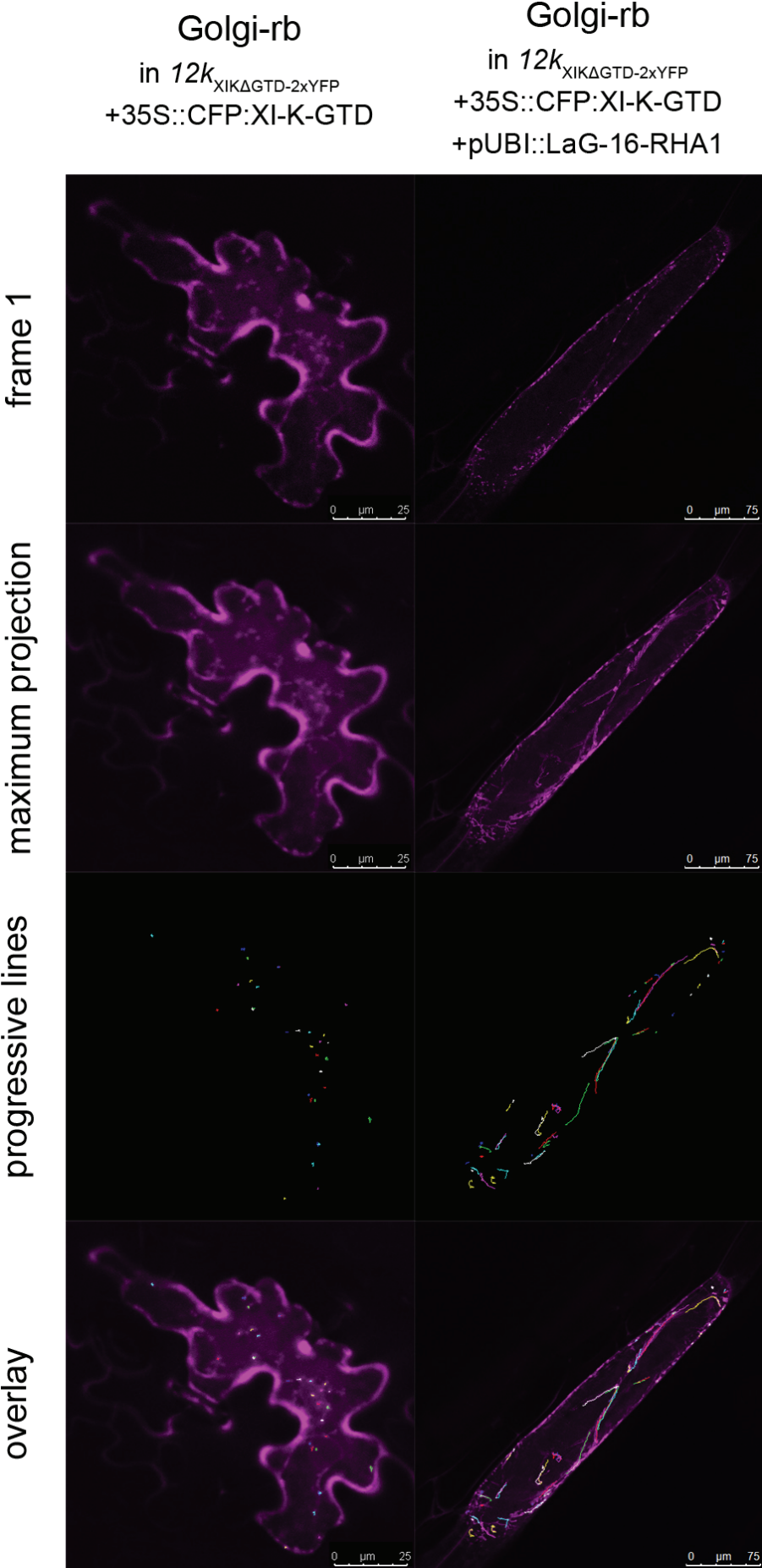


Figure 22: Bridging of cargo blocking by GTDs. The $12k_{XIK\Delta GTD-2xYFP}$ transgenic line was transiently transformed by bombardment with (first column) 35S::CFP:XI-K-GTD and the Golgi-rb marker, or (second column) 35S::CFP:XI-K-GTD, the nanobody construct pUBI::LaG-16-RHA1 and the Golgi-rb marker. Golgi movement was tracked manually over 50 frames (54.39 sec). Frame 1 displays the initial position of the Golgi bodies, in the maximum projection all frames of the video are stacked. Progressive lines indicate the trajectories of the Golgi bodies.

Results

Figure 22 displays the results of Golgi movement analyses in the $12k_{XI-K\Delta GTD-2xYFP}$ transgenic line in the presence of 35S::CFP:XI-K-GTD with or without the nanobody construct pUBI::LaG-16-RHA1. Frame 1 displays the initial position of the Golgi bodies, in the maximum projection all frames of the video are stacked. Progressive lines indicate the trajectories of the Golgi bodies analysed by manual tracking. The results displayed are representative for sets of 10 cells per setup. In the absence of the nanobody construct, the Golgi movement was almost fully impaired. The Golgi bodies were only capable of extremely restricted movement. In contrast, in the presence of the nanobody construct, the dominant negative effect of the XI-K-GTD was strongly decreased, and medium to long range movement is possible again. These results support the hypothesis that the free GTD domains indeed block the cargo binding sites, as this effect could be bridged by the nanobody construct in this conditional rescue line.

(3) Myosin dimerisation

First results which were obtained during my master thesis suggest not only the existence of myosin homodimers, but cooperative action of different myosins by heterodimerisation. A systematic yeast 2-hybrid assay including the tail and coiled coil fragments of the four myosins revealed that these proteins have the capacity to build heterodimers, although the extend to do so differs in between the different myosins (Table 12).

Table 12: Yeast 2-hybrid results of interactions of myosin tails and coils.

Interaction between myosin XI tails N-terminally fused to the GAL4-AD and myosin XI coils N-terminally fused to the GAL4-BD and vice versa. Selection was carried out on selective dropout medium lacking leucine, tryptophan, and histidine, supplemented with 3-15 mM 3-aminotriazole (3-AT). GFP N-terminally fused to the GAL4-AD was included as a negative control. The results displayed are the sum of 3-9 independent replicates. “-“ – no interaction in any set, “+“ – interactions in all sets tested, “+/-“ – differential results between sets.

		coiled coil				tail			
		XI-1	XI-2	XI-I	XI-K	XI-1	XI-2	XI-I	XI-K
coiled coil	XI-1	+	-	-	-	+	-	+	-
	XI-2	-	+	-	-	-	+	-	-
	XI-I	-	-	+	-	+	-	+	-
	XI-K	-	-	-	+	-	-	-	+
tail	XI-1	+	-	+	-	+	+/-	+	+
	XI-2	-	+	-	-	+/-	+	+/-	-
	XI-I	+	-	+	-	+	+/-	+	+/-
	XI-K	-	-	-	+	+	-	+/-	+

The results show that - at least in the yeast system - the coiled coil domains can only build homodimers. Additionally, the coil of XI-1 is able to build heterodimers with the tail of XI-I

Results

and vice versa. The results of tail interactions can be split into two groups: clear heterodimers were found for XI-1 with XI-I and XI-K, while results for interactions of XI-2 with XI-1 and XI-I, as well as XI-I with XI-K were not consistent between the replicates. XI-2 was found to be not capable of forming heterodimers with XI-K.

To further verify these findings and proof the existence of heterodimers *in planta*, a multitude of experiments have been performed. Transient expressions via particle bombardment as well as tobacco leaf infiltration, with all combinations depicted in Table 12, with varying destination vectors and fluorophores where not successful. It was only possible to express either one myosin exclusively, or both with an extremely weak and/or altered signal. This led to the conclusion that the expression of two myosins or myosin parts at once is extremely adverse for plant cells and therefore not possible in this setup. This finding was further confirmed since particle bombardment of said constructs on the *12k^R* line (*12k* mutant line rescued with pMDC32:XI-K:YFP, kindly provided by Valera Peremyslov) caused similar effects.

3.3 Myosin full length constructs – from functional to function?

The lack of functional full length myosin constructs, and/or the restriction to only one fluorophore, limits the prospect of finding novel myosin functions and characteristics. For this work, full length constructs were created under the control of the 35S or ubiquitin promoter, C-terminally fused to YFP, CFP or RFP/mCherry, respectively (see Table 22). Unfortunately, only the YFP tagged versions showed strong signals. Both, RFP/mCherry and CFP tagged myosins were rather weak (data not shown).

Localisation

Similar to the fragments tested in former studies, the full length constructs of myosins XI-1, XI-2 and XI-K localise to the cytoplasm and in strands throughout the cell. Not many dot structures can be seen, but sometimes occur (Figure 23).

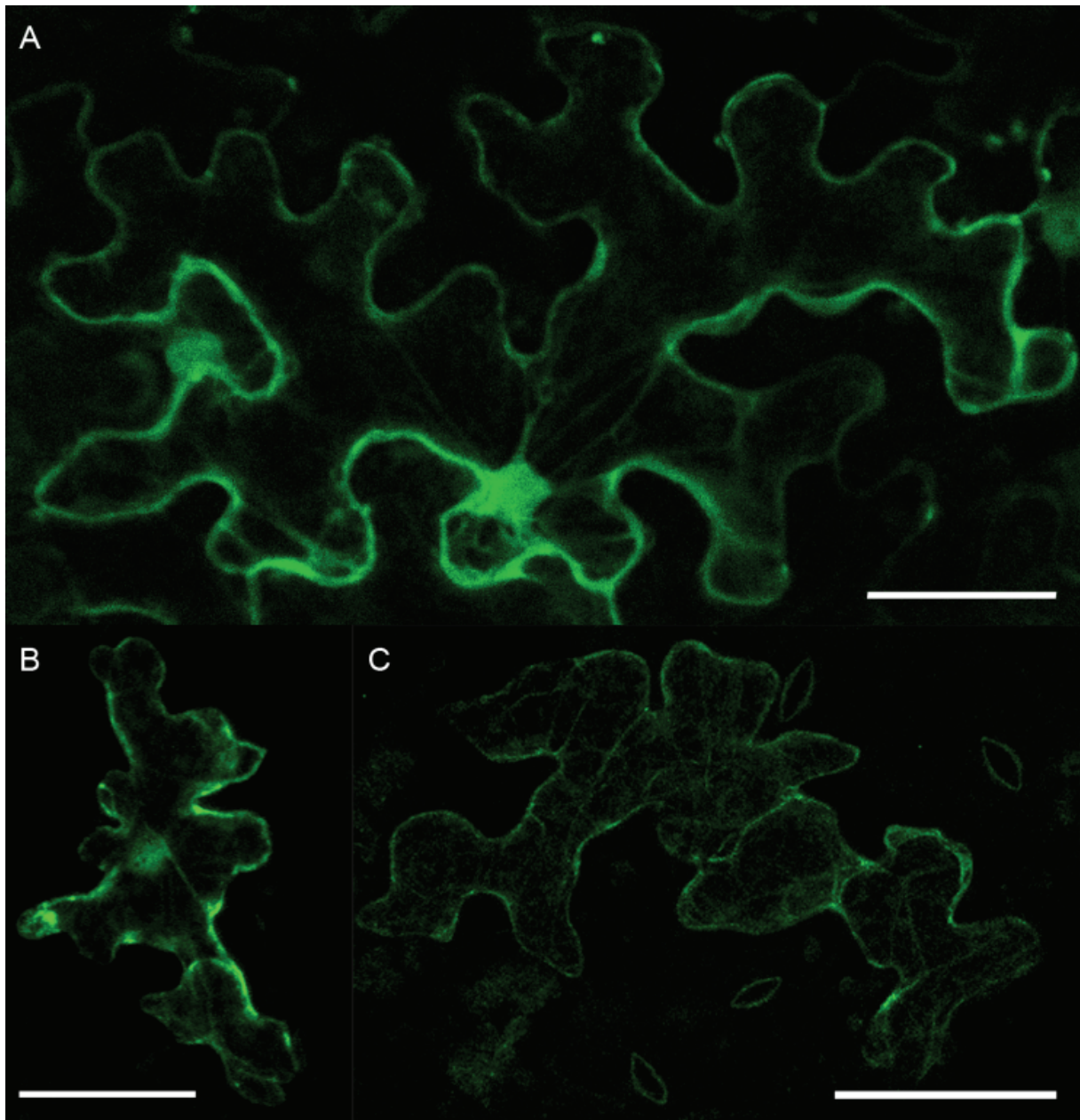


Figure 23: Localisation of myosin full length constructs in Arabidopsis leaf cells. Transient expression of A – 35S::XI-1-YFP in Col-0, B – 35S::XI-2-YFP in 2IK, C – 35S::XI-K-YFP in Col-0. The scale displays 50 µm.

When expressed together with 35S::LifeAct-CFP, a distinct co-localisation with the actin cytoskeleton could be observed for all three myosins (Figure 24).

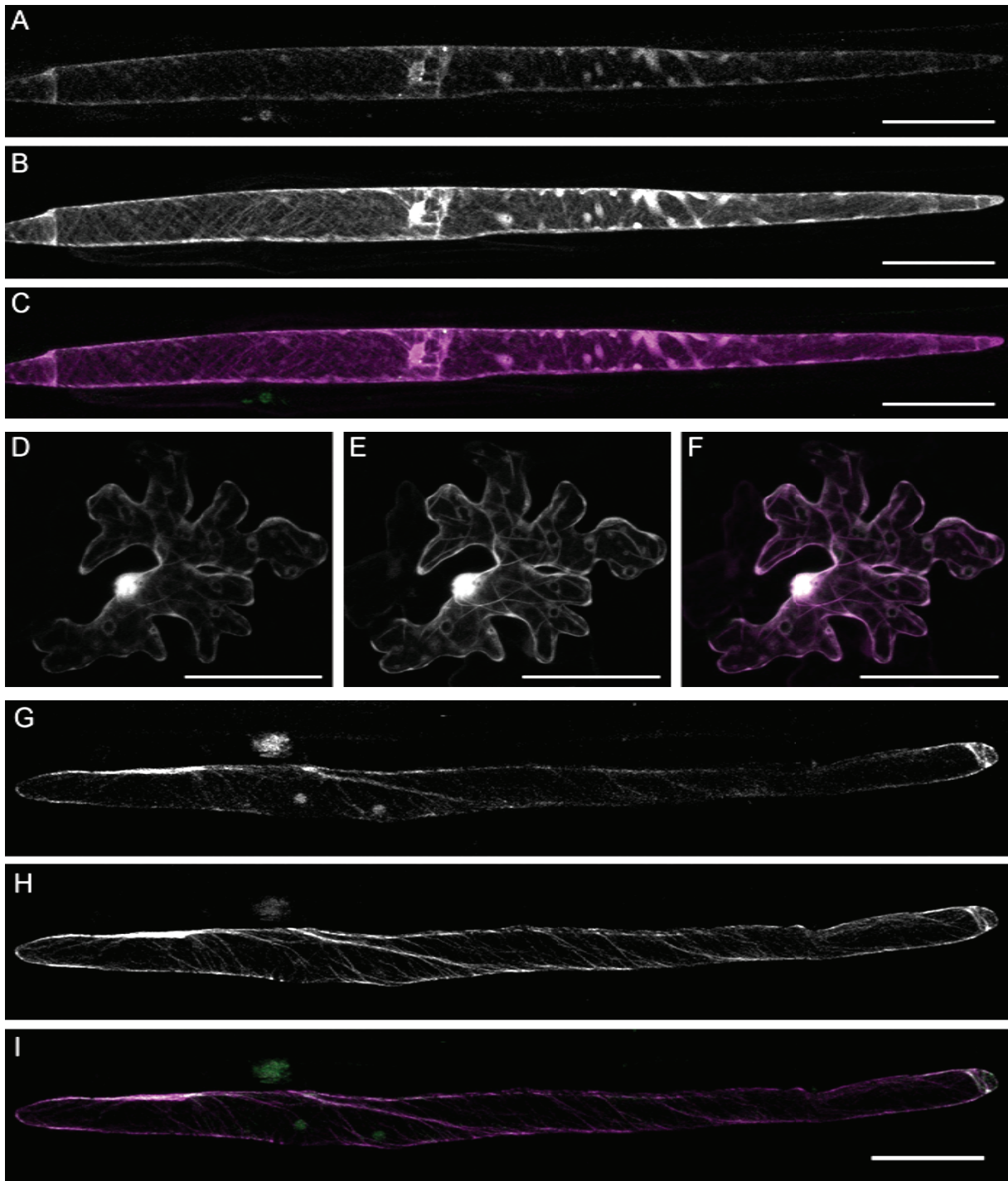


Figure 24: Localisation of myosin full length constructs and 35S::LifeAct-CFP in Col-0 leaf cells. Transient expression of A-C – 35S::XI-1:YFP, D-F – 35S::XI-2:YFP, G-I – 35S::XI-K:YFP. The scale displays 100 μm (A-C and G-I) or 50 μm (D-F).

The expression of the tagged myosins did not alter the actin organisation (compare Figures 23 and 24).

In conjunction with the finding from chapter 3.2 that the truncated forms of the myosins can often not be expressed in the same cell, sets of two full length myosin constructs were used to transiently transform tobacco leaves (Figure 25). Here as well, the localisation of at least one

Results

of the myosins was strongly altered in presence of a second one. In most cases, the signal was weakened and shifted to the cytoplasm. The characteristic fine strands of actin were only visible in few cells and aggregates built up.

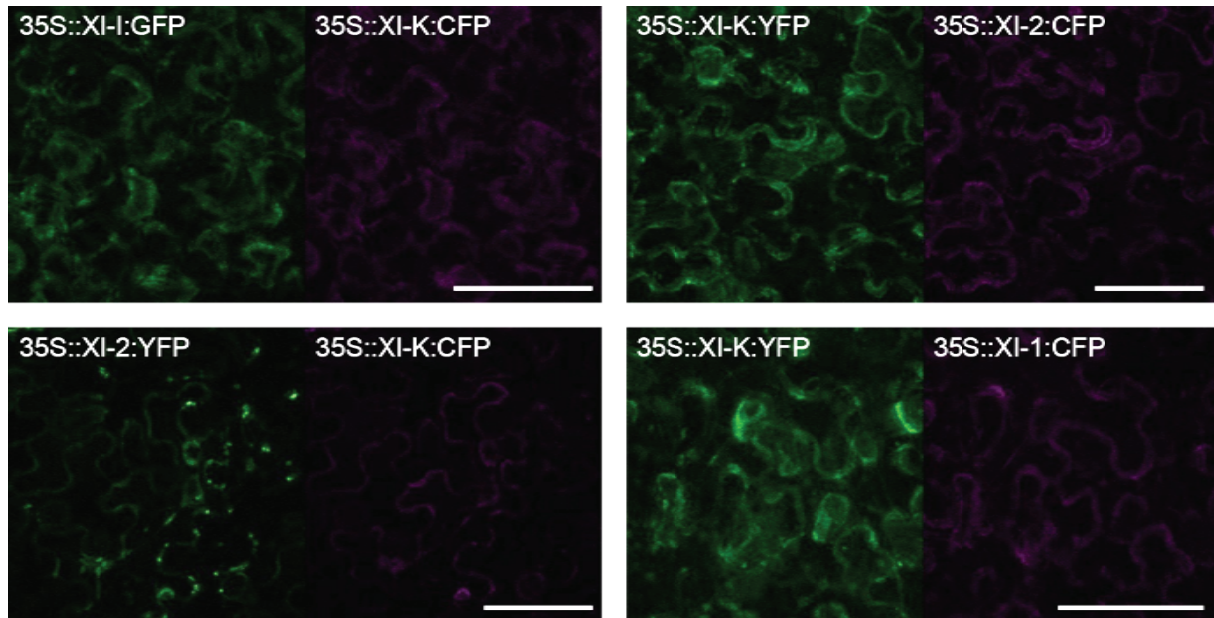


Figure 25: Co-localisation of myosin full length constructs.

The pictures show tobacco leaf cells infiltrated with myosin constructs. The scale displays 75 μ m.

Functionality of the full length constructs

The localisation of the full length constructs was found to be exactly as expected. However, it was necessary to determine if the constructs were also functional. To test this, several mutant lines were transformed with the full length constructs of XI-1, XI-2 and XI-K, C-terminally tagged with YFP, under the control of the 35S promoter or the ubiquitin promoter (only XI-2 and XI-K), respectively. Unfortunately, no stable lines expressing a full length myosin were obtained. Since the BASTA selection clearly showed multiple transformed plants, it can be assumed that the transformation was successful. However, no fluorescence could be detected and – in case of mutants transformed with myosin XI-K – no rescue of the trichome phenotype was visible.

As stable lines could not be generated, the functionality was tested transiently at least for the XI-K full length construct, by bombarding mutant rosette leaves with the respective constructs and a marker to check for a rescue of organelle movement (Figure 26). The peroxisome long range movement was clearly restored, indicating that the 35S::XI-K:YFP construct is functional.

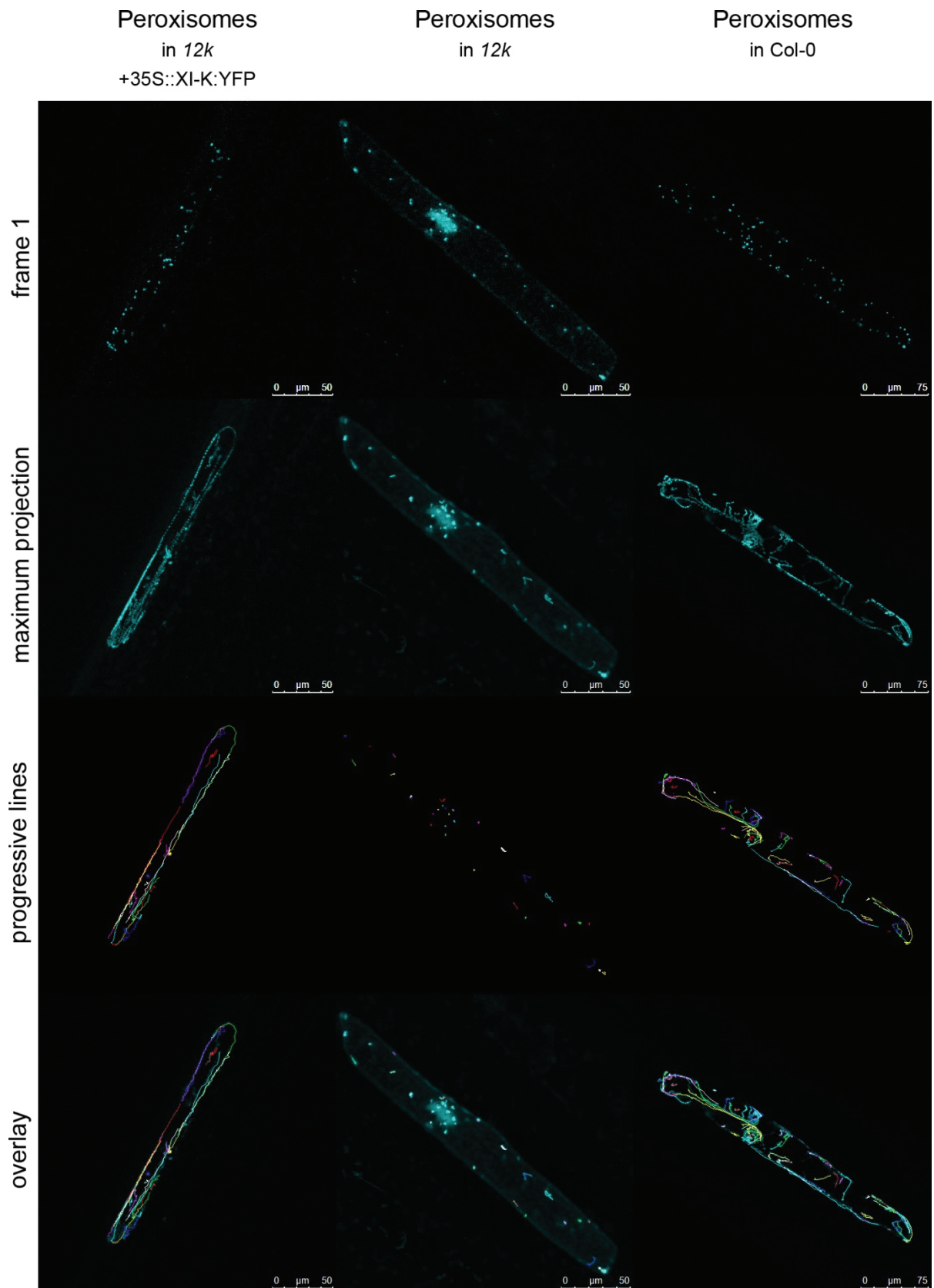


Figure 26: Rescue of peroxisome movement in the *12k* mutant with 35S::XI-K:YFP. The peroxisome marker 35S::CFP:SKL was transiently expressed in leaf cells by bombardment in (first column) the *12k* mutant together with 35S::XI-K:YFP, (second column) the *12k* mutant, (third column) Col-0. Peroxisome movement was tracked manually over 50 frames (63.21 sec). Frame 1 displays the initial position of the peroxisomes, in the maximum projection all frames of the video are stacked. Progressive lines indicate the trajectories of the peroxisomes.

3.4 Stirring and passive flow of cytoplasm

Cytoplasmic streaming consists of both, the active transport and the hydrodynamic flow. In this work, the passive component of cytoplasmic streaming is analysed regarding two different characteristics: the stirring effect and Brownian motion of molecules.

3.4.1 Is stirring sufficient for movement?

Stirring is the passive motion or bulk flow of the cytoplasm, caused by the directed movement of myosins (Avisar et al., 2008). In order to investigate the relevance of this effect for organelle movement, the XI-K Δ GTD-2xYFP construct (M. Jakoby, chapter 3.2 (2)) was utilised as a molecular stirrer. Triple *12k* knockout lines and *12k* stable lines expressing XI-K Δ GTD-2xYFP (*12k*_{XI-K Δ GTD-2xYFP}) were transiently transformed with organelle markers for Golgi, peroxisomes, P-bodies and mitochondria, respectively. Movement of the organelles was tracked to evaluate the stirring effect caused by the XI-K Δ GTD-2xYFP construct. Since myosin XI-K is essential for actin stability (Ueda et al., 2010), it was first analysed if the XI-K Δ GTD-2xYFP construct can rescue the actin organisation, since this could also restore movement but would be independent of the stirring effect (Figure 27).

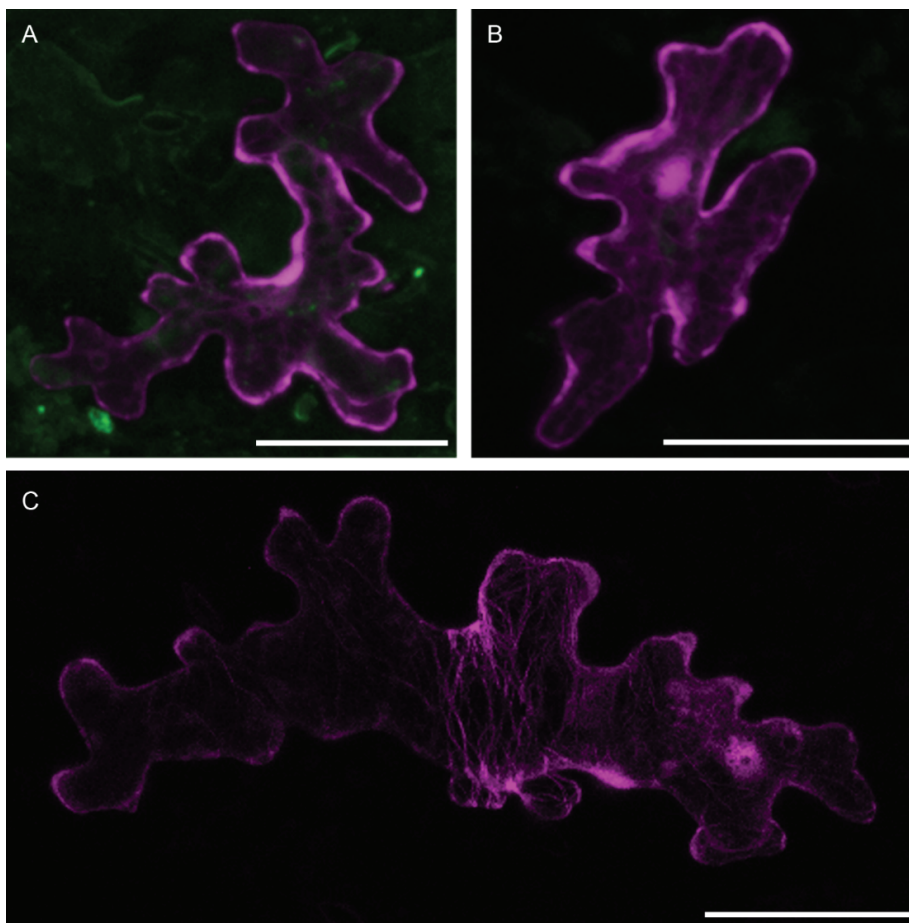


Figure 27: Actin organisation in Arabidopsis leaf epidermal cells. Transient 35S::LifeAct-CFP expression in A - *12k*_{XI-K Δ GTD-2xYFP}, B - *12k*, C – Col-0. The scale displays 50 μ m.

Results

The XI-K Δ GTD-2xYFP construct was not able to restore normal actin organisation in the *12k* mutant. Thus, it can be assumed that the effects of this construct on organelle movement are caused by its function as a molecular stirrer.

In order to find out if stirring is sufficient to accelerate organelles, movement of peroxisomes was tracked in the *12k* mutant and the *12k*_{XI-K Δ GTD-2xYFP} line (Figure 28).

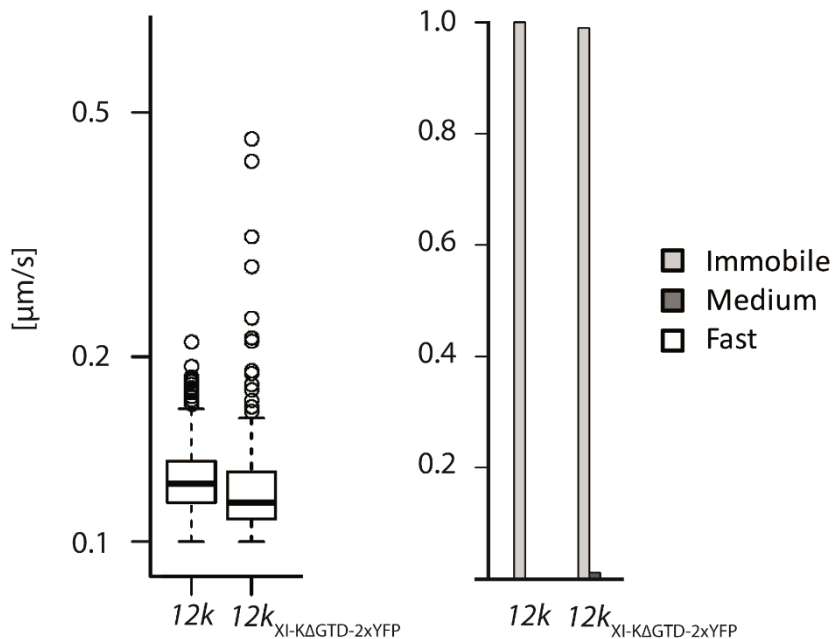


Figure 28: Effect of molecular stirrer on peroxisome movement. Movement of peroxisomes was manually tracked in the *12k* mutant and the *12k*_{XI-K Δ GTD-2xYFP} conditional rescue line. Peroxisomes were marked using 35S::CFP:SKL.

In the *12k* mutant, movement of peroxisomes is extremely restricted. All peroxisomes classify as immobile and never accelerate over approx. 0.22 $\mu\text{m}/\text{sec}$. In presence of the molecular stirrer, the average speed does not increase. However, single peroxisomes are able to move with approx. up to 0.5 $\mu\text{m}/\text{s}$, which classifies as medium speed. Hence, it was not possible to restore movement of peroxisomes. However, peroxisomes are occasionally swept along by the XI-K Δ GTD-2xYFP construct. In addition, no obvious rescue of the phenotype was observed for mitochondria or Golgi bodies (data not shown).

Brownian motion

A variety of molecules in the cytoplasm of a cell move by Brownian motion, which is the random motion of particles in a fluid. Even though this way of movement follows a random pattern for each particle, directional movement can be caused by a concentration gradient, e.g.

Results

through consumption of specific molecules at one place in the cell. A study in tobacco (Esseling-Ozdoba et al., 2008) has shown that this random movement of the cytoplasm is accelerated by the motive force of the actomyosin system in large cells. In addition, it has been found that this movement defines plant size by controlling diffusion of nutrients, metabolites, cell-wall precursors and hormones, and thus controlling the cell expansion (Tominaga et al., 2013).

Hence, it is crucial to determine the role of the passive flow as a baseline for the movement. In this work, Fluorescence Recovery after Photobleaching (FRAP) was used to determine the recovery of free RFP in the cytoplasm of transiently transformed *Arabidopsis* epidermal pavement cells. An area of $2.5 \times 2.5 \mu\text{m}$ was bleached and the recovery and half life time of RFP was determined. Figure 29 shows an exemplary FRAP series from a Col-0 leaf epidermal pavement cell.

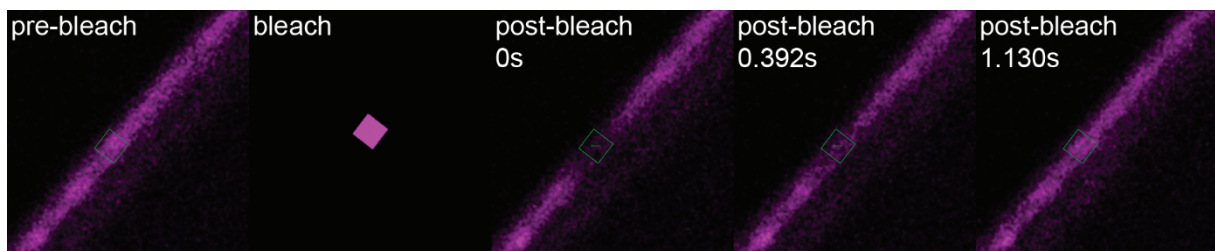


Figure 29: FRAP series in Col-0 epidermal pavement cell.

Pre-bleach, bleach and post-bleach images of a cell transiently transformed with 35S::mCherry. The region of interest (ROI) covers an area of $2.5 \times 2.5 \mu\text{m}$.

The FRAP experiment was carried out for Col-0 and *12k*, Col-0 treated with Latrunculin B, which disrupts the actin cytoskeleton, and Col-0 after fixation with paraformaldehyde and glutaraldehyde (Figure 30).

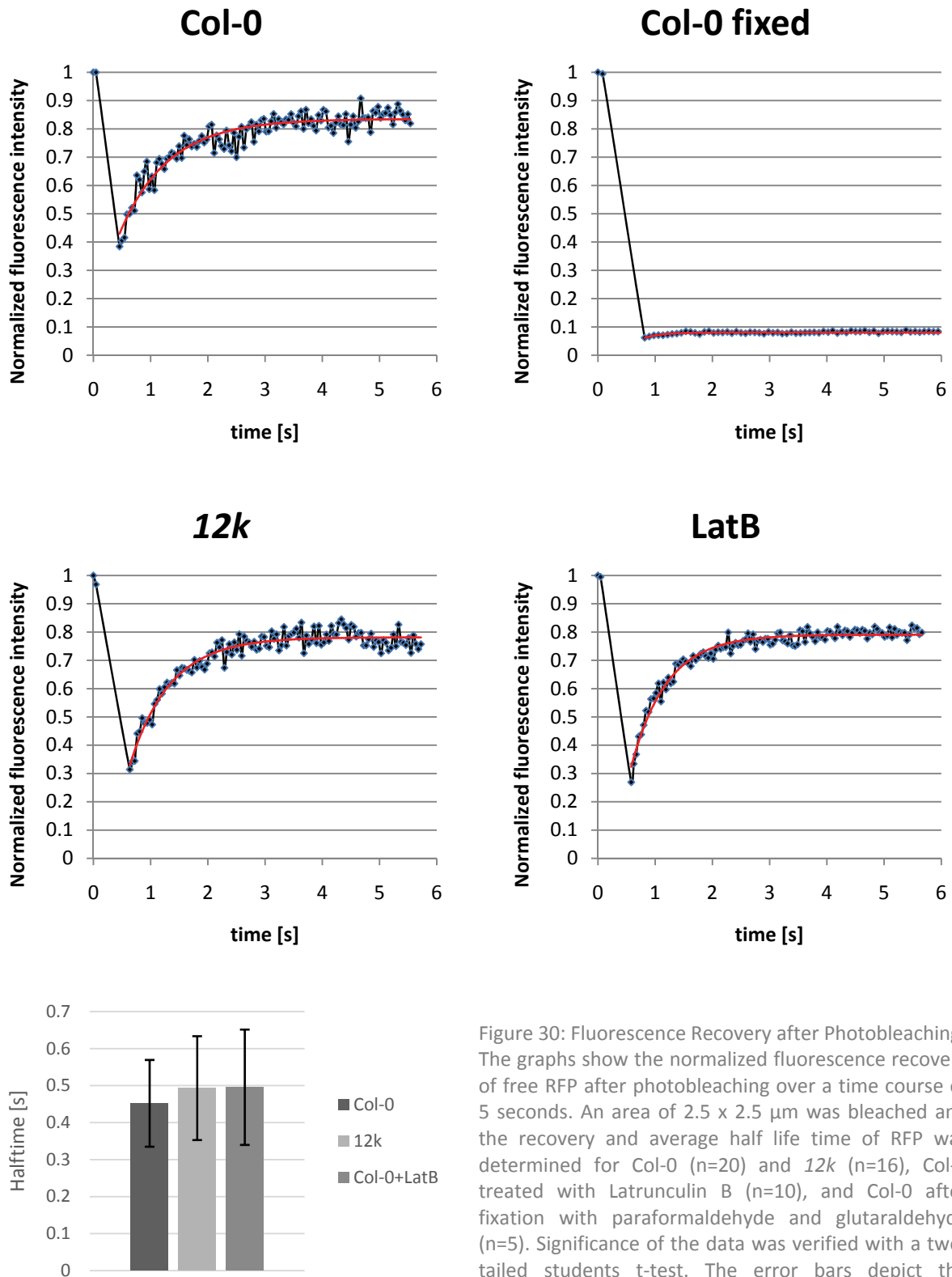


Figure 30: Fluorescence Recovery after Photobleaching. The graphs show the normalized fluorescence recovery of free RFP after photobleaching over a time course of 5 seconds. An area of $2.5 \times 2.5 \mu\text{m}$ was bleached and the recovery and average half life time of RFP was determined for Col-0 ($n=20$) and 12k ($n=16$), Col-0 treated with Latrunculin B ($n=10$), and Col-0 after fixation with paraformaldehyde and glutaraldehyde ($n=5$). Significance of the data was verified with a two-tailed students t-test. The error bars depict the standard deviation.

The results show that the curve progressions of all samples were as expected. All living samples show a strong decrease upon bleaching to approx. 30% of the initial fluorescence and a fast recovery of the RFP signal. The fixed cells show no recovery. The average half lifetime

Results

of Col-0 (0.45 ± 0.12 sec) was slightly decreased compared to the triple mutant *12k* (0.49 ± 0.14 sec) and the latrunculin B treated cells (0.50 ± 0.16 sec). However, the values were not significantly different. Since former studies showed that movement of the cytoplasm is faster in larger cells, the experiment was carried out with cells of different sizes and the results were compared. However, no significant difference was visible (data not shown). These results indicate that there is no relevance of stirring for the speed of the passive bulk flow in the examined cells.

II. SPIRRIG

In Arabidopsis, the BEACH domain protein SPIRRIG was found to act as both, a facilitator of membrane dynamics and as a part of the salt response/P-body machinery (De Lozanne, 2003; Steffens et al., 2015). However, its molecular function is unknown and its exact role in morphology could not be determined yet. In this work, a detailed characterisation of *Arabidopsis alpina spi* mutants was carried out, in order to elucidate differences in comparison to Arabidopsis and pinpoint sites of functional relevance in the protein or connect phenotypes with certain pathways.

3.5 The SPIRRIG protein

The BEACH domain protein families of both, Arabis and Arabidopsis, contain six BEACH domain genes which are clustered into four groups (A-D), while group A and C contain two BEACH homologues, respectively (Table 13). It was already shown that group D is a plant-specific outgroup which is characterized by a kinase domain, possibly with plant-specific functions (Teh et al., 2014). This, however, is not true for group A, suggesting a more general function of its members, including the SPI protein. In Chlorophyta, only one homologue of BEACH domain proteins is present. Neither in *Chlamydomonas reinhardtii* nor in *Ostreococcus tauri*, it is possible to classify these. With exclusive focus on the BEACH domain, these proteins are most similar to members of the group D, however, they lack the typical kinase domain.

Results

Table 13: The BEACH domain protein family in the plant kingdom.

“+” – protein exists in this species, “-” – protein does not exist in this species, “(…)” – protein cannot be assigned to one specific group.

			Organism	A1	A2	B	C1	C2	D		
Chlorophyta (Green Algae)			<i>Ostreococcus tauri</i>			(+)					
			<i>Chlamydomonas reinhardtii</i>			(+)					
Landplants	Bryophyte (moss)		<i>Physcomitrella patens</i>		(+)	+	+	-	-		
	Lycophyte (clubmoss)		<i>Selaginella moellendorffii</i>	-	-	-	-	-	+		
	Angiosperms	Monocots		<i>Sorghum bicolor</i>	+	+	+	-	+	+	
				<i>Oryza sativa</i>	+	+	+	++	-	+	
		Eudicots	Brassicaceae		<i>Vitis vinifera</i>		(+)	+	+	-	+
					<i>Arabidopsis thaliana</i>	+	+	+	+	+	+
					<i>Capsella rubella</i>	+	+	+	+	+	+
					<i>Camelina sativa</i>	+	+	+	+	+	+
					<i>Arabidopsis lyrata</i>	+	+	+	+	+	+
					<i>Thellungiella halophila</i>	+	+	+	+	+	+
					<i>Leavenworthia alabamica</i>	+	+	+	+	+	+
					<i>Sisymbrium irio</i>	+	+	+	-	+	+
					<i>Aethionema arabicum</i>	+	+	+	-	+	+
					<i>Arabis alpina</i>	+	+	+	+	+	+
		<i>Brassica oleracea</i>	+	+	+	+	+	+			
		<i>Brassica rapa</i>	+	+	+	+	+	+			
<i>Brassica napus</i>	+	+	+	+	+	+					

Results



Figure 31: Phylogram of the BEACH domains in the plant kingdom.

The tree is based on the amino acid sequences of the BEACH domains and was created using the Neighbour Joining method with the Ugene software and subsequently modified. Numbers at branches display bootstrap values. The table shows the abundance of BEACH domain protein family members within the plant kingdom.

Results

The SPIRRIG proteins of *A. thaliana* and *A. alpina* are highly conserved, especially in the C-terminus (Figure 32). The sequence identity reaches 94% for the whole protein and 97% for the PBW domain.

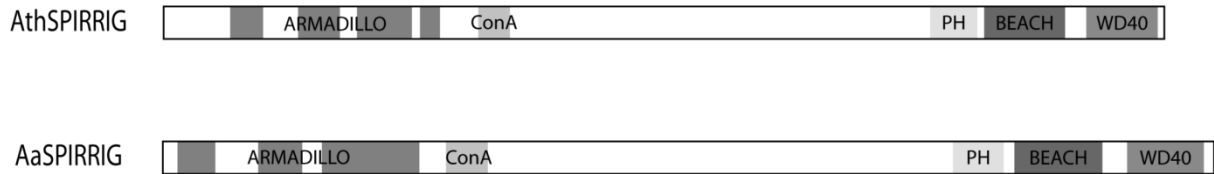


Figure 32: The SPIRRIG protein in *Arabidopsis thaliana* and *Arabis alpina*.

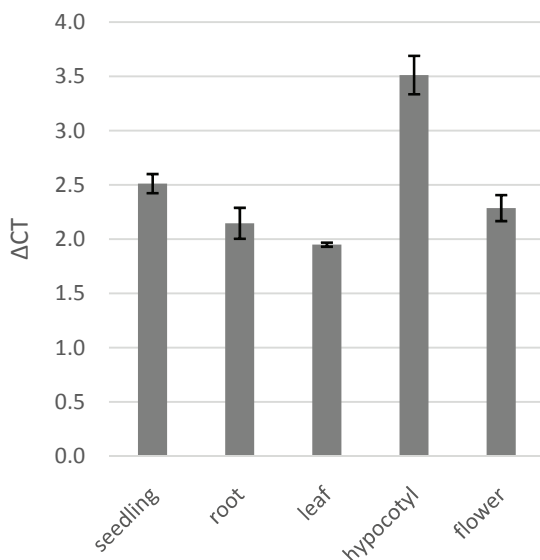
ARMADILLO - Armadillo repeat domain, ConA – Concanavalin A-like lectin domain, PH - Pleckstrin-Homology domain, BEACH – Beige and Chediak Higashi domain, WD40 – WD40 repeat domain. Domains were annotated using PROSITE (Hulo et al., 2007).

The expression pattern of SPIRRIG was tested in whole seedlings, roots, mature leaves, hypocotyls and flowers (Figure 33). The transcript is expressed throughout the whole plant, similar to the expression pattern in *Arabidopsis* (Saedler et al., 2009). The expression is at slightly lower levels in the hypocotyl, compared to other tissues of the plant.

A



B



C

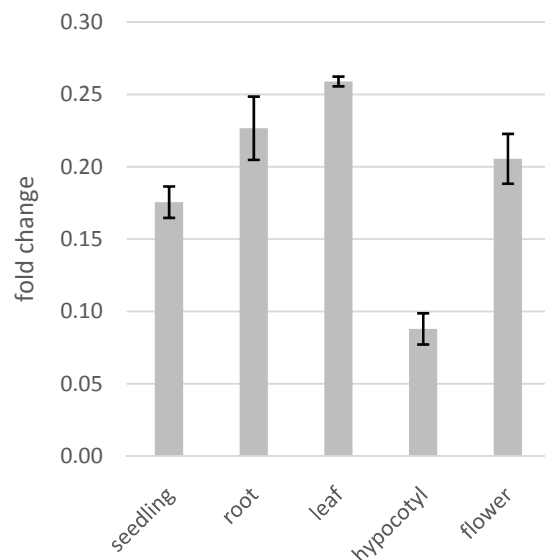


Figure 33: SPIRRIG expression in different tissues of *Arabis alpina*.

A – position of qPCR primers in the *AaSPl* gene. Grey areas mark exons. B – ΔC_t values of SPIRRIG expression, C – fold change values of SPIRRIG expression. The results were obtained by qPCR, data was normalized against RAN3. Error bars depict standard deviations.

3.6 *spi* mutants in *Arabidopsis thaliana*

In 2014, D. Chopra identified three putative *spi* mutants derived from an EMS mutagenesis in *Arabidopsis thaliana pep1* (Wang et al., 2009) based on their trichome phenotype. Sequencing of these mutants revealed early stop codons in all three lines: upstream of the BEACH domain (*spi-1*), within the WD40 repeats (*spi-2*) and in the N-terminus (*spi-3*), respectively (Figure 34). In addition, *spi-1* shows an E to K exchange within one of the Armadillo repeats.

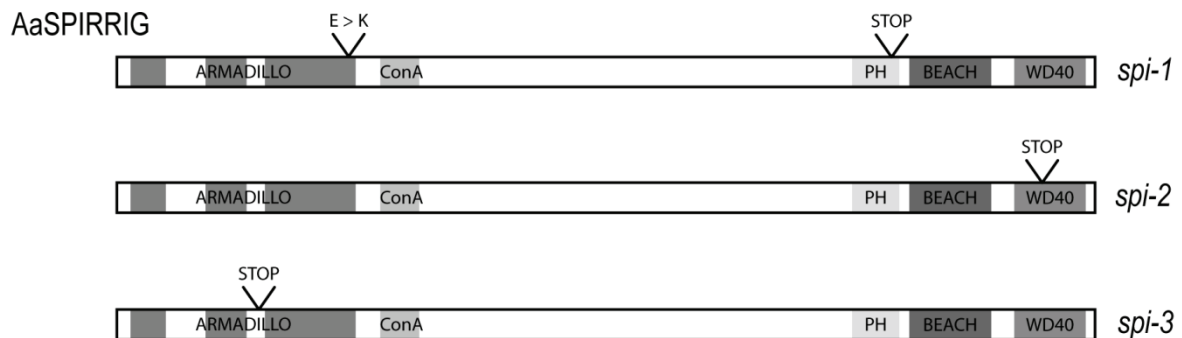


Figure 34: Schematic representation of the *SPIRRIG* gene in three EMS *spi* mutants. ARMADILLO - Armadillo repeat domain, ConA – Concanavalin A-like lectin domain, PH - Pleckstrin-Homology domain, BEACH – Beige and Chediak Higashi domain, WD40 – WD40 repeat domain.

A complementation test was carried out to prove that the mutations in the *SPI* gene are causative for the observed trichome phenotype: All lines were crossed with each other and the F1 offspring were analysed for the *spirrig* trichome phenotype. Complementation, meaning a rescue of the mutant phenotype, only occurs if the mutations are in different genes. For the three *spi* mutant crossings, all F1 progeny showed the distorted phenotype (Figure 35).

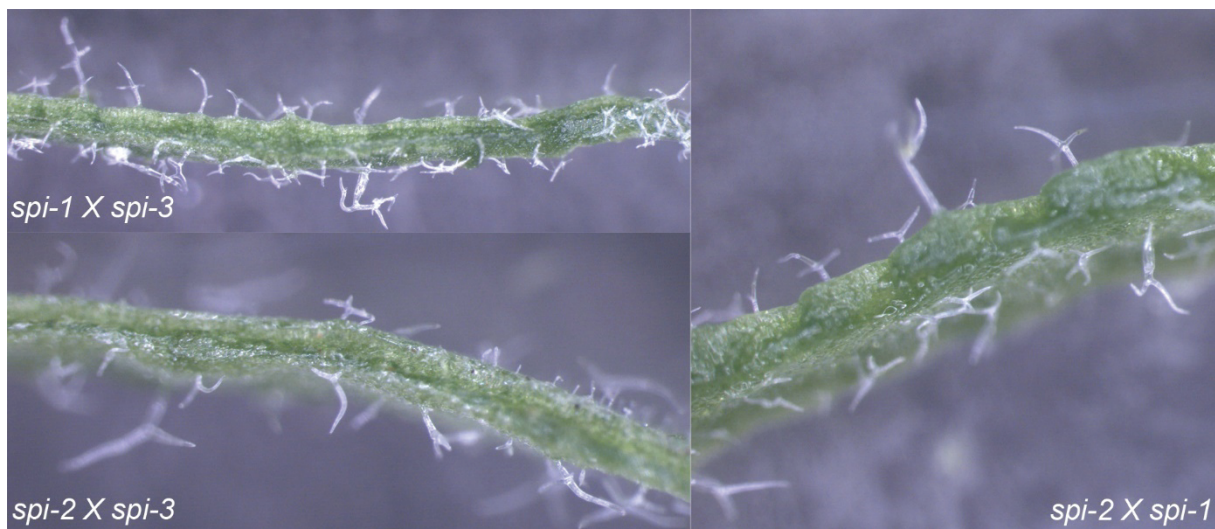


Figure 35: Complementation assay of *spi* EMS mutants. The pictures show leaf cross sections of F1 progenies of crossings between *spi* mutant alleles 1, 2 and 3. All progenies show distorted trichomes.

Results

In the three mutant alleles and their background *pep1*, the mRNA of SPIRRIG is expressed to the same extent (Figure 36).

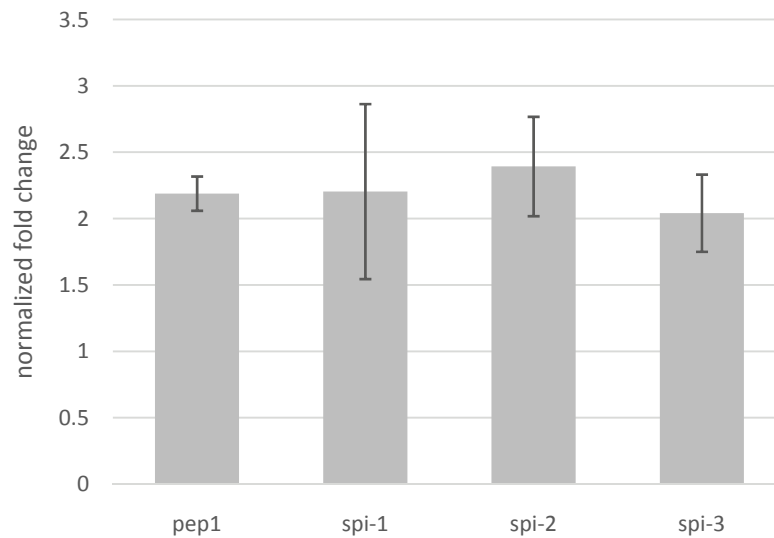


Figure 36: Expression of SPIRRIG in *pep1* and *spi* mutants.

The results were obtained by qPCR and normalized against TUA5 and CAC. Significance of the results was tested with a Mann-Whitney-U test at a level of $p < 0.10$.

3.6.1 Common phenotypes in Arabis and Arabidopsis

Since the exact molecular functions of SPI have not been determined so far, known phenotypes are the most promising traits to compare and analyse similarities and differences between Arabidopsis and Arabis. Common phenotypes in both Brassicaceae indicate highly conserved functions of the *SPIRRIG* gene.

Cell complexity

In Arabidopsis, *spi* epidermal pavement cells on rosette leaves show less lobing and less complexity than wild type cells (Figure 37; Table 16; Saedler et al., 2009). In Arabis, this experimental setup is not applicable, since the cells on true leaves vary too much within one plant to achieve any comparison (data not shown). However, a similar approach was used on cotyledons, which are not as diverse. Here it could be shown that *spi* cells are less lobed and thus less complex than *pep1* cells.

Results

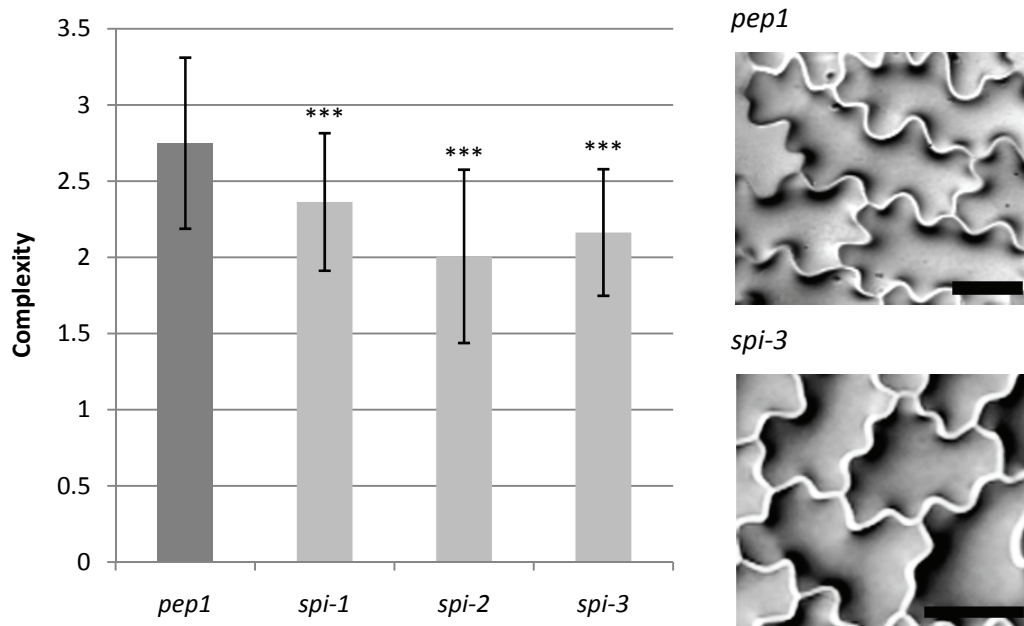


Figure 37: Complexity of 10 day old cotyledon cells in *pep1* and *Aaspi* mutants.

The graph displays the mean complexity of 50 cells per line (10 cells on 5 leaves). The complexity was calculated with the formula $\text{Complexity} = \frac{\text{perimeter}^2}{4 \cdot \pi \cdot \text{area}}$ (Dewitte et al., 2003), significance was tested with a one way ANOVA at a significance level of 0.001 (***), 0.02 (**) and 0.05 (*). The pictures show representative agarose imprints of epidermal pavement cells on cotyledons of *pep1* and *spi-3*. The scale displays 50 μm .

Root hair length

The root hairs of all *Aaspi* mutant alleles are significantly shorter than those of *pep1* (Figure 38), like it was also shown in *A. thaliana spi* (Saedler et al., 2009).

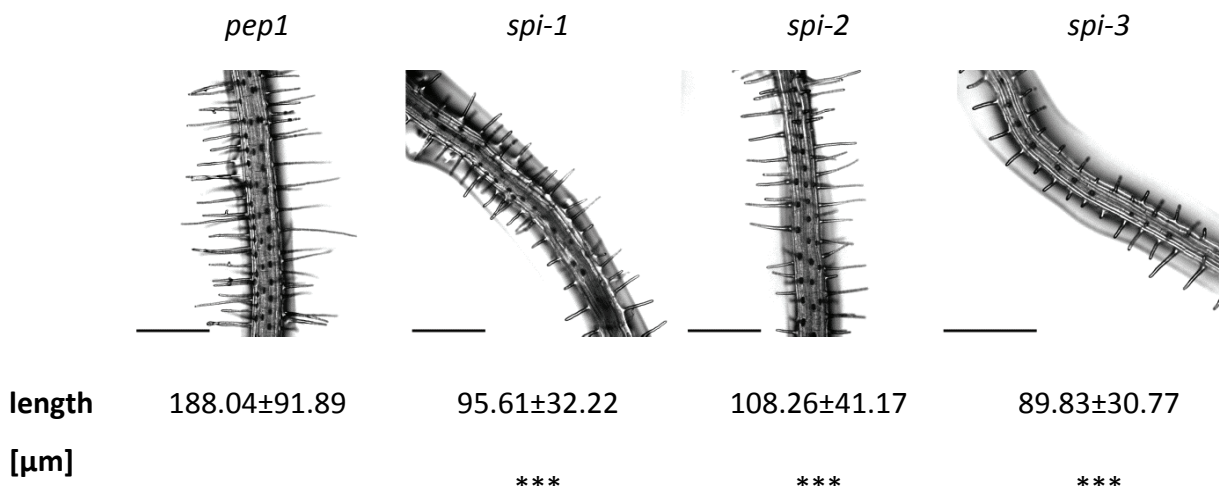


Figure 38: Root hairs of seven day old seedlings in *pep1* and *Aaspi* mutants.

The individual length of 150 seven day old root hairs per line was measured 1 mm below the intersection of hypocotyl and root for 15 root hairs per sample. Significance of the data was calculated with a Wilcoxon signed-rank test at a significance level of 0.001 (***), 0.02 (**) and 0.05 (*). The scale displays 300 μm .

Results

Trichomes

The trichome phenotype was the initial trait which identified the *spi* mutants in the EMS screen of *Arabis alpina*, meaning it is similar to that in *Arabidopsis*: trichomes are weakly distorted and single branches tend to be elongated. Apart from that, trichomes in *Arabis* have a higher number of branches than in *Arabidopsis* (Figure 39).

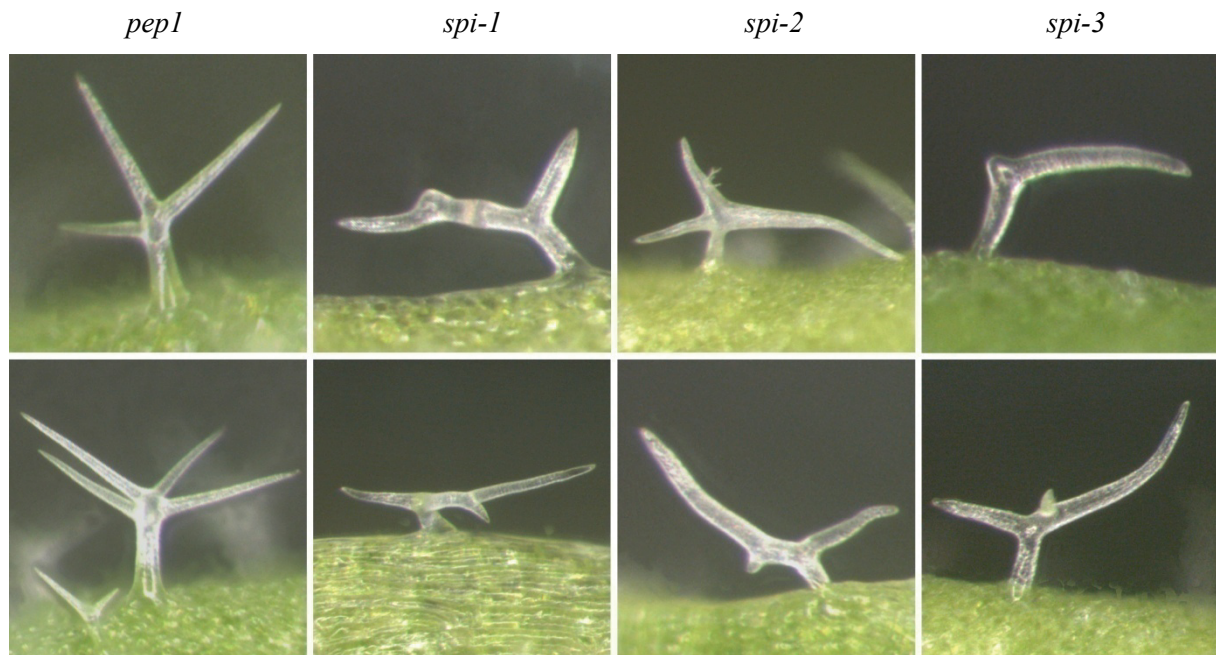


Figure 39: Trichome shapes in *pep1* and *Aaspi* mutants.
For size comparison see Table 14.

For *Arabidopsis*, it was shown that the stalk length of trichomes, their width and the average branch length were decreased in *spi* mutants. For the stalk length, the same observation was made in *Arabis*. For both, stalk width and branch length, the results were inconsistent within the three mutant lines (Table 14).

Table 14: Trichome measurements in *Arabis alpina*.

The stalk length is defined as the distance between leaf surface and the first branch, the stalk width was measured at the middle point of the stalk. The table shows the mean and standard deviation of 100 measurements per line and trichome parameter on mature leaves. Significance of the data was calculated with a Wilcoxon signed-rank test at a significance level of 0.001 (***) , 0.02 (**) and 0.05 (*).

	<i>pep1</i>	<i>spi-1</i>	<i>spi-2</i>	<i>spi-3</i>
stalk length [µm]	143±59	110±72 ***	94±41 ***	88±65 ***
stalk width [µm]	26±7	26±8	22±5 ***	25±7
branch length [µm]	159±59	163±75	122±52 ***	153±69

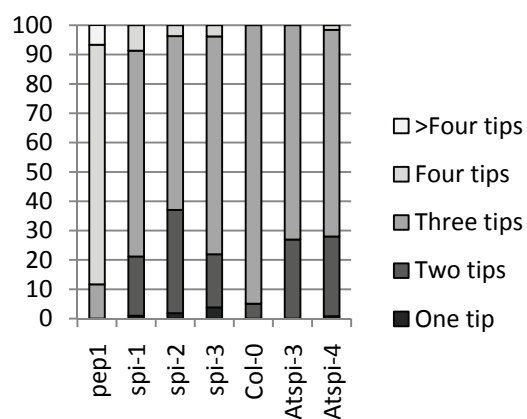
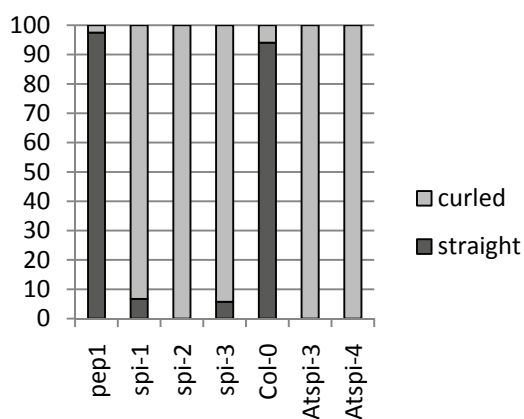
Results

Despite these two parameters not being consistent within the different alleles, the general shape of trichomes in *Arabis* and *Arabidopsis spi* mutants is similar. To further support these observations, the frequency of certain trichome shapes in both brassicaceae was analysed (Table 15).

Table 15: Classes of different trichomes in *pep1*, *Col-0* and *spi* mutants.

Table and graphs shows the relative abundance in % in >100 trichomes per line.

			<i>pep1</i>	<i>spi-1</i>	<i>spi-2</i>	<i>spi-3</i>	<i>Col-0</i>	<i>Atspi-3</i>	<i>Atspi-4</i>
One tip	straight		-	-	-	-	-	-	-
	curled		-	1.0	1.9	3.8	-	-	0.8
Two tips	straight		-	1.0	-	-	4.2	-	-
	straight		-	-	-	1.0	-	-	-
	curled		-	4.8	25.0	9.5	0.8	20.0	24.0
	curled		-	14.4	10.2	7.6	-	7.0	3.2
Three tips	straight		11.7	4.8	-	2.9	89.8	-	-
	curled		-	15.4	14.8	21.0	-	12.2	15.2
	curled		-	50.0	44.4	50.5	5.1	60.9	55.2
Four tips	straight		79.2	1.0	-	1.9	-	-	-
	curled		2.5	7.7	3.7	1.9	-	-	1.6
>Four tips			6.6	-	-	-	-	-	-



Results

The *spi* trichome types in between both species turned out to be comparable: in summary, *spi* trichomes are more curled and have a lower number of branches than their corresponding wild type/background.

3.6.2 Unique phenotypes in Arabis *spi* mutants

Phenotypes which differ in Arabidopsis and Arabis are of specific interest. Given that both species are highly similar, little differences might give insight in the general functions of the gene and also hint to the responsible motives or domains.

Hypocotyl morphology

In Arabidopsis, *spi* mutants show a decrease of almost 2 fold in hypocotyl length of young seedlings (Saedler et al., 2009). For Arabis *spi*, a decrease in hypocotyl length could not be observed (Table 16), on the contrary, the hypocotyls of the mutants were (significantly) longer than those of *pep1*.

Table 16: Hypocotyl length in *pep1* and *Aaspi* mutants.

The hypocotyls length was measured in 50 seven day old seedlings per line. Significance of the data was calculated with a Wilcoxon signed-rank test at a significance level of 0.001 (***) , 0.02 (**) and 0.05 (*).

	<i>pep1</i>	<i>spi-1</i>	<i>spi-2</i>	<i>spi-3</i>
hypocotyl length [cm]	2.27±0.46	2.43±0.55	2.69±0.47	2.56±0.47
			***	**

In addition, it was reported that dark grown Arabidopsis *spi* seedlings exhibit out-curved and disconnected hypocotyl cells (Saedler et al., 2009). This phenotype could not be observed in Arabis *spi* mutants. All tested lines showed elongated hypocotyls cells, indicating that the fast growth of the cells had indeed occurred. However, no out-curved and disconnected hypocotyl cells could be found in two independent experiments (N>30 per line, Figure 40).

Results

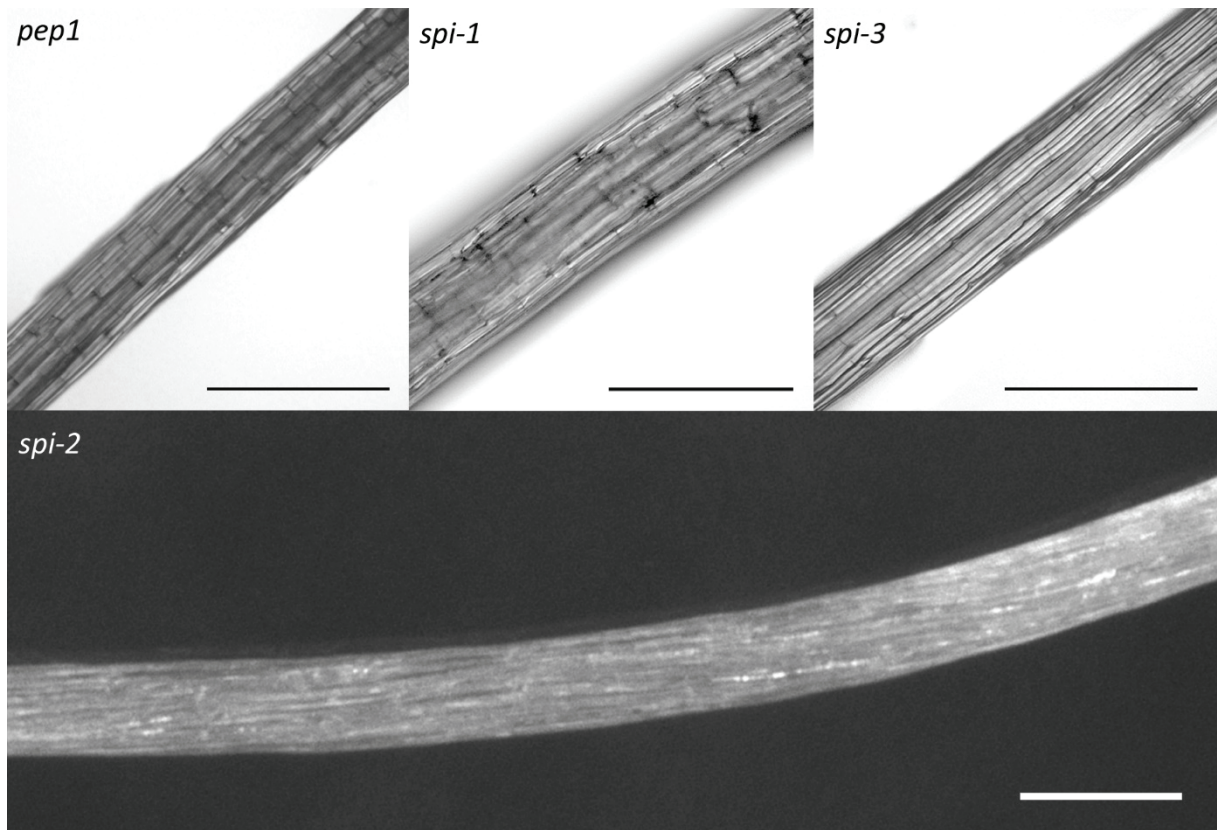


Figure 40: Dark grown hypocotyls of *pep1* and *Aaspi* mutants. Light-microscopic pictures of hypocotyls. The scale displays 500 μm .

Fragmented vacuoles

It was found that the *Arabidopsis spi* mutants show a 10 fold increased number of fragmented vacuoles in root hairs compared to the wild type (Saedler et al., 2009). In *Arabis*, no difference was visible between *pep1* and the *spi* mutants (Figure 41, Table 17).

Table 17: Fragmented root hair vacuoles in *pep1* and *Aaspi* mutants.

Root hairs were stained with FDA and integrity of vacuoles was analysed in >100 root hairs per line.

	<i>pep1</i>	<i>spi-1</i>	<i>spi-2</i>	<i>spi-3</i>
normal vacuoles [%]	93.58	94.17	93.16	93.79
fragmented vacuoles [%]	6.42	5.83	6.84	6.21

Results

Fragmented vacuoles could be observed, however, they only occurred rarely (Figure 41).

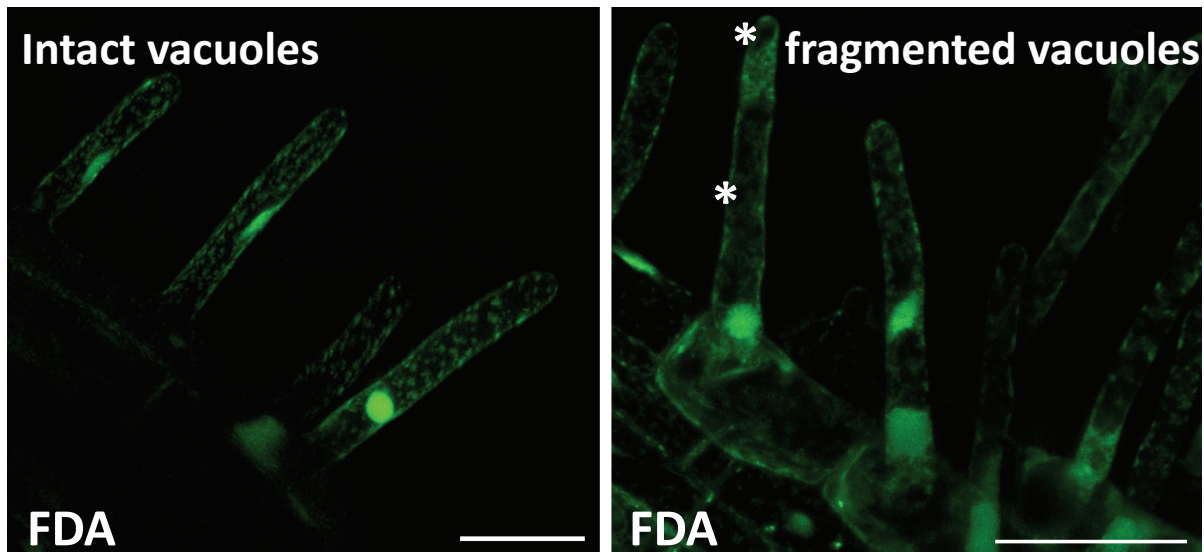


Figure 41: FDA staining of Arabis root hairs. Asterisks indicate fragmented vacuoles. Scale displays 50 μm .

3.6.3 *spi* and salt stress responses

Since the role of SPI in P-body formation and salt stress response is showing a novel feature of BEACH domain proteins, it is of high relevance for illuminating their biological mechanisms other than membrane trafficking.

3.6.3.1 Phenotypes

To learn more about the salt stress response in *spi*, stress assays were carried out under transpiring and non-transpiring conditions, as well as in different developmental stages.

Germination

Germination of *pep1* and the three *spi* mutants was analysed on MS plates and MS plates supplemented with 125 mM NaCl in three independent sets. The relative number of seeds germinated on salt media was normalized against the values from media containing no salt and combined between the sets (Figure 42).

Results

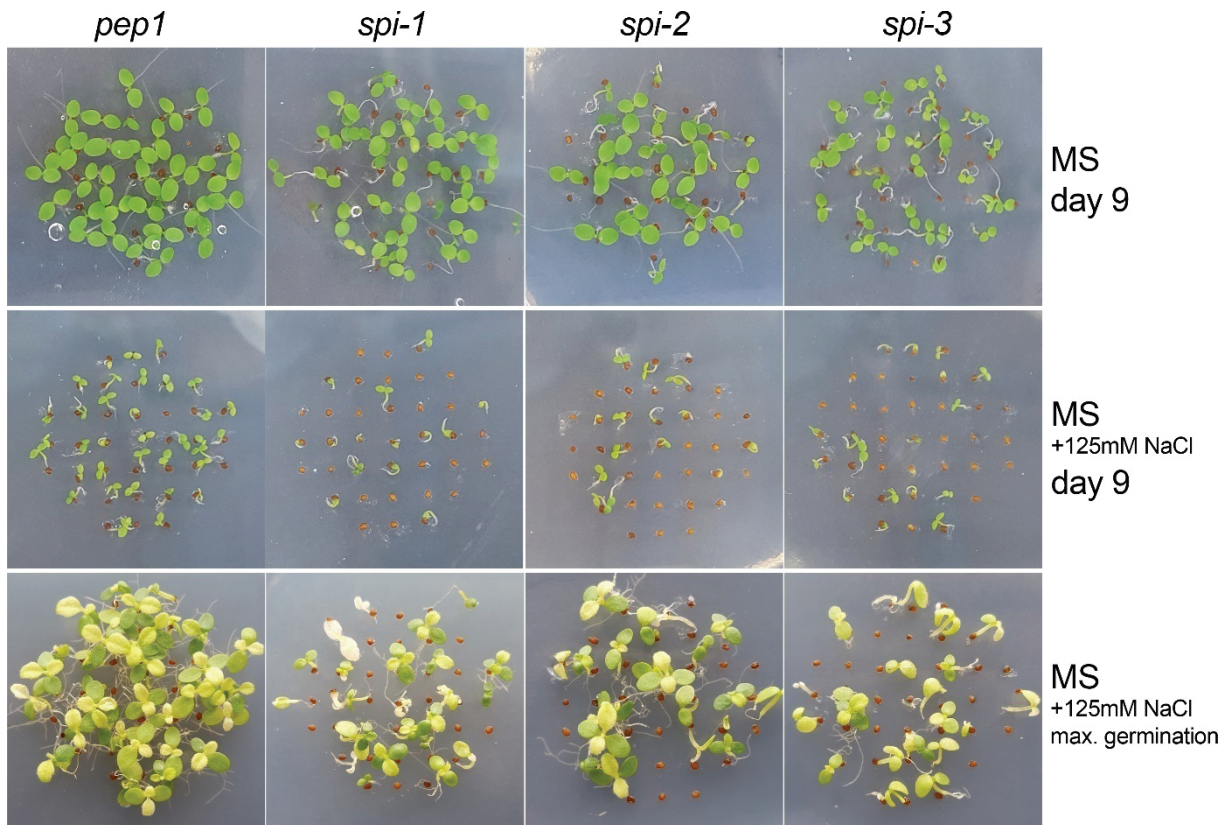
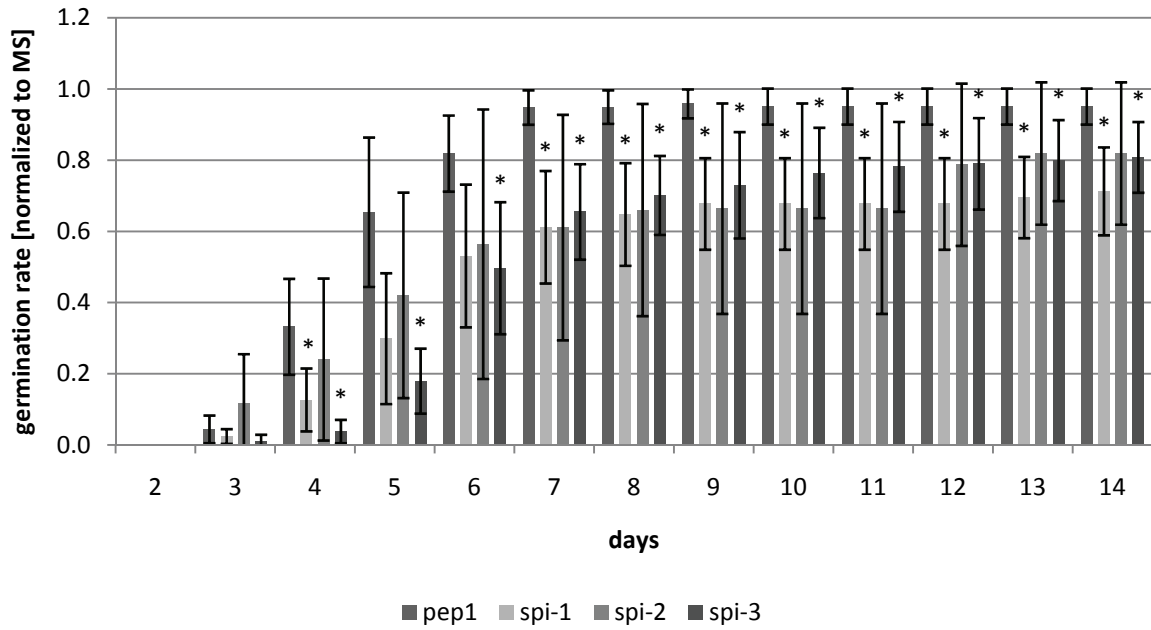


Figure 42: Germination of *pep1* and *spi* mutants under salt stress.

Germination of *pep1* and the three *spi* mutants was analysed on MS plates and MS plates supplemented with 125 mM NaCl in three independent sets (N>115 per line and condition). The relative number of seeds germinated on salt media was normalized against the values from media containing no salt and combined between the sets. Error bars depict standard deviations. Significance was tested using Mann-Whitney-U at a level of $p < 0.10$.

For *spi-1*, the delay in germination is not significant compared to *pep1*. However, the tendency towards later germination is still visible. The second allele showed the strongest

Results

variation in between the sets, resulting in the least reliable mean values. Despite highly similar average germination rates compared to *spi-1*, the germination of *spi-2* is not significantly different compared to *pep1*. In contrast, the delay in germination and the inhibition of germination under salt stress are significant for *spi-3*.

In addition to the slight differences in germination, the representative images in Figure 42 also display how the size of the germinated seedlings seems to be most comparable in between *pep1* and *spi-2*. So despite the obvious variability of the *spi-2* values between sets, the fact that the mean values were not significantly different in between *pep1* and *spi-2* might indeed reflect a phenotypic trait.

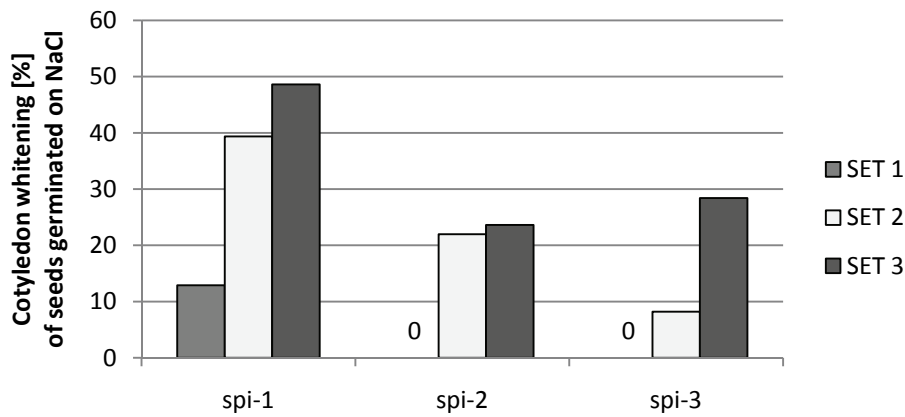
Cotyledon whitening

Cotyledon whitening was analysed after direct germination on salt (Figure 43A), transfer to salt 5 days after germination (Figure 43B) or transfer to salt 10 days after germination (Figure 43C).

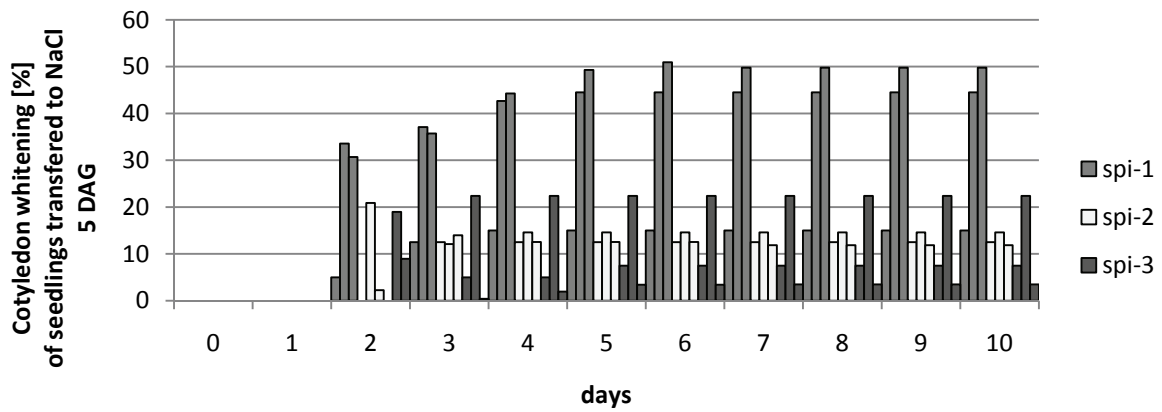
Due to extreme variations in between the sets, the cotyledon whitening assay was found to be rather unreliable in *Arabis*. Accordingly, the results will not be included. However, one aspect of this experiment was rather striking and the same tendency was observed for all sets: the general salt sensitivity decreases with the age of the plants. For *spi-1*, cotyledon whitening happens at a rate of 10-50% over background levels when exposed to salt for an extended period during germination and after five days of normal seedling growth, respectively. This percentage strongly decreases, to max. 25%, if seedlings are older when salt exposure starts. The other two alleles showed a less severe reaction to salt, however, the same tendency was also seen for *spi-2* and *spi-3*. The cotyledon whitening in *pep1* was at about 10% for each setup, showing that the salt response was not altered in the wild type depending on the age of the seeds/seedlings.

Results

A



B



C

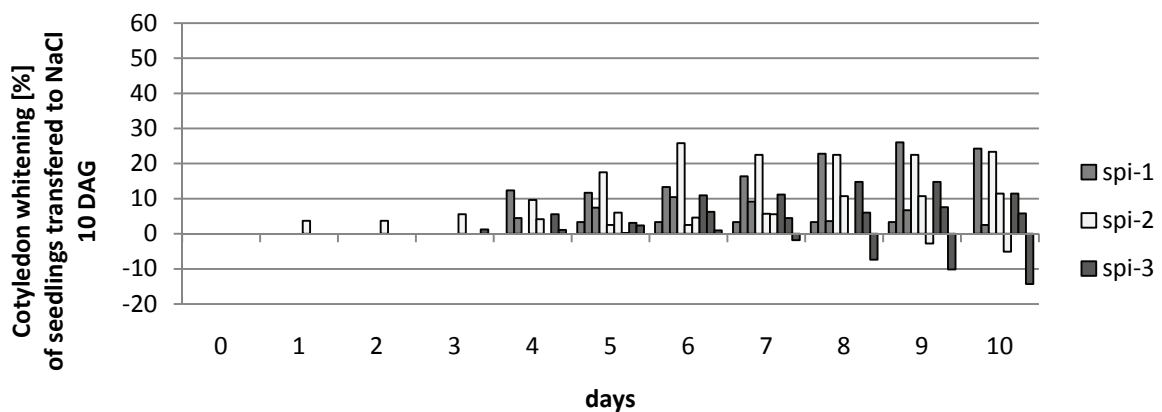


Figure 43: Cotyledon whitening of *Aaspi* mutants.

Values were normalized against *pep1*. The three independent sets are shown in the same shade, respectively. Cotyledon whitening was analysed A - after direct germination on salt (N=59-78 plants per line), B - transfer to salt five days after germination (N=63-88 plants per line), C - transfer to salt 10 days after germination (N=59-86 plants per line).

Results

Primary root growth

Primary root growth was determined on plates containing 0 mM NaCl, 75 mM NaCl and 125 mM NaCl for *pep1* and the three *spi* lines. Figure 44 displays the results after 4 days of growth. These did not differ from the results after eight days (data not shown). The standard deviations clearly show that the primary root growth within the lines was highly diverse. In addition, the three sets differed significantly and could therefore not be combined. Hence, the results have to be analysed with caution.

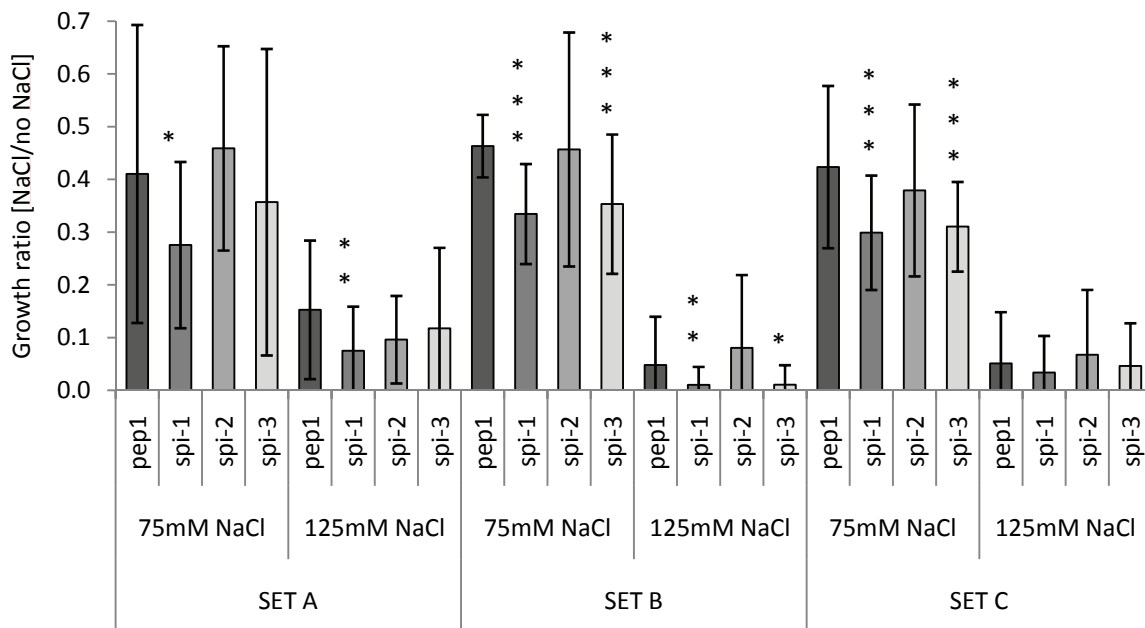


Figure 44: Primary root growth of *pep1* and *Aaspi* on different concentrations of NaCl after four days. Primary root growth under salt stress conditions was tested in three independent experiments (Sets A-C). The assays were carried out on plates containing 0 mM NaCl, 75 mM NaCl and 125 mM NaCl, respectively. Roots were measured after four days of growth. Significance of the data was tested using an ANOVA with $p < 0.001$ (***), $p < 0.01$ (**) and $p < 0.05$ (*). Total N per line per condition 93-128.

Especially at 75 mM NaCl, it is visible that the three lines show the same tendencies in each set: *spi-1* seems to have the strongest salt response, followed by *spi-3*, while *spi-2* seems to behave similar to *pep1*. At 125 mM salt, these tendencies are similar, only *spi-3* in set A seems to show a weaker reaction to salt. However, considering the high standard deviations, this observation cannot be fully trusted. After changing the measuring method for the root growth from set B onwards, the standard deviations seem to slightly decrease, thus, set B and C might be more reliable.

Results

Seedling growth

In *Arabidopsis*, seedling growth under salt stress conditions can be easily investigated by watering a mixture of sand and soil with MS medium containing different concentrations of salt. However, *Arabidopsis* plants were not capable of healthy growth under these conditions. The sand/soil mixture proved to be insufficient for the roots to anchor the plant. Hence, it was necessary to find other growth conditions to enable a salt treatment.

Two different kinds of hydroponic growth systems were tested, using agarose medium or stone wool. The agarose system proved to be unsuitable for *Arabidopsis* plants, due to their defects in gravitropism which often prevent the roots to grow straight downwards. The stone wool system was slightly more efficient, however, the survival rate of the plants was at about 20% due to early plant death within the first two weeks after germination. The plants which did survive the first two weeks were rather healthy. Figure 45 displays the relative weight of the plants after the treatment.

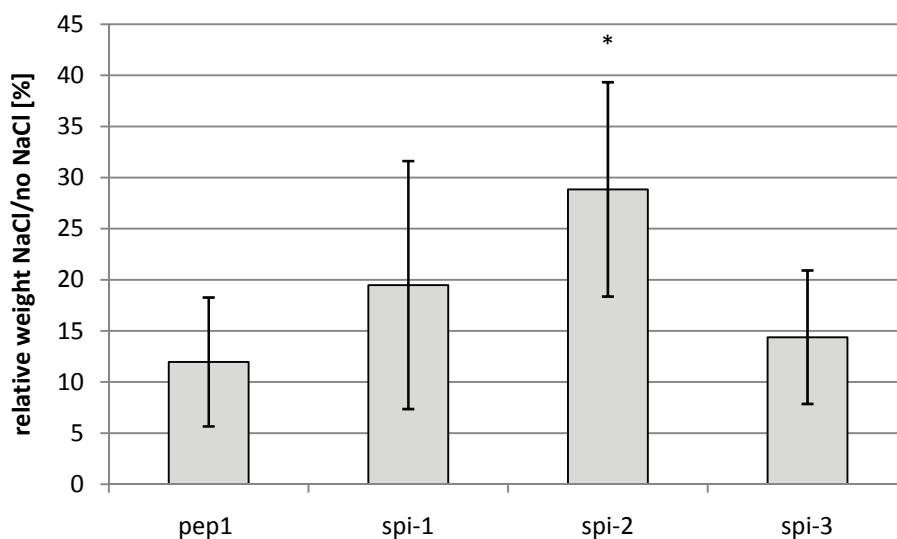


Figure 45: Seedling growth of *Arabidopsis alpine* lines on stone wool under salt stress.

Seedling growth under salt stress conditions was carried out on 77er trays supplemented with stone wool cubes. Plants were watered every 3-4 days from below with $\frac{1}{2}$ MS for the first 20 days, subsequently plants were watered with either $\frac{1}{2}$ MS or $\frac{1}{2}$ MS with 125 mM NaCl (N=5-12 per line and condition). The weight of the seedlings was determined after 30 days. Significance of the data was tested using a t-Test with $p < 0.001$ (***) , $p < 0.01$ (**) and $p < 0.05$ (*).

The fresh weight of all plants was reduced upon salt stress to 10-30% of the weight under non-stress conditions. The relative weight of *pep1*, *spi-1* and *spi-3* did not differ significantly. Surprisingly, *spi-2* was able to cope better with the salt treatment than *pep1*. However, due to the low number of plants which could be analysed, this experiment was only taken as a hint

Results

towards a reduction of the salt hypersensitivity in the *spi* mutants in later stages of development.

Since proper growth of *Arabidopsis* on sand/soil, agarose and stone wool was not possible, salt stress was applied to plants grown on soil. This method is not preferable, due to saline build-up that happens with organic matter in the soil. To counteract this problem, flood irrigation was used, which can wash out excess salt. Figure 46 displays the relative weight of the plants after the treatment.

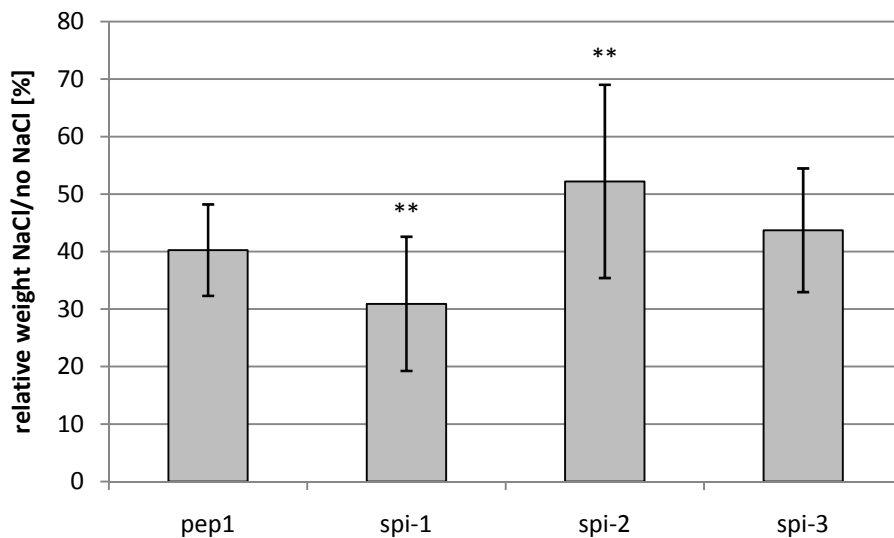


Figure 46: Seedling growth of *Arabidopsis* lines on soil under salt stress.

Seedling growth under salt stress conditions was carried out on soil. Plants were watered every 3-4 days with water for the first 20 days, subsequently plants were watered with either water or water with 125 mM NaCl (N=27-31 per line and condition). The weight of the seedlings was determined after 30 days. Significance of the data was tested using ANOVA with $p < 0.001$ (***) , $p < 0.01$ (**) and $p < 0.05$ (*).

As already seen for the growth on stone wool, *spi-3* does not exhibit salt hypersensitivity at this stage of development. Here as well, *spi-2* seems to be adapted to salt even better than *pep1*. In contrast to the first experiment, *spi-1* still shows salt hypersensitivity. Here again, the results should be discussed with caution, since so far only one experiment could be conducted.

3.6.3.2 Effect of salt stress on the localisation of SPI

The SPIRRIG gene encodes one of the longest proteins in Arabidopsis. With its CDS of 10802 bp, it is nearly ten times longer than the average Arabidopsis CDS, which is about 1200 bp. To date, it was only successful to amplify SPI in five parts and integrate these into vectors. Since AtSPI already proved to be a rather complicated gene to reconstruct (personal

Results

communication, M. Jakoby), it was unfortunate but not surprising that all attempts to create larger fragments of AaSPl by alignment PCR, restriction and general cloning methods, as well as Gibson Assembly (NEB) failed so far. With the NEBuilder technique (NEB), it was possible to create the C-terminal fragment, the PH-BEACH-WD40 (PBW) domain. This fragment shows the same localisation behaviour as the full length construct in Arabidopsis and was shown to be necessary and sufficient for protein binding.

The C-terminus of AaSPlRRIG shows a cytoplasmic localisation upon transient expression in tobacco and Arabidopsis (Figure 47), similar to the localisation of AtSPl and AtSPl-PBW.

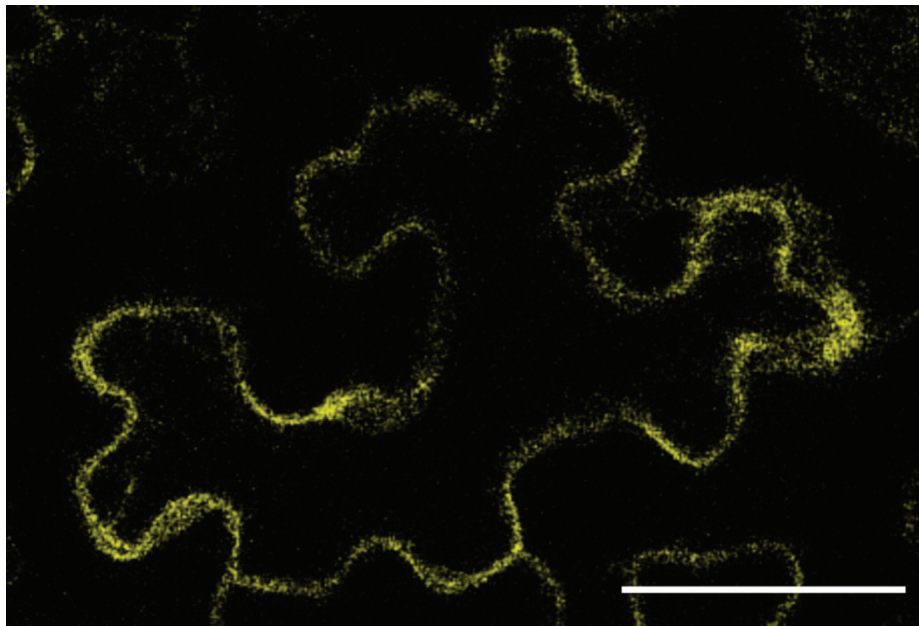
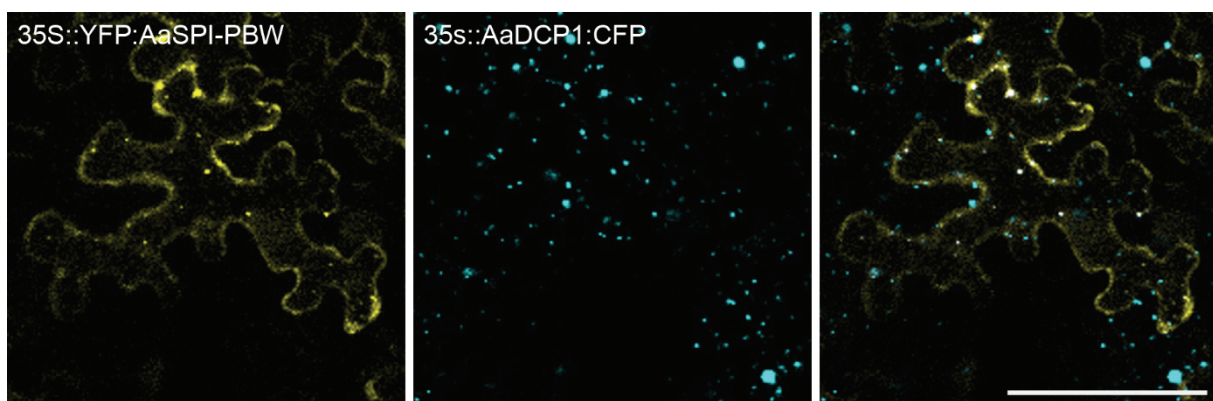


Figure 47: Localisation of 35S::YFP-SPI-PBW in tobacco leaves cells. Tobacco cells were transiently transformed by leaf infiltration with *Agrobacterium tumefaciens*. Scale shows 50 μm .

Under salt stress, SPI-PBW starts to accumulate in dot structures, which co-localise with DCP1 (Figure 48).



Results

Figure 48: Localisation of SPI-PBW under salt stress.

Tobacco cells were transiently transformed by leaf infiltration with *Agrobacterium tumefaciens* and stressed with 125 mM NaCl for 60 min. Scale shows 100 μ m.

Since this reaction of AaSPI to salt was also observed for AtSPI (Steffens et al., 2015), it is possible that in both species, SPI has a function at P-bodies, hence it might be involved in mRNA processing.

3.6.3.3 Effects of salt stress on transcript levels

It was found that AtSPIRRIG stabilizes a variety of transcripts in a salt dependent manner (Saedler et al., 2009). To carry out similar analyses via qPCR in Arabis, it was essential to first establish reliable reference genes and test those for their stability under salt stress.

Establishing new reference genes for *Arabis alpina*

The used reference genes were chosen due to their stable expression in other species, robust expression levels over different developmental stages or by considering their essential function for the organism (Table 18). All reference gene primers perform at a very good efficiency between 94 and 107% and a correlation between -0.99 and -1. These values lie well within the optimal range defined by the MIQE guidelines (Bustin et al., 2009). A detailed list of primers, their sequences and source, as well as the standard curves of the dilution series are attached in the appendix (Table 25, Figure 57).

Table 18: Primer efficiencies and correlation of reference genes for *Arabis alpina*.

Gene	Efficiency [%]	R ²
<i>ATPase</i>	98.33	-0.996
<i>Thioredoxin</i>	101.92	-0.992
<i>HCF</i>	99.98	-0.997
<i>EIF4a</i>	107.01	-0.992
<i>RAN3</i>	102.30	-0.998
<i>UBQ10</i>	102.52	-0.999
<i>Actin 2</i>	102.85	-0.999
<i>PSB33</i>	99.51	-1.000
<i>Histone H3</i>	99.14	-0.999
<i>NdhO</i>	94.34	-0.999
<i>TUA5</i>	98.32	-1.000
<i>18srRNA</i>	98.65	-1.000
<i>CAC</i>	98.07	-0.999
<i>SAND</i>	96.42	-0.999
<i>HSP81.2/90</i>	96.74	-0.999

Results

Reference gene stability under salt stress

All reference genes were tested on cDNA from Arabis seedlings grown under normal and salt stress conditions. The quantity values of both treatments are displayed in Figure 49. Here, strong differences between salt and no salt conditions are visible for HCF, EIF4a, RAN3 and HSP81.2/90. In contrast, the expression of TUA5, PSB33 and CAC turned out to be extremely similar under both conditions.

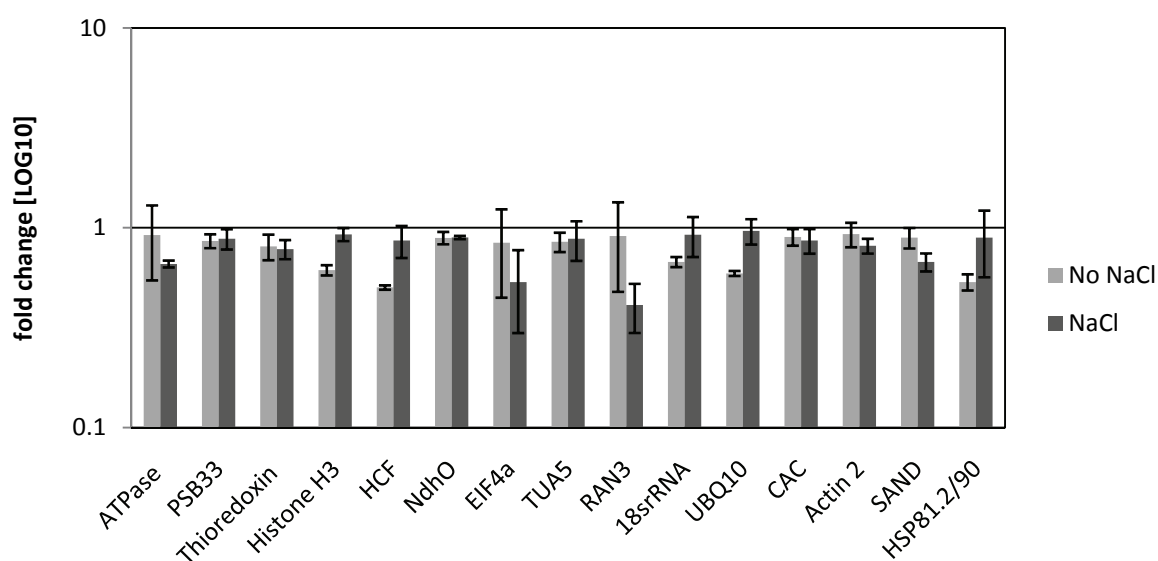


Figure 49: Quantity values of reference gene expression under control and salt stress conditions. The error bars depict the standard deviation.

The stability values of the reference genes were calculated with the NormFinder, BestKeeper and geNorm software, respectively. The results are displayed in Table 19.

Table 19: Gene expression stability under salt stress.

Genes were ranked using the three commonly used software programs NormFinder, BestKeeper and geNorm.

Rank	NormFinder		BestKeeper		geNorm	
	Gene	Stability	Gene	Stability	Gene	Stability
1	<i>PSB33</i>	0.086	<i>TUA5</i>	1.161	<i>CAC</i>	0.540
2	<i>TUA5</i>	0.088	<i>CAC</i>	1.180	<i>PSB33</i>	0.547
3	<i>Thioredoxin</i>	0.100	<i>Actin 2</i>	1.190	<i>TUA5</i>	0.555
4	<i>CAC</i>	0.103	<i>18srRNA</i>	1.192	<i>Thioredoxin</i>	0.555
5	<i>Actin 2</i>	0.153	<i>PSB33</i>	1.225	<i>Actin 2</i>	0.555
6	<i>NdhO</i>	0.155	<i>SAND</i>	1.234	<i>Histone H3</i>	0.596
7	<i>Histone H3</i>	0.230	<i>Thioredoxin</i>	1.243	<i>NdhO</i>	0.611

Rank	NormFinder		BestKeeper		geNorm	
	Gene	Stability	Gene	Stability	Gene	Stability
8	<i>SAND</i>	0.267	<i>NdhO</i>	1.255	<i>UBQ10</i>	0.630
9	<i>18srRNA</i>	0.286	<i>Histone H3</i>	1.255	<i>SAND</i>	0.655
10	<i>UBQ10</i>	0.300	<i>UBQ10</i>	1.330	<i>18srRNA</i>	0.706
11	<i>HCF</i>	0.363	<i>HCF</i>	1.404	<i>HCF</i>	0.707
12	<i>ATPase</i>	0.387	<i>ATPase</i>	1.594	<i>ATPase</i>	0.832
13	<i>EIF4a</i>	0.500	<i>HSP81.2/90</i>	1.902	<i>HSP81.2/90</i>	1.090
14	<i>HSP81.2/90</i>	0.688	<i>EIF4a</i>	1.968	<i>EIF4a</i>	1.163
15	<i>RAN3</i>	0.728	<i>RAN3</i>	2.461	<i>RAN3</i>	1.413

The stability values are not comparable between the different software, due to different statistical models used. However, the simple addition of the ranks leads to a ranking of the best reference genes over all three methods (Table 20).

Table 20: Ranking of stable reference genes under salt stress.

Gene	NormFinder	BestKeeper	geNorm	SUM
<i>TUA5</i>	2	1	3	6
<i>CAC</i>	4	2	1	7
<i>PSB33</i>	1	5	2	8
<i>Actin 2</i>	5	3	5	13
<i>Thioredoxin</i>	3	7	4	14
<i>NdhO</i>	6	8	7	21
<i>Histone H3</i>	7	9	6	22
<i>SAND</i>	8	6	9	23
<i>18srRNA</i>	9	4	10	23
<i>UBQ10</i>	10	10	8	28
<i>HCF</i>	11	11	11	33
<i>ATPase</i>	12	12	12	36
<i>HSP81.2/90</i>	14	13	13	40
<i>EIF4a</i>	13	14	14	41
<i>RAN3</i>	15	15	15	45

The geNorm software was used to calculate the number of reference genes which should be used for an adequate normalization under salt stress conditions (Figure 50). The maximum value marking a good stability is a pair wise variation of 0.15 according to the geNorm

Results

manual. For the given setup of the experiment, it is therefore possible to work with only two reference genes since the pair wise variation of two to three genes (V2/3) is already well beneath the cut-off with a pair wise variation of 0.08.

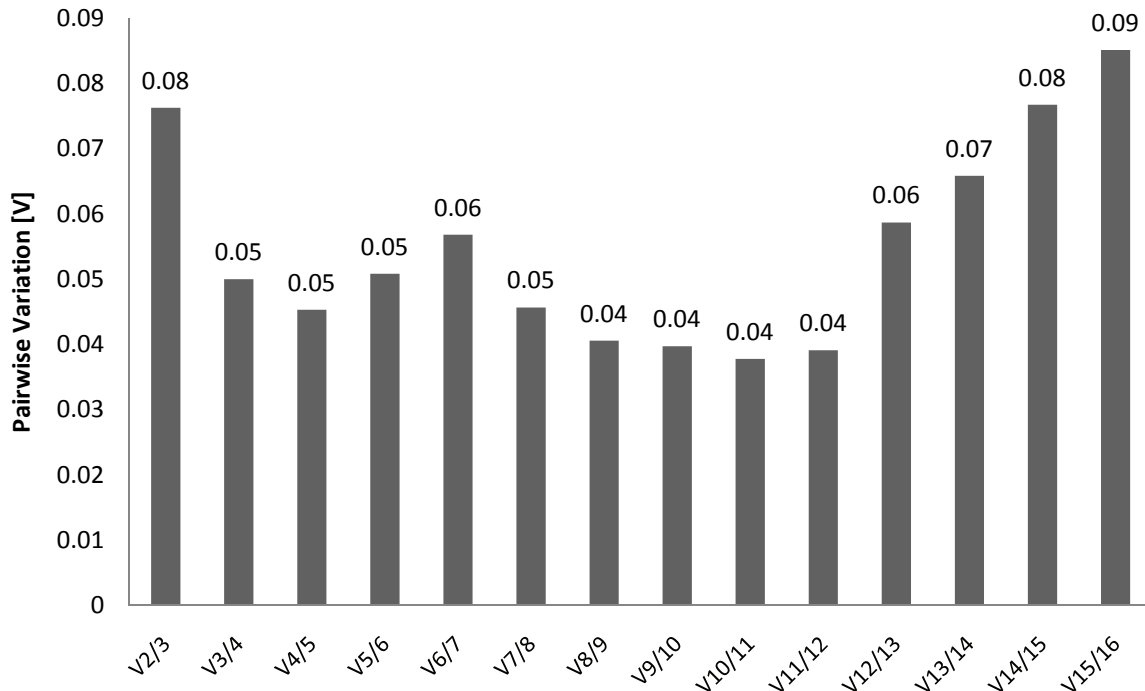


Figure 50: Determination of the optimal number of control genes for normalization. Pair wise variation was determined using the geNorm software (Vandesompele et al., 2002). Threshold for adequate variation is 0.15.

Hence, TUA5 and CAC were chosen for normalization of expression data from plants grown under salt stress in *Arabidopsis thaliana*.

Monitoring salt stress

Apart from adequate normalization, it is essential for the qPCR experiment to verify that a specific treatment was successful. Hence, RNAseq data from *Arabidopsis thaliana* (Steffens et al., 2015) was used to identify a gene which is strongly upregulated under salt stress, making it a suitable salt stress indicator.

The protein chosen was ethylene and salt inducible 1 (ESI1), an integrase-type DNA-binding superfamily protein which encodes a member of the ERF (ethylene response factor) subfamily B-3 of the ERF/AP2 transcription factor family (www.ncbi.nlm.nih.gov). The primers used for qPCR analysis reached an efficiency of 104% and a correlation of -0.99 (Table 25, Figure 57). Figure 51 displays the relative fold change under salt stress.

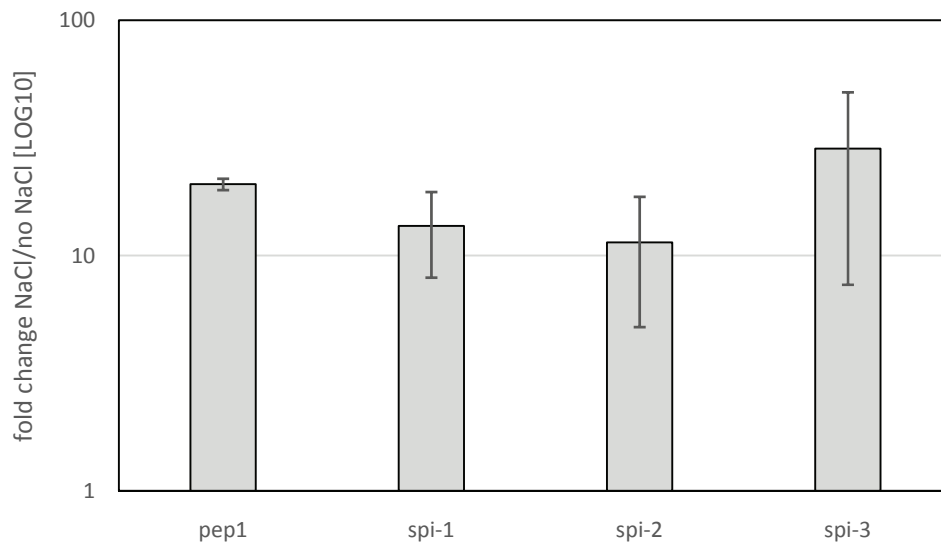


Figure 51: Transcript levels of AaESE1 under salt stress. Normalisation was carried out against CAC and TUA5. Error bars depict standard deviation. Significance was determined using a Mann-Whitney-U test at $p < 0.10$.

For all lines tested, fold changes of more than 10 fold could be observed in the salt treated samples.

Differential regulation of transcripts in *spi* mutants

In Arabidopsis, 483 genes were found to be differentially regulated in between the wild type and *spi* (Steffens et al., 2015). Within this group, several genes were of particular interest, due to their extreme up- or downregulation in *spi* or due to the pathways they are involved in. 5 transcripts were chosen for a qPCR analysis in Arabis.

The first protein which was chosen, TSPO-related (OUTER MEMBRANE TRYPTOPHAN-RICH SENSORY PROTEIN-related), showed an upregulation in RNAseq of more than 1.41 fold in the *spirrig* mutant under normal conditions and 0.22 fold under salt stress, compared to Col-0 under the same conditions. TSPO-related is a membrane-bound protein which can be induced in vegetative tissues by osmotic or salt stress, as well as abscisic acid treatment. The protein is located in the endoplasmic reticulum and Golgi stacks (Berardini et al., 2015b). In accordance with its function in salt stress, it was upregulated 179 fold (*spi*) and 791 fold (Col-0) in salt treated samples. The primers used for qPCR analysis reached an efficiency of 104% and a correlation of -0.99 (Table 25, Figure 57).

Results

Figure 52 shows the results of the qPCR analysis in *Arabidopsis*: the expression levels in the *spi* mutants under normal conditions were comparable to *pep1*. When treated with salt, the transcript levels in all lines increased strongly, however, no significant difference was visible comparing *pep1* and the *spi* mutants.

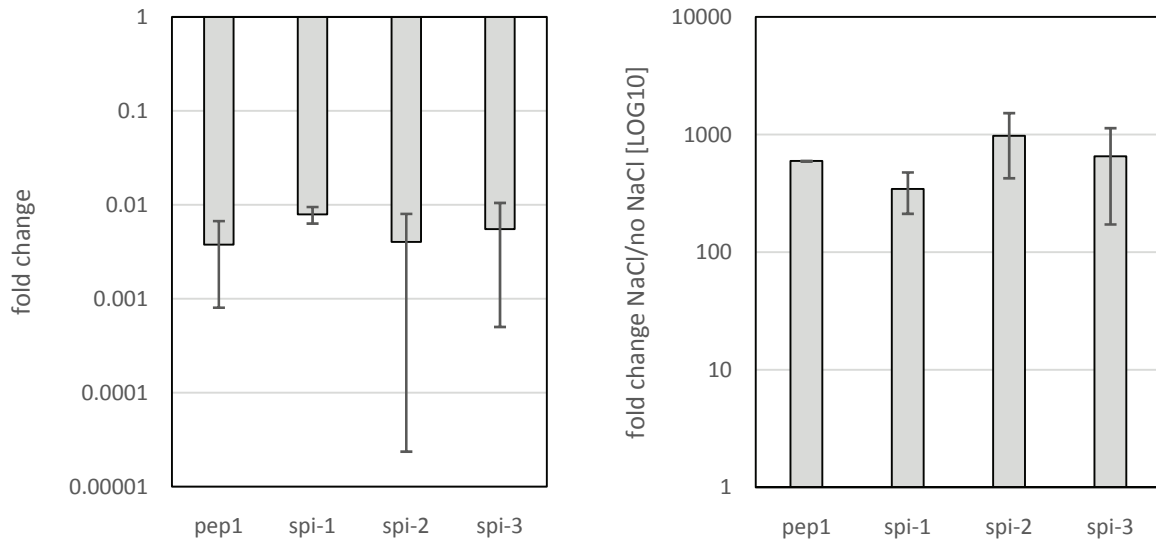


Figure 52: Relative transcript levels of TSPO-related protein in response to salt stress. Normalisation was carried out against CAC and TUA5. Error bars depict standard deviation. Significance was determined using a Mann-Whitney-U test at $p < 0.10$.

The next transcript chosen was downregulated 0.25 fold when comparing the salt responses of *spi* with that of the wild type: AT3G07250 is a nuclear transport factor 2 (NTF2) family protein. The NTF2 domain is named after a homodimer, which is able to stimulate the transport of a cargo protein to the nucleus. In addition, AT3G07250 has a function in RNA binding and is likely to function as a ribonucleoprotein complex (Lamesch et al., 2012). The primers used for qPCR analysis reached an efficiency of 93 % and a correlation of -0.99 (Table 25, Figure 57).

The transcript is slightly downregulated in the mutants, even significantly downregulated in *spi-3* (Figure 53). In addition, NTF2 family protein mRNA levels are strongly increased under salt stress, with a significantly higher upregulation in all three mutants.

Results

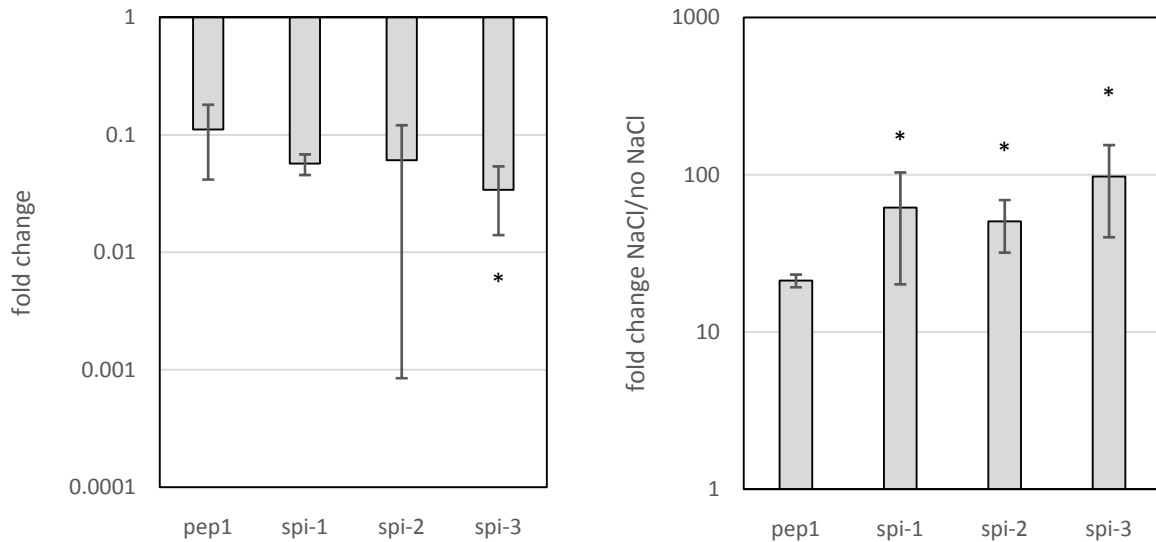


Figure 53: Relative transcript levels of NTF2 family protein in response to salt stress. Normalisation was carried out against CAC and TUA5. Error bars depict standard deviation. Significance was determined using a Mann-Whitney-U test at $p < 0.10$.

The third gene, AT5G59310, encodes lipid transfer protein 4. Proteins of this family are able to bind fatty acids and acylCoA esters. They can transfer phospholipids and function in response to abscisic acid, salt stress and drought (Lamesch et al., 2012). In the RNAseq analysis, this transcript was upregulated 4.28 fold when comparing the salt responses of *spi* with that of Col-0. The primers used for qPCR analysis reached an efficiency of 92% and a correlation of -0.99 (Table 25, Figure 57).

For this gene, transcript levels were comparable between *pep1*, *spi-1* and *spi-3* in qPCR. In contrast, *spi-2* showed strongly decreased amounts of transcript compared to *pep1*, and a much stronger upregulation in salt conditions (Figure 54).

Results

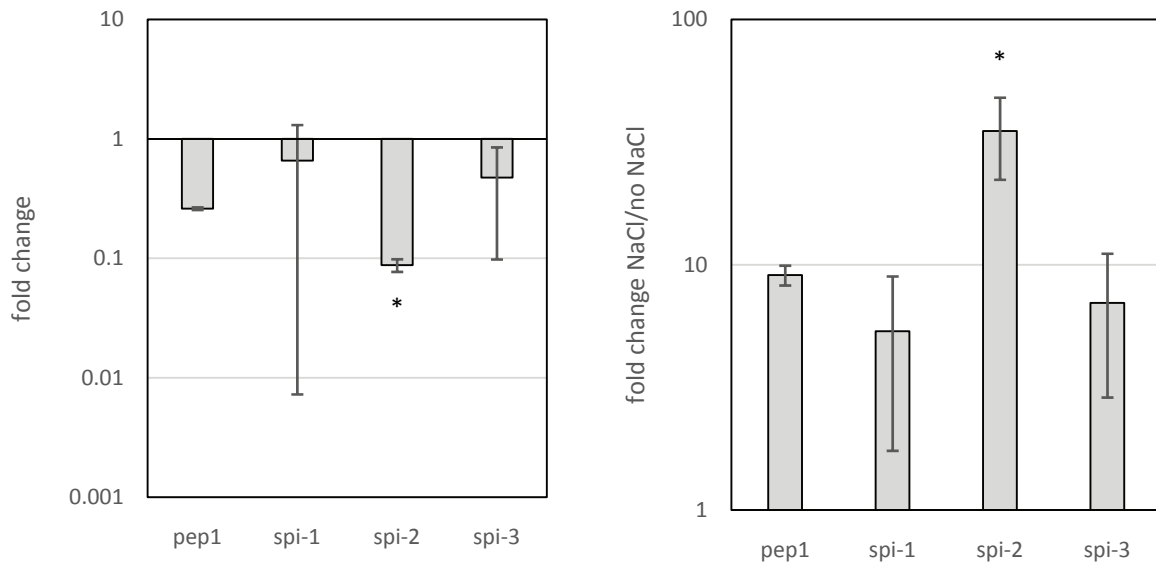


Figure 54: Relative transcript levels of lipid transfer protein 4 in response to salt stress. Normalisation was carried out against CAC and TUA5. Error bars depict standard deviation. Significance was determined using a Mann-Whitney-U test at $p < 0.10$.

The fourth gene is AT1G71520, an integrase-type DNA-binding superfamily protein with DNA-binding transcription factor activity which is involved in ethylene-activated signalling, regulation of transcription and response to chitin (Lamesch et al., 2012). In the RNAseq analysis, it was upregulated in the mutant under normal conditions by 3.73 fold, and downregulated 0.23 fold more under salt than the wild type. The primers used for qPCR analysis reached an efficiency of 88% and a correlation of -0.99 (Table 25, Figure 57).

In the qPCR analysis, *pep1*, *spi-2* and *spi-3* were comparable under normal conditions. However, the transcript of the integrase-type DNA-binding superfamily protein was much higher in *spi-1* compared to all other lines. Under salt conditions, all *spi* mutants showed a decreased upregulation compared to *pep1*, with *spi-1* having the least severe reaction to salt (Figure 55).

Results

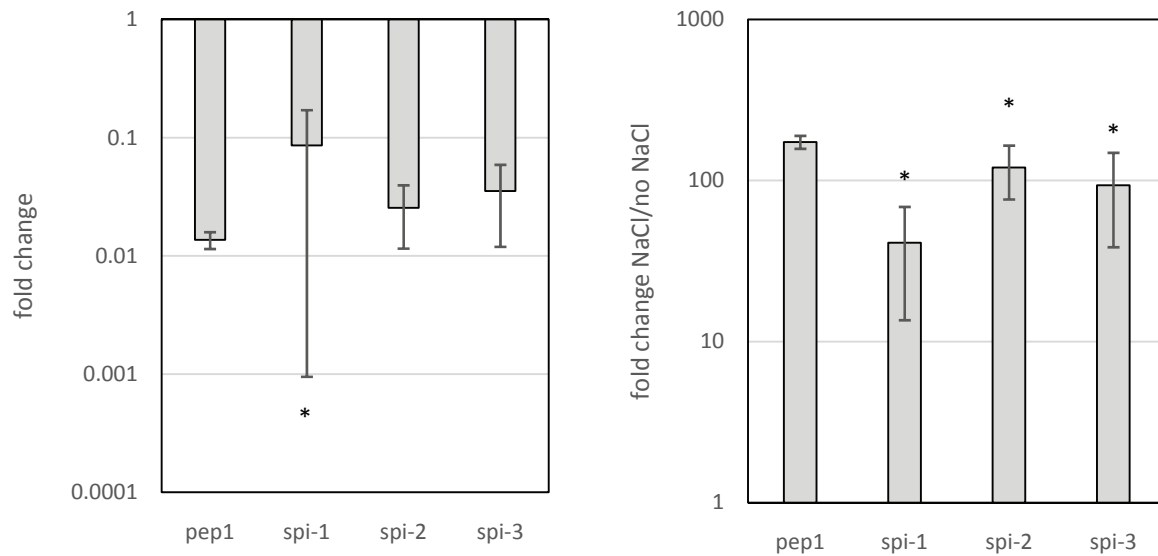


Figure 55: Relative transcript levels of an integrase-type DNA-binding superfamily protein in response to salt stress.

Normalisation was carried out against CAC and TUA5. Error bars depict standard deviation. Significance was determined using a Mann-Whitney-U test at $p < 0.10$.

The last gene chosen was AT3G44860, which encodes FARNESOIC ACID CARBOXYL-O-METHYLTRANSFERASE (FAMT). The role of farnesoic acid in plants has not been revealed so far. However, it is known that in insects, Juvenile hormone III is produced by methylated farnesoic acid. This hormone regulates crustacean development and it was found that plants with high levels of it have a better defence against insects. However, the transcript level of FAMT is increased upon various stresses, indicating that it might have more general functions in stress responses (Yang et al., 2006). In the RNAseq analysis, the transcript was upregulated 13 fold in the mutant, and 0.12 fold less upregulated under salt stress. The primers used for qPCR analysis reached an efficiency of 89% and a correlation of -0.99 (Table 25, Figure 57).

In the qPCR, transcript levels were shown to behave similarly for *pep1*, *spi-2* and *spi-3* under both conditions (Figure 56). In *spi-1*, transcript levels showed a tendency to be higher under normal conditions, however, this difference was not significant. Under salt stress, the increase of transcript was significantly less in *spi-1* compared to *pep1*.

Results

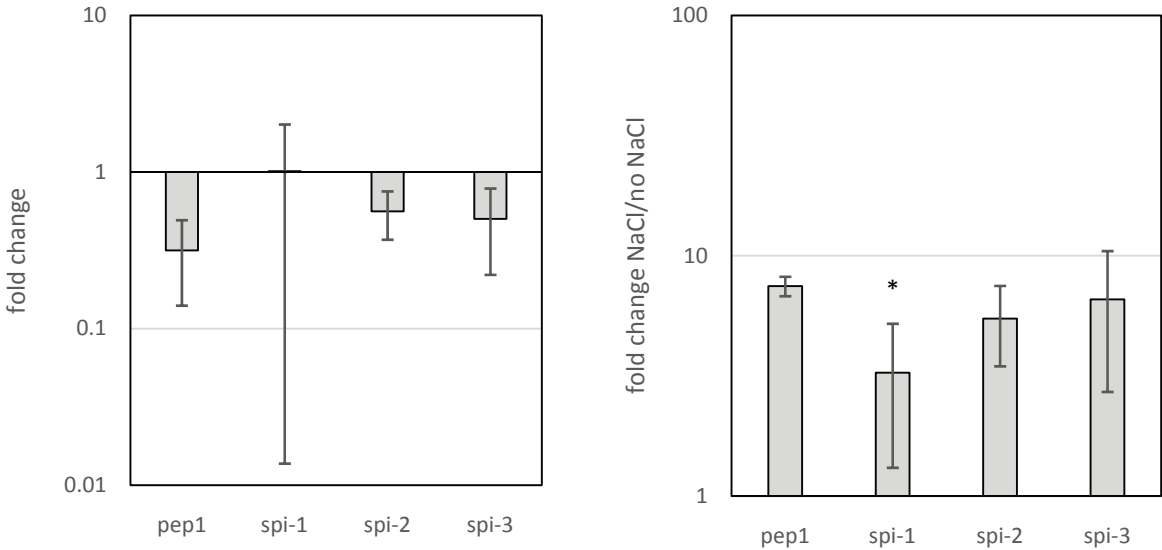


Figure 56: Relative transcript levels of FAMT in response to salt stress. Normalisation was carried out against CAC and TUA5. Error bars depict standard deviation. Significance was determined using a Mann-Whitney-U test at $p < 0.10$.

4 Conclusions

I. Cytoplasmic streaming

Over the last decades, the actomyosin system has been in the focus of numerous studies. Actin is of such great importance for plant performance that scientists were initially surprised to find that the loss of certain myosins does not have a significant effect on plant morphology (Duan and Tominaga, 2018; Peremyslov et al., 2008). Over the years, the high level of redundancy of these molecular motors was revealed, and has been most challenging for experimental design (Duan and Tominaga, 2018).

In order to reveal the dynamics of cytoplasmic streaming, and the roles of myosins XI-1, XI-2, XI-I and XI-K in particular, a broad spectrum of analyses was carried out in this study. Surprisingly, the obtained results put various former hypotheses about cytoplasmic streaming in question.

Stirring is not sufficient to enhance organelle movement or bulk flow in Arabidopsis leaves

In 2008, the concept of cytoplasmic streaming as a unidirectional, constant flow of cytoplasm was found to be incompatible with organelle movement patterns. As organelles were found to have multidirectional, saltatory movements with varying velocities, cytoplasmic stirring was proposed to be the more adequate concept to describe the mechanisms behind cytoplasmic streaming (Avisar et al., 2008; Prokhnevsky et al., 2008). It was assumed that directionally moving myosins locally stir the cytoplasm and thereby accelerate it. This would lead to both, an increased bulk flow and - as a result - faster movement of organelles or vesicles in the cytoplasm. However, the results obtained in this study indicate that both assumptions have to be rejected.

The bulk flow of the cytoplasm in Arabidopsis leaf cells was found to be unaltered by myosin loss or disintegration of the actin cytoskeleton. Although this observation seems contradictory at first, it indeed is coherent with a study in tobacco, which was able to show that the bulk flow is only accelerated in large cells with vigorous directed movement (Esseling-Ozdoba et al., 2008). In Arabidopsis pavement cells, neither the size nor the velocity of myosin mediated transport reaches the necessary threshold. Thus, it can be assumed that stirring does not have a significant effect on the passive flow in these cells in Arabidopsis.

Conclusions

In addition, it was shown in this work that the molecular stirrer XI-K Δ GTD-2xYFP is not capable of restoring movement of organelles in the *12k*_{XI-K Δ GTD-2xYFP} transgenic line to a significant extent. Its functionality can be assumed, due to the occasional entrainment of organelles and its visible movement. Nevertheless, the stirring effect of XI-K Δ GTD-2xYFP was found to be negligible in Arabidopsis leaf cells. Considering the small size of the YFP-YFP tag in comparison to an organelle, it could be assumed that the sheer size of the stirrer might play a role for its effect on organelle movement. Nevertheless, the actual entrainment of organelles could only be mediated by acceleration of the bulk flow. This however, was shown to be independent of stirring in this study.

In addition, it was found that the defects of the actin cytoskeleton cannot be restored by XI-K Δ GTD-2xYFP. This was a rather surprising result, considering that the molecular stirrer is capable of fast movements. At this point, it can only be assumed that the GTD itself, or the stabilisation of the myosin dimer by cargo binding (Li and Nebenführ, 2008a) are essential to maintain an intact actin cytoskeleton. Indeed, first results indicate that upon cargo binding via the nanobody construct, actin organisation can be restored in *12k* mutants expressing XI-K Δ GTD-2xYFP (data not shown).

Myosin XI-K is essential for long range transport of P-bodies and peroxisomes

Myosin XI-K has been found to be essential for long range transport of P-bodies (Steffens et al., 2014b) and was proposed to mediate peroxisome movement together with XI-2 (Peremyslov et al., 2008; Prokhnevsky et al., 2008). In this work, movement of P-bodies was systematically analysed in single and multiple mutants of myosins XI-1, 2, I and K, in order to elucidate the involvement of all four myosins.

For P-body transport, it was found that XI-K is indeed the only factor mediating fast movements. In addition, Myosin XI-I is least redundant to XI-K, showing no synergistic effects in the *ik* double mutant, in contrast to strong effects in *1k* and *2k*. Furthermore, XI-I is likely to be more redundant to XI-1 than XI-2, since *1IK* shows a significantly stronger decrease in speed than *2IK*. These results are coherent with the phylogenetic analysis, as well as the results gained regarding myosin dimerisation: XI-1 and XI-I seem to be highly redundant, are capable of forming heterodimers, and are most closely related. In contrast, XI-2 is likely to only function as a homodimer. It shows the least sequence similarity to the other three myosins and seems to be the least involved in P-body binding, according to the analysis of the dominant negative effect. In contrast, myosin K is essential for long range movement

Conclusions

and is capable of forming heterodimers with XI-1 and XI-I, making it the most important myosin for P-body movement.

The peroxisome movement was analysed for the *xi-2* mutant, as a strong involvement of myosin 2 in peroxisome transport was contradictory to results obtained in this work. It was shown, that peroxisome movement in the *xi-2* mutant was similar to wild type. This observation, together with former results (Duan and Tominaga, 2018; Peremyslov et al., 2008) indicate that only XI-K is essential for long range transport of peroxisomes.

The dominant negative effect is mostly mediated by blocking of cargo binding sites

The results obtained in this study indicate that there is probably no myosin activation and deactivation through conformational change. However, even if the yeast 2-hybrid data does not reflect the situation *in planta*, it is very unlikely that conformational change is involved in the dominant negative effect of GTDs. It was shown that the dominant negative effect of GTDs can be reversed by providing alternative anchoring of myosins and Golgi bodies, which is bridging the blockage of cargo binding sites.

The distorted phenotype can be induced despite an intact actin cytoskeleton

The findings of this study allow the assumption that the morphological phenotypes seen in the *xi-k* deficient mutants are not caused by the consequences of reduced bulk flow. Hence, the actual cause is either the loss of directed transport by XI-K itself and/or the alterations of the actin cytoskeleton. However, it was shown in the transgenic Col-0_{35S::YFP:XI-K-GTD} line that distorted trichomes are formed although the actin cytoskeleton is intact and XI-K is present. Here, only the cargos were blocked by free GTDs, indicating that the directed transport of XI-K cargos is the underlying reason for the distorted trichomes.

Myosin loss causes a selection disadvantage under non-optimal conditions

In the early 2000s, it was an unexpected discovery that none of the myosin *xi* mutants in *Arabidopsis* exhibit obvious phenotypes under normal conditions (Prokhnevsky et al., 2008). Even though this is a reflection of their high level of functional redundancy, it is striking that even quadruple mutants perform rather well in optimal conditions (Prokhnevsky et al., 2008).

In this study, it was shown that the triple mutants *12k* and *2ik* show a reduced reaction to long term heat, while the quadruple mutant shows no heat reaction at all. These results indicate an involvement of all four myosins in the morphogenic changes *Arabidopsis* plants undergo as a response to heat. However, there seems to be no absolute necessity for fast movement

Conclusions

mediated by XI-K for this process, as *xi-k* single, double and the *lik* triple mutant do not have a heat phenotype. Furthermore, myosins XI-1, 2 and K seem to be most involved in the underlying process, as the reaction to heat is more reduced in the *l2k* mutant than in *2ik*.

In addition, it was found that these three lines show (significant) reduction of hypocotyl growth in the dark. While *l2k* only shows a slight tendency towards shorter hypocotyls, growth in *2ik* and the quadruple mutant is severely reduced. Here again, XI-K loss does not explain the phenotype. Although the defect is strongest in the quadruple mutant, myosins 2, I and K seem to have the most impact on this rapid cell growth.

Since the heat reaction and skotomorphogenesis can be essential for plant survival, it can be concluded that myosins XI-1, XI-2, XI-I and XI-K have synergistic effects in and are of great importance for morphological adaptation under non optimal conditions.

Outlook

It was found that myosin XI-K is solely mediating long range transport of P-bodies and peroxisomes. Consequently, it will be a challenge in the future to distinguish between the effects of movement inhibition of each organelle. It will be crucial to re-mobilise each organelle individually and create stable lines, allowing detailed analyses of the phenotypes.

It was successful to generate the coding sequences of three full length myosins. The XI-K full length construct was already shown to express a functional protein. In the future, the CDS sequence of this construct can be introduced into vectors encoding stronger fluorophore tags emitting blue or red, to finally build a set of functioning constructs. In order to express these together and create stable lines with all myosins, it might be helpful to create constructs under the endogenous promoters, as this proofed to be successful in the *l2k^R* line (Peremyslov et al., 2012).

II. SPIRRIG

The Brassicaceae *Arabis alpina* was selected for the analysis of the BEACH domain protein SPIRRIG, since it is closely related to Arabidopsis, allowing a direct comparison, while being distant enough to expect different phenotypes and molecular functions. In accordance, it was found in this work that three EMS *Aaspirrig* mutants do indeed show strong similarities and differential behaviour. Thus, it was possible to draw several conclusions, which will proof valuable to reveal more details about SPIRRIG function in the future.

Conclusions

The distorted phenotype is similar in *Arabis* and *Arabidopsis*

In this work, three *Arabis spirrig* mutant alleles in the *pep1* background were analysed. *spi-1*, with a premature stop codon within the PH domain; *spi-2*, truncated by only 193 amino acids within the WD40 repeats; and *spi-3*, in which no functional domain remained intact, due to a very early stop codon within the Armadillo repeats. These mutant alleles share three phenotypes: lower cell complexity of cotyledon cells, short root hairs and distorted trichomes. These phenotypes are well conserved in *Arabidopsis* and *Arabis*, indicating similar functions of the SPIRRIG protein. For both species, it was shown that the mRNA of SPIRRIG is expressed at wild type level, indicating that these phenotypes are not influenced by the amount of transcript. However, it is still to be determined if altered translation, post-translational modification or folding of the protein play a role in the phenotype. On the DNA/mRNA level, the only common feature of all three alleles is the (partial) lack of the WD40 repeats, indicating that this domain might play a role in the observed phenotypes.

SPIRRIG is differentially regulated in *Arabis* hypocotyls

The phenotypic analysis of *pep1* and *spirrig* revealed that the hypocotyls of the mutants were (significantly) longer than those of *pep1*. This phenotype is opposed to *Arabidopsis spi*, in which the hypocotyls were found to be half as long as the wild type's. In addition, no out-curved and disconnected hypocotyl cells of dark grown seedlings were observed in *Arabis*. However, this observation has to be treated with caution, since this phenotype was found to be hard to reproduce even in *Arabidopsis* (personal communication, M. Hülkamp).

One possible explanation for these observations could be the expression of the SPIRRIG mRNA in *Arabis* hypocotyls. In this work, it was shown that the levels of transcript are reduced in the hypocotyl compared to other tissues of the plant. This might not have a functional relevance, or could just as well be the underlying reason why the loss of the functional protein does not have a severe negative effect.

SPIRRIG is not essential for vacuolar integrity in *Arabis* root hairs

WD40/BEACH domain proteins are known mediators of vacuolar integrity. They evolved before the separation of plants and animals and consist of four distinct groups (De Lozanne, 2003). The *SPI* gene belongs to the same clade as the WD40/BEACH domain protein *LvsA* from *Dictyostelium* (Saedler et al., 2009), whose loss causes fragmentation of the contractile vacuole (Gerald et al., 2002). Based on this knowledge, vacuoles in root hairs of *Arabidopsis spi* were studied and found to have a strongly increased number of fragmented vacuoles as

Conclusions

well (Saedler et al., 2009). In *Arabis*, this phenotype could not be observed. Fragmented vacuoles were found rarely and to the same extent in background and mutant. This is quite surprising, given the conservation of this function beyond kingdoms. Nevertheless, the results obtained in this work indicate that the *Arabis* version of the SPIRRIG protein is not essential for vacuolar integrity (in root hairs).

The salt stress response differs in between *spi* alleles

It was shown in this work that the distorted phenotype of trichomes, the reduced complexity of cotyledon cells and the decreased length of root hairs do not differ in the three *spi* alleles investigated. This, however, is not the case for the salt stress phenotypes. The *spi-1* allele lacks a part of the PH domain, the BEACH domain and the WD40 repeats. This line shows the full salt stress phenotype, including delayed and decreased germination, shorter primary roots as well as reduced growth of the seedlings. This mutant closely resembles the *Arabidopsis* alleles investigated before, in which all T-DNA insertions lie before the PH domain (Steffens et al., 2015). This would indicate that the PBW domain or parts of it are essential for a proper salt response. At this point it is not clear though, if other functional domains or a specific fold of the protein might play a role in salt stress responses.

In contrast, the *spi-2* allele which is mutated in the end of the WD40 repeats, does not show a salt phenotype. In some experiments this allele was even found to be slightly hyposensitive to salt stress. Since the salt response is not weaker than in *pep1*, it can be assumed that the slightly truncated protein is still able to function in salt response. Hence, it can be assumed that the WD40 domain, or at least its missing part in *spi-2*, is not essential under these conditions. In accordance with the results obtained from *spi-1*, this would indicate that the PH BEACH domain is essential for salt stress tolerance in *Arabis*.

The observations made for the third allele, *spi-3*, turned out to be less definite. Although *spirrig* is truncated most severely in this line – only leaving a part of the ARMADILLO repeats intact – it showed the typical salt response only for germination and primary root growth, but wild type behaviour in seedling growth. This however might be due to the fact that the differences at this stage of development are quite small, as were the number of replicates.

SPIRRIG is most important for salt response in seeds and young seedlings

In all *spi* mutant alleles analysed, the salt stress phenotype seemed to decrease with age. The cotyledon whitening decreased with increasing time before the transfer to salt, and the

Conclusions

seedling growth on soil showed only approx. 10% difference between *pepl* and the strongest allele *spi-1*. Since the salt response did not decrease with the age of the plants for *pepl*, this indicates a more important role of SPRRIG in seeds/younger seedlings.

New reference genes for *Arabis alpina* – new tools for expression analyses

In 2009, the Minimum Information for Publication of Quantitative Real-Time PCR Experiments (MIQE) guidelines were published, addressing the issue that there is no consensus on correct performance and interpretation of qPCR experiments (Bustin et al., 2009). Nearly 10 years later, the effects of inappropriate reference genes for normalization are still widely disregarded, and consequently, qPCR data in various publications still are poorly normalized. Proper reference genes exhibit a stable expression and should reflect the total amount of mRNA in a sample. The efficiency of the corresponding primers should be evaluated with a dilution series and reach 90 to 110% (optimal) or 80 to 120% (minimal), with a correlation of -0.99 to -1. The same conditions apply to primers for the transcripts of interest. Given these requirements, normalization enables the comparison of transcripts in different samples, controlling for variations in yields of extraction and reverse-transcription, as well as efficiency of amplification. In this work, 13 new reference genes were established for *Arabis alpina* and the most reliable reference gene combination under salt stress was determined: TUA5 and CAC. In addition, ESE1 was identified as a suitable transcript for monitoring salt stress.

Differentially regulated transcripts in *spirrig* under salt stress

The qPCR analyses of potential differentially regulated genes in *spi* mutants in *Arabis* was based on the results found in RNAseq of *Arabidopsis thaliana* (Steffens et al., 2015). It is commonly known that RNAseq results can give valuable hints on interesting candidates, yet might not be reproducible in qPCR experiments. Since both experiments were performed in different, albeit closely related species, it was expected to find some inconsistent and contradicting results. Thus, the qPCR data will be discussed independently from the results of the RNAseq.

TSPO-related did not show differential regulation in the *spi* mutants compared to *pepl*. However, it is strongly upregulated under salt stress and could be used as a very sensitive salt stress detector.

In contrast, NTF2 family protein was found to have a (significantly) lower expression in the *spi* mutants under normal conditions and it showed an increased upregulation under salt stress

Conclusions

in all *spi* alleles. This indicates a connection between this transcript and SPIRRIG, however, it cannot be (solely) responsible for the salt phenotype, since its transcript levels are also altered in *spi-2*, which shows no phenotype under salt stress conditions.

Lipid transfer protein 4 has decreased transcript values in *spi-2* under normal conditions and strongly increased transcript levels in *spi-2* under salt stress. Since this protein is known to function in salt response, it is a putative candidate for mediating the salt adaptability of *spi-2*.

The integrase-type DNA-binding superfamily protein is known to possess DNA-binding transcription factor activity (Lamesch et al., 2012). Under salt conditions, its transcript levels in *spi* mutants were significantly lower than in *pep1*, indicating a possible connection between these two genes. In addition, the integrase-type DNA-binding superfamily protein mRNA in *spi-1* showed the least severe reaction to salt, which might be reflective of *spi-1* having the strongest salt stress phenotype.

FAMT transcript levels were shown to be comparable for *pep1*, *spi-2* and *spi-3* under normal and salt conditions. In *spi-1* under salt stress, the increase of transcript was significantly less compared to *pep1*. Here again, this observation might correlate with *spi-1* having the most severe salt phenotype.

Outlook

In this study, it was found that despite the distorted phenotype being similar in *Arabis* and *Arabidopsis*, SPIRRIG is not essential for vacuolar integrity in *Arabis* root hairs. This indicates that both phenotypes are connected to different functions of SPI: Provided that translation and folding of the SPIRRIG protein is not significantly altered, the observations could lead to the hypotheses that proper cell morphology is – at least partially - mediated by the WD40 repeats, but not by the function of SPIRRIG in vacuolar integrity. However, it is yet to be determined, if AaSPIRRIG has a function in membrane fusion or membrane composition independent of the root hair vacuoles. The primary function of WD40 repeats is protein-protein interaction, which can mediate the assembly of protein complexes or transient interactions among proteins. Thus, it will be crucial to find new interactors of SPIRRIG, which can explain the alterations in morphology in the corresponding mutants.

In addition, the different salt stress responses in between *spi* alleles let to the hypothesis that the PH BEACH domain is essential for the salt stress phenotype. To further verify this, it would be most helpful to create a set of mutant lines with specific mutations in the PH BEACH domain. These could be generated using CRISPR/CAS, or by stable transformation

Conclusions

of *spirrig* mutants with mutated constructs. These lines could then be analysed regarding their salt stress response.

The new reference genes for *Arabis alpina* were used in qPCR expression analyses, which revealed four differentially regulated transcripts in *spirrig* under salt stress. In the future, these have to be investigated in more detail to verify their possible interrelation with SPIRRIG. Finally, studying these interesting candidates might reveal the exact function of SPIRRIG in salt stress response.

Appendix

Table 21: List of primers, donor constructs and construct sources.

ID	vector	Insert gene ID	stop	source/primer (forward/reverse)
	pDONR201	AaVPS20.2 Aa_G130450	-	GGGGACAAGTTTGTACAAAAAAGCAGGCTTAATGGG GAATTTGTTTGTGAA/ GGGGACCACTTTGTACAAGAAAGCTGGGTTTCCACCT TCCAAAGGTTCTT
LS461	pDONR207	AaSPl-PBW Aa_G228370	+	GGGGACAAGTTTGTACAAAAAAGCAGGCTTAAAAGG GTCTGAAGATCCGGAATGGCAGCT/ GGGGACCACTTTGTACAAGAAAGCTGGGTTCTATGA AGCCTGTTTCAATG
LS467	pDONR201	AaDCP1 Aa_G368370	+	GGGGACAAGTTTGTACAAAAAAGCAGGCTTAATGTC TCAAACGGGAAGCT/ GGGGACCACTTTGTACAAGAAAGCTGGGTTTCTMTGA TTGATGTGCATTTT
	pDONR207	AaMYC1 Aa_G511730		B. Zhang
LS338	pDONR201	AtNOT1 AT1G02080	+	GGGGACAAGTTTGTACAAAAAAGCAGGCTCAATGAC TCCCTCAAGGTCGCCGGTC/ GGGGACCACTTTGTACAAGAAAGCTGGGTATCMGTG AGAATTGTCTGAGACCCAACC
MJ887	pDONR201	AtSPl-PBW AT1G03060	+	M. Jakoby
AST242	pDONR201	AtDCP1 AT1G08370	+	A. Steffens
AST243	pDONR201	AtDCP1 AT1G08370	-	A. Steffens
LS294	pDONR201	AtXI-1 tail AT1G17580	-	GGGGACAAGTTTGTACAAAAAAGCAGGCTCAatgCTG AAAATGGCTGCAAGAGACACCGGT/ GGGGACCACTTTGTACAAGAAAGCTGGGTATCMATC TGACCTTTCCAACAAGAACATGA
LS161	pDONR201	AtXI-1-coil AT1G17580	+	GGGGACAAGTTTGTACAAAAAAGCAGGCTCAatgCTG AAAATGGCTGCAAGAGACACCGGT/ GGGGACCACTTTGTACAAGAAAGCTGGGTATCMCGG TGAGATGGTAAGAGTTTGTGTC
LS450	pDONR201	AtXI-1 full length AT1G17580	-	GGGGACAAGTTTGTACAAAAAAGCAGGCTTAATGGC TGCTCCAGTCATAAT/ GGGGACCACTTTGTACAAGAAAGCTGGGTATCMATC TGACCTTTCCAACAAGAACATGA
LS155	pDONR201	AtXI-1-GTD AT1G17580	+	GGGGACAAGTTTGTACAAAAAAGCAGGCTCAatgAAA TCGCTTAATCAGAAACAGCAG/ GGGGACCACTTTGTACAAGAAAGCTGGGTATCMATC TGACCTTTCCAACAAGAACATGA
LS514	pDONR201	AtXI-1-Motor AT1G17580	-	GGGGACAAGTTTGTACAAAAAAGCAGGCTTAATGGC TGCTCCAGTCATAAT/ GGGGACCACTTTGTACAAGAAAGCTGGGTTTCTGAAG GAAAATCTTTGTCT
LS436	pDONR207	AtXI-1-GTD AT1G17580	-	GGGGACAAGTTTGTACAAAAAAGCAGGCTCAatgAAA TCGCTTAATCAGAAACAGCAG/

Appendix

ID	vector	Insert gene ID	stop	source/primer (forward/reverse)
				GGGGACCACTTTGTACAAGAAAGCTGGGTATCMATC TGACCTTCCAACAAGAACATGA
MJ1303	pENTR/D-TOPO	AtXI-1 tail AT1G17580	+	M. Jakoby
AST244	pDONR201	AtDCP5 AT1G26110	+	A. Steffens
AST245	pDONR201	AtDCP5 AT1G26110	-	A. Steffens
AST104	pDONR201	AtVCS AT3G13300	+	A. Steffens
LS296	pDONR201	AtXI-I tail AT4G33200	-	GGGGACAAGTTTGTACAAAAAAGCAGGCTCAatgCTT AAACAGGTTGCTAATGAAGCAG/ GGGGACCACTTTGTACAAGAAAGCTGGGTATCMAAT GATCTGCTTTGAGGTTGAAGCTA
LS158	pDONR201	AtXI-I-coil AT4G33200	+	GGGGACAAGTTTGTACAAAAAAGCAGGCTCAatgCTT AAACAGGTTGCTAATGAAGCAG/ GGGGACCACTTTGTACAAGAAAGCTGGGTATCMTGG CGAAATAGCAAGTGCCTGTTGACG
LS157	pDONR201	AtXI-I-coil AT4G33200	-	GGGGACAAGTTTGTACAAAAAAGCAGGCTCAatgCTT AAACAGGTTGCTAATGAAGCAG/ GGGGACCACTTTGTACAAGAAAGCTGGGTATCMTGG CGAAATAGCAAGTGCCTGTTGACG
LS171	pDONR201	AtXI-I-GTD AT4G33200	+	GGGGACAAGTTTGTACAAAAAAGCAGGCTCAatgAAA TTAACCGCAGAAAAGAAACCTGGA/ GGGGACCACTTTGTACAAGAAAGCTGGGTATCMAAT GATCTGCTTTGAGGTTGAAGCTA
LS164	pDONR201	AtXI-I-GTD AT4G33200	-	GGGGACAAGTTTGTACAAAAAAGCAGGCTCAatgAAA TTAACCGCAGAAAAGAAACCTGGA/ GGGGACCACTTTGTACAAGAAAGCTGGGTATCMAAT GATCTGCTTTGAGGTTGAAGCTA
LS511	pDONR201	AtXI-I-Motor AT4G33200		GGGGACAAGTTTGTACAAAAAAGCAGGCTCAATGAG AAATTGTCTTCCAATGGAATTGA/ GGGGACCACTTTGTACAAGAAAGCTGGGTTTCTTAGG AACACTTTTGTCC
MJ1306	pENTR/D-TOPO	AtXI-I tail AT4G33200	+	M. Jakoby
LS397	pFASTR06:GFP	AtXI-I AT4G33200	+	K. Tamura
MJ1441	pENTR223	AtXRN4 AT4G33211	+	M. Jakoby
AST272	pDONR201	AtDCP2 AT5G13570	+	A. Steffens
AST269	pDONR201	AtDCP2 AT5G13570	-	A. Steffens
LS297	pDONR201	AtXI-K tail AT5G20490	-	GGGGACAAGTTTGTACAAAAAAGCAGGCTCAatgCTT AAGATGGCCGCACGAGACACAG/ GGGGACCACTTTGTACAAGAAAGCTGGGTATCCTCCC GATGTACTGCCTTCTTTACGTGT
LS159	pDONR201	AtXI-K-coil AT5G20490	+	GGGGACAAGTTTGTACAAAAAAGCAGGCTCAatgCTT AAGATGGCCGCACGAGACACAG/ GGGGACCACTTTGTACAAGAAAGCTGGGTATCMTGG CGAAATAGCAAGTGCCTGTTGACG
LS423	pDONR201	AtXI-K full length AT5G20490	-	GGGGACAAGTTTGTACAAAAAAGCAGGCTCAATGGT TGGCCAGTCAATATAATAG/

ID	vector	Insert gene ID	stop	source/primer (forward/reverse)
				GGGGACCACTTTGTACAAGAAAGCTGGGTATCCTCCC GATGTACTGCCTTCTTTACGTGT
LS160	pDONR201	AtXI-K-GTD AT5G20490	+	GGGGACAAGTTTGTACAAAAAAGCAGGCTCA atgGAAAAGCAACAGGAAAACCAGGA/ GGGGACCACTTTGTACAAGAAAGCTGGGTATCaCGAT GTACTGCCTTCTTTACGTGTGAG
LS512	pDONR201	AtXI-K-Motor AT5G20490	-	GGGGACAAGTTTGTACAAAAAAGCAGGCTCAATGGT TGGCCCAGTCAATATAATAG/ GGGCAGTTACTTGTACAGcCTaGgcgggTcCGTCGACG atccTGTCTCAATTCTTTTCG
MJ1571	pDONR207	AtXI-K-GTD AT5G20490	-	M. Jakoby
MJ1308	pENTR/D- TOPO	AtXI-K tail AT5G20490	+	M. Jakoby
AST530	pDONR201	AtXI-2 tail AT5G43900	+	A. Steffens
LS295	pDONR201	AtXI-2 tail AT5G43900	-	GGGGACAAGTTTGTACAAAAAAGCAGGCTCA CTTAAGATGGCTGCTAGAGAAACTGG/ GGGGACCACTTTGTACAAGAAAGCTGGGTATCCGTG CAAGAATACAAATGCTGGA
LS162	pDONR201	AtXI-2-coil AT5G43900	+	GGGGACAAGTTTGTACAAAAAAGCAGGCTCA CTTAAGATGGCTGCTAGAGAAACTGG/ GGGGACCACTTTGTACAAGAAAGCTGGGTATCMAGG AGTGCTTATTGTTTGCTGATGCA
LS156	pDONR201	AtXI-2-coil AT5G43900	-	GGGGACAAGTTTGTACAAAAAAGCAGGCTCA CTTAAGATGGCTGCTAGAGAAACTGG/ GGGGACCACTTTGTACAAGAAAGCTGGGTATCMAGG AGTGCTTATTGTTTGCTGATGCA
LS163	pDONR201	AtXI-2-GTD AT5G43900	+	GGGGACAAGTTTGTACAAAAAAGCAGGCTCA GGGAAATCTGCTGCAGAACGTCAAAT/ GGGGACCACTTTGTACAAGAAAGCTGGGTATTAGTG CAAGAATACAAATGCTGGA
LS513	pDONR201	AtXI-2-Motor AT5G43900	-	GGGGACAAGTTTGTACAAAAAAGCAGGCTCAATGGT TGCTAACTTCAATCCATCAGT/ GGGGACCACTTTGTACAAGAAAGCTGGGTCCGCAG AAAAACTTTCGTCT
LS422	pDONR201	AtXI-2 full length AT5G43900	-	GGGGACAAGTTTGTACAAAAAAGCAGGCTCAATGGT TGCTAACTTCAATCCATCAGT/ GGGGACCACTTTGTACAAGAAAGCTGGGTATCCGTG CAAGAATACAAATGCTGGA
LS437	pDONR207	AtXI-2-GTD AT5G43900	-	GGGGACAAGTTTGTACAAAAAAGCAGGCTCA GGGAAATCTGCTGCAGAACGTCAAAT/ GGGGACCACTTTGTACAAGAAAGCTGGGTATCCGTG CAAGAATACAAATGCTGGA
AST167	pACT	GFP	+	A. Steffens
AST168	pAS	GFP	+	A. Steffens
MJ1417	pENSG:CFP	SKL motif	-	M. Jakoby
CD3-968	pFGC	golgi-rb		(Nelson et al., 2007)
MJ1653	pUBI::AUBERG INE	IVDH AT3G45300		M. Jakoby
MJ1574	pMDC32:XI-KΔGTD-2xYFP			M. Jakoby
MJ1872	pUBI::LaG-16-RHA1			M. Jakoby

ID	vector	Insert gene ID	stop	source/primer (forward/reverse)
	pENTR1A	LifeAct-CFP		GCCGCACTCGAGATGGGTGTCGAGATTTGATCAAG AAATTCGAAAGCATCTCAAAGGAAGAAGGGGATCCA CCGGTCGCCACCATGGTGTAGCAAGGGCGAGGA/ GCTGGGTCTAGATTACTTGTACAGCTCGTCCA
AST534	pENSG:YFP	XI-2 tail		A. Steffens
AST535	pENSG:CFP	XI-2 tail		A. Steffens
AST551	pENSG:CFP	XI-1 tail		A. Steffens
AST554	pENSG:CFP	XI-I tail		A. Steffens
AST555	pENSG:CFP	XI-K tail		A. Steffens
MJ1315	pENSG:YFP	XI-1 tail		M. Jakoby
MJ1320	pENSG:YFP	XI-K tail		M. Jakoby

Table 22: List of destination vectors created using the gateway system.

insert																	
	stop	pACT	pAS	pCL112	pCL113	pSYC	pSYN	pENSG:CFP	pENSG:YFP	pEXSG:CFP	pEXSG:YFP	pUBI:EXSG:GW:YFP	pAUB	pPACIFIC	pXI-KAGTD:GW:YFP	pUBI:EXSG:XI-2AGTD:GW:YFP	pUBI:EXSG:XI-KAGTD:GW:YFP
AaVPS20.2	-						+										
AaSPl-PBW	+	+	+	+	+			+	+								
AaDCP1	+	+	+	+	+			+									
AaMYC1					+												
AtNOT1	+	+	+												+		
AtSPl-PBW	+	+	+														
AtDCP1	+	+	+												+		
AtDCP1	-									+	+		+				
AtXI-1 tail	-									+	+						
AtXI-1-coil	+	+	+					+	+								
AtXI-1 full length	-	+	+	+	+					+	+		+				
AtXI-1-GTD	+	+	+					+	+						+		
AtXI-1-Motor	-	+	+								+						

Appendix

insert	stop	pACT	pAS	pCL112	pCL113	pSYC	pSYN	pENSG:CFP	pENSG:YFP	pEXSG:CFP	pEXSG:YFP	pUBI:EXSG:GW:YFP	pAUB	pPACIFIC	pXI-KΔGTD:GW:YFP	pUBI:EXSG:XI-2ΔGTD:GW:YFP	pUBI:EXSG:XI-KΔGTD:GW:YFP
		AtXI-1-GTD	-														+
AtXI-1 tail	+	+	+	+	+												
AtDCP5	+								+						+		
AtDCP5	-									+	+			+			
AtVCS	+														+		
AtXI-I tail	-									+	+						
AtXI-I-coil	+	+	+					+	+								
AtXI-I-coil	-									+							
AtXI-I-GTD	+	+	+					+	+						+		
AtXI-I-GTD	-														+	+	+
AtXI-I-Motor		+	+								+						
AtXI-I tail	+	+	+	+	+												
AtXRN4	+														+		
AtDCP2	+								+						+		
AtDCP2	-									+	+						
AtXI-K tail	-									+	+						
AtXI-K-coil	+	+	+					+	+								
AtXI-K full length	-	+	+			+	+	+	+			+	+				
AtXI-K-GTD	+	+	+					+	+						+		
AtXI-K-Motor	-	+	+							+	+						
AtXI-K-GTD	-														+	+	+
AtXI-K tail	+	+	+	+	+												
AtXI-2 tail	+	+	+	+	+												
AtXI-2 tail	-									+	+						
AtXI-2-coil	+	+	+					+	+								
AtXI-2-coil	-									+	+						
AtXI-2-GTD	+	+	+					+	+						+		
AtXI-2-	-	+	+								+				+		

insert	stop	pACT	pAS	pCL112	pCL113	pSYC	pSYN	pENSG:CFP	pENSG:YFP	pEXSG:CFP	pEXSG:YFP	pUBI:EXSG:GW:YFP	pAUB	pPACIFIC	pXI-KΔGTD:GW:YFP	pUBI:EXSG:XI-2ΔGTD:GW:YFP	pUBI:EXSG:XI-KΔGTD:GW:YFP
		Motor															
AtXI-2 full length	-					+	+			+	+	+	+				
AtXI-2-GTD	-														+	+	+

Table 23: Detailed overview on genotyping and/or selfing of myosin mutants.

mutant	knocked out alleles	Origin/genotyped by
<i>xi-1</i>	SALK_022140, SALK_134363	SALK /A. Steffens
<i>xi-2</i>	SALK_127984	SALK /A. Steffens
<i>xi-i</i>	SALK_92443	SALK /A. Steffens
<i>xi-k</i>	SALK_067972, GK_164_D12	SALK /A. Steffens
<i>xi-1 xi-2</i>	SALK_022140, SALK_127984	SALK /A. Steffens
<i>xi-1 xi-i</i>	SALK_134363, SALK_92443	SALK /plant provided by A. Steffens was segregating for <i>xi-i</i> , LS (see Table 24)
<i>xi-1 xi-k</i>	SALK_134363, GK_164_D12	AS
<i>xi-2 xi-i</i>	GK_115_C01, SALK_92443	SALK /plant provided by A. Steffens was segregating for <i>xi-i</i> , LS
<i>xi-2 xi-k</i>	GK_115_C01, GK_164_D12	SALK /A. Steffens
<i>xi-i xi-k</i>	SALK_92443, GK_164_D12	LS (see Table 24)
<i>xi-1 xi-2 xi-i</i>	SALK_022140, SALK_127984, SALK_92443	LS (see Table 24)
<i>xi-1 xi-2 xi-k</i>	SALK_022140, SAIL_632_D12, SALK_067972	(Peremyslov et al., 2010)
<i>xi-1 xi-i xi-k</i>	SALK_022140, SALK_92443, GK_164_D12	LS (see Table 24)
<i>xi-2 xi-i xi-k</i>	SALK_127984, SALK_92443, GK_164_D12	LS (see Table 24)
<i>xi-1 xi-2 xi-i xi-k</i>	SALK_022140, SALK_127984, SALK_92443, GK_164_D12	LS (see Table 24)

Table 24: Genotyping primer for SALK lines.

mutant	allele/line	primer	wild type
<i>xi-1</i>	SALK_022140	Forward Reverse wt	GAATGCTGCCAGAGTCATTTCAGAGGC CAAAGAATCGATCTTCTCTGTATCTTC

Appendix

		Reverse T-DNA (LBa1)	TGGTTCACGTAGTGGGCCATCG
<i>xi-2</i>	SALK_127984	Forward	GTCTACGAACTCTATATAGCTCCAG
		Reverse wt	TTCAGCGTCGTGGCAGCCATTCTCCAT
		Reverse T-DNA (LBa1)	TGGTTCACGTAGTGGGCCATCG
<i>xi-i</i>	SALK_92443	Forward	TGCACTCATTAATGGTAGCCAGCCTAG
		Reverse wt	GGGCTTCTGCAATTCAATTCAGGCA
		Reverse T-DNA (LBa1)	TGGTTCACGTAGTGGGCCATCG
<i>xi-k</i>	GK_164_D12	Forward	CATCTCACACATTCTTACTACAAGC
		Reverse wt	AATATGGCCTTTTTCTGTTGATTG
		Reverse T-DNA (LBa1)	TGGTTCACGTAGTGGGCCATCG

Table 25: List of qPCR primers.

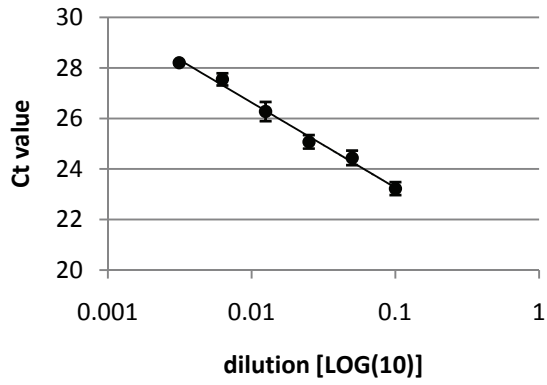
NN – no number

Number	Gene	Primer	Source	
Aa_G9730 AT2G25610	ATPase	Forward Reverse	GCCAACCTTGTATGCGGGTTA GTTGGCCATGTTGCTTGTGC	
Aa_G337160 AT5G03880	Thioredoxin	Forward Reverse	GATTGGTCGTGCCGAAAGG TCTCGAGCAATTCCTGCTTTG	
Aa_G363210 AT4G37200	HCF (HIGH CHLOROPHYLL FLUORESCENCE 164)	Forward Reverse	AAGGTAATGTTGTCGGGAGGCT CGGCTCGGGCATGAGGAAT	
Aa_G472320 AT3G13920	EIF4a (eukaryotic translation initiation factor 4A1)	Forward Reverse	CCAGCTTCTCCACCCAAGA GCTCGTCACGCTTCACCAAG	
Aa_G442020 AT5G55190	RAN3 (RAN GTPASE 3)	Forward Reverse	CACAGGAAAAACACATTTCGT CCATCCCTAAGACCACCAAT	(Wang et al., 2009)
Aa_G41880 AT4G05320	UBQ10 (UBIQUITIN 10)	Forward Reverse	AAGGCCCAAAACACAAACG CGTCTCCGTGGTGGTTTCTA	Provided by P. Jiang
NN AT3G18780	Actin 2	Forward Reverse	AGCTGTTCTCTCCCTGTACG AACCTCGTAGATTGGCACA	
Aa_G319470 AT1G71500	PSB33 (PHOTOSYSTEM B PROTEIN 33)	Forward Reverse	TGGCGACCACTGCATCTTCA ATCGACGGTCACGACGGAGA	
NN At5g65360	Histone H3	Forward Reverse	CTCACGGAGAGCGACGGTTC GCAACTCGCGACGAAAGCAG	
Aa_G477070 AT1G74880	NdhO (NAD(P)H:plastoqui none dehydrogenase complex subunit O)	Forward Reverse	GCGGCGAGGTCTTGACATT TCGCTCGTAAACAAGTTTCTCAGACT	
NN AT5G19780	TUA5 (TUBULIN ALPHA 5)	Forward Reverse	TGTGACCCGAGGCACGGAAA CCAGTAGGGCACCAGTCAACA	
NN AT3G41768	18srRNA	Forward Reverse	CTCCGATCCCGAAGGCCAAC CCTTAAGTGGCCGGGTCGTG	
Aa_G26240 AT5G46630	CAC (Clathrin adaptor complexes medium subunit family protein)	Forward Reverse	TGGACAAGACCACCAATCCA CACTCGACCGTGTGTAACC	
Aa_G18160 AT2G28390	SAND (SAND family protein)	Forward Reverse	TTGCAGGATTTCGATTGAGG TCCAAAGGGACCTCCTGTTC	
NN AT5G56030	HSP81.2/90 (Heat Shock Protein 81.2/90)	Forward Reverse	CGTCTGGTGAGGCTCTTGGT AGCCTACGCTCCTCAAGGTACT	

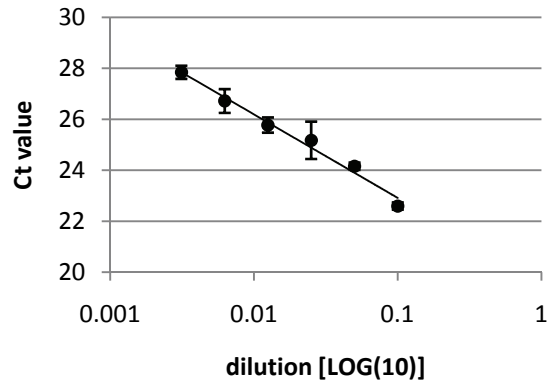
Appendix

Number	Gene	Primer	Source
Aa_G12840 AT2G47770	TSPO(outer membrane tryptophan-rich sensory protein)- related	Forward Reverse	GTGGACGGTGGGTCCACAA CACACCACAAGCCCGGCTAA
Aa_G664320 AT3G23230	Integrase-type DNA-binding superfamily protein (EFE1)	Forward Reverse	TGCAGCAGAGATCCGAGACC TCATAAGCCCGAGCGGCATC
Aa_G46100 AT5G24240	<i>Arabis alpina</i> Phosphatidylinosito l 3- and 4-kinase	Forward Reverse	TCCGCACGGACAGACTGTTT TGTTTCGTGGTCCAGTCATGGG
	<i>Arabidopsis thaliana</i> Phosphatidylinosito l 3- and 4-kinase	Forward Reverse	TCCGCATGGACAGCCTGTTT AGTTCGTGGTCCAGTCATAGG
Aa_G228370 AT1G03060	<i>Arabis alpina</i> SPIRRIG	Forward Reverse	AACCGGTCACCGCTCTCCAT CCCAGATGAATCGCCGCTCA
NN AT3G44860	FARNESOIC ACID CARBOXYL-O- METHYLTRANSFERA SE (FAMT)	Forward Reverse	gctcgacgctttcaagttgcc acctcaatcgtgtagcaccca
NN AT1G71520	Integrase-type DNA-binding superfamily protein	Forward Reverse	ggaatccgtcgtcggaaatggg agctgcacctctgctgtgg
Aa_G499040 AT5G59310	lipid transfer protein 4	Forward Reverse	CCGGTTCCGTGCTGTGTAGG TCGGCATGCTTGTTGACGGT
Aa_G78660 AT3G07250	nuclear transport factor 2 (NTF2) family protein	Forward Reverse	CGGCCAAACGGTAACGGTAGTT TGCCCTCTGGTCCGTTACCT

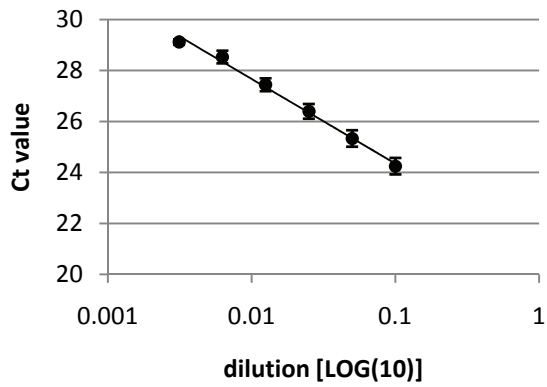
ATPase



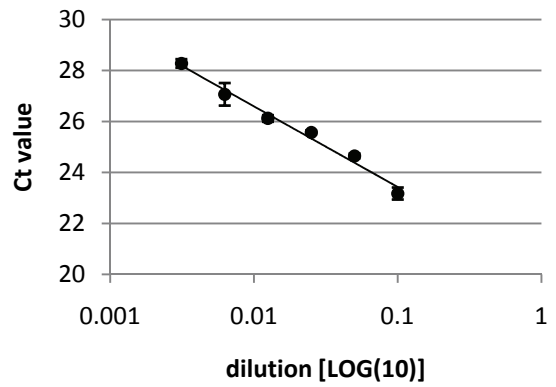
Thioredoxin



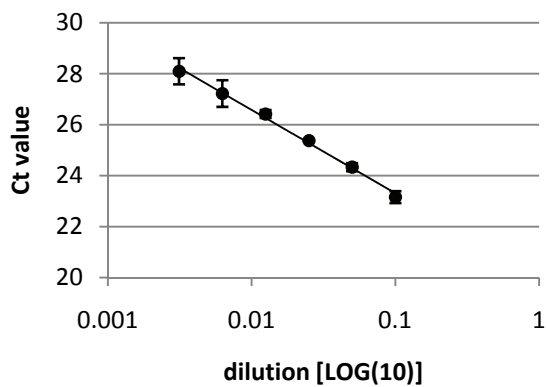
HCF



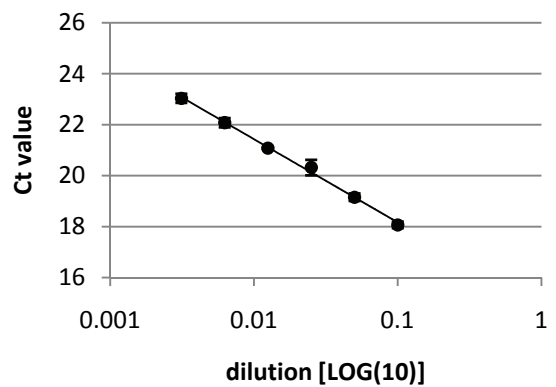
EIF4a



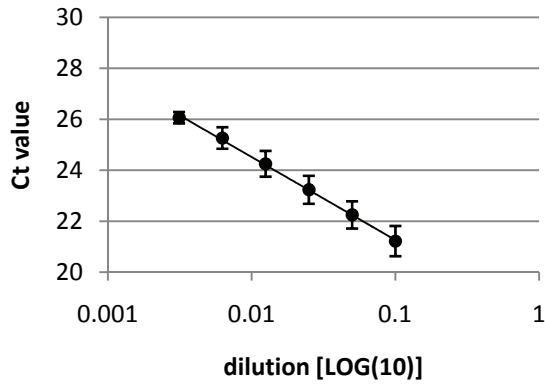
RAN3



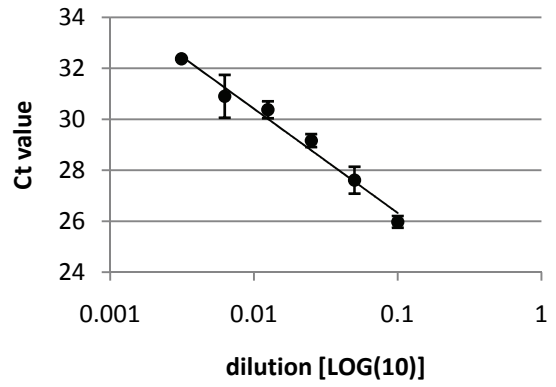
UBQ10



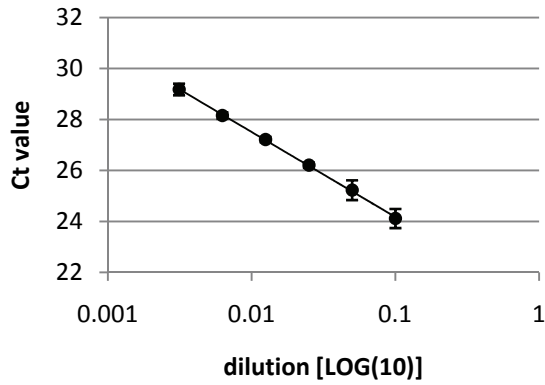
Actin 2



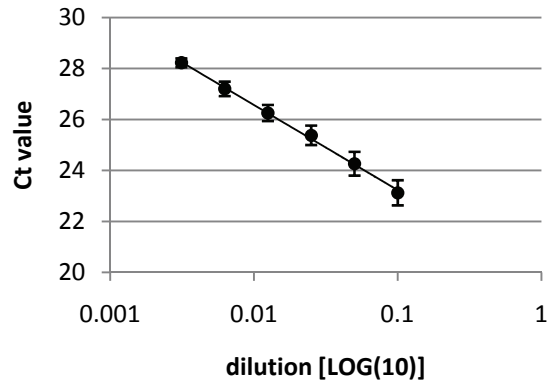
PP2A



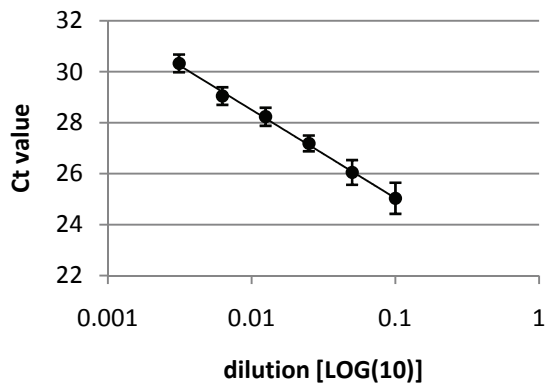
PSB33



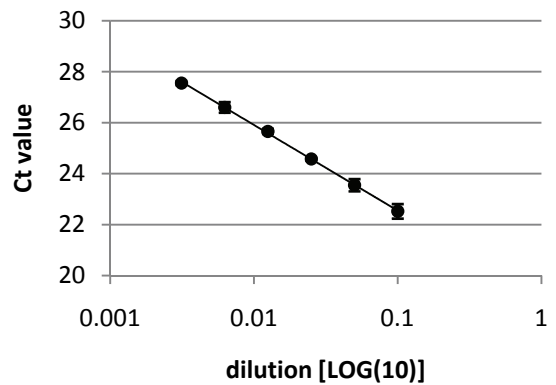
Histone H3



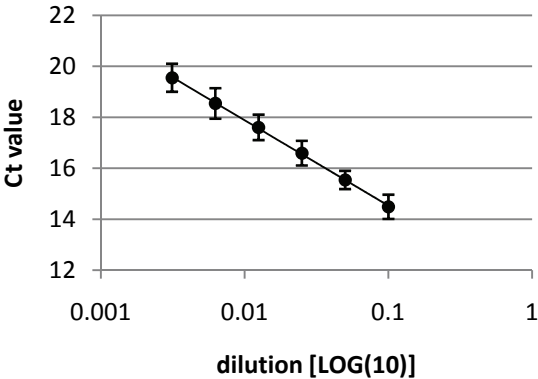
NdhO



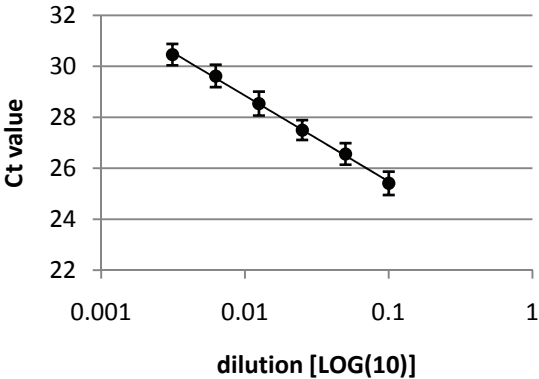
TUA5



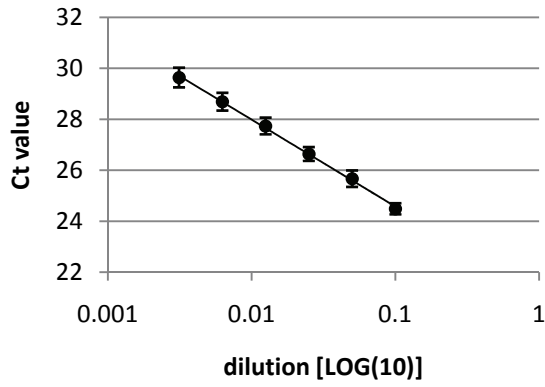
18srRNA



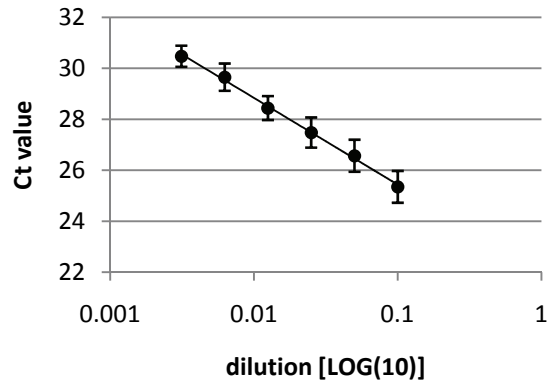
CAC



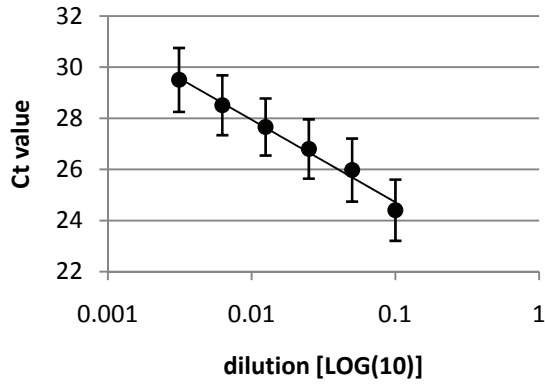
SAND



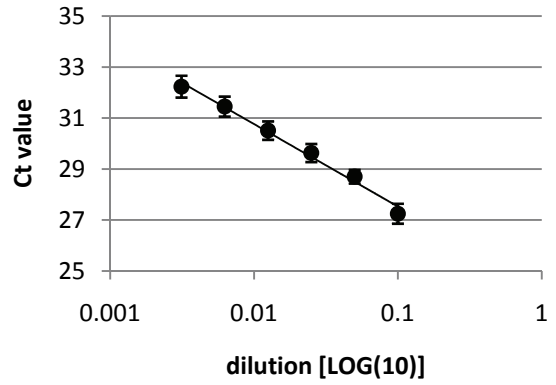
HSP81.2/90



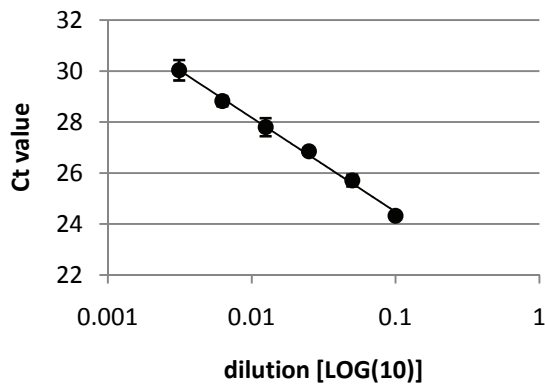
TSPO-related



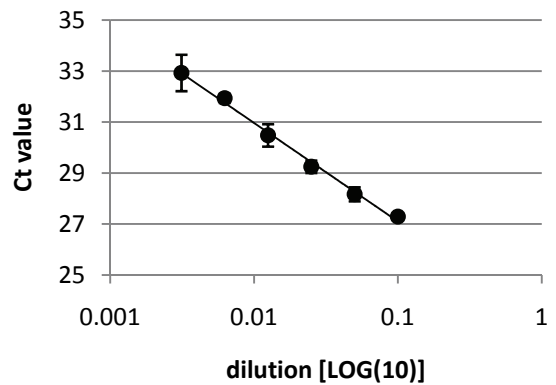
EFE1



AaPI4Kc3



AtPI4Kc3



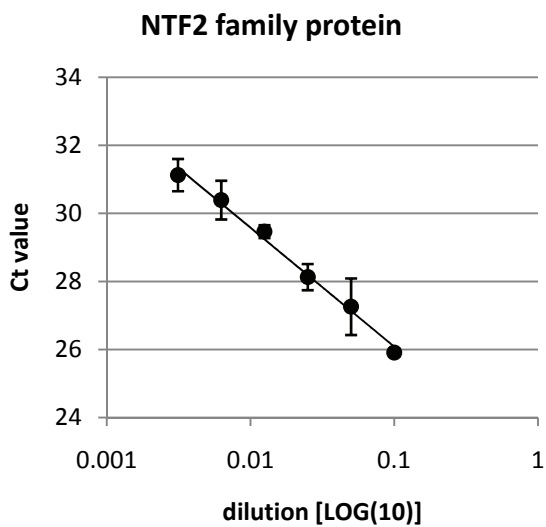
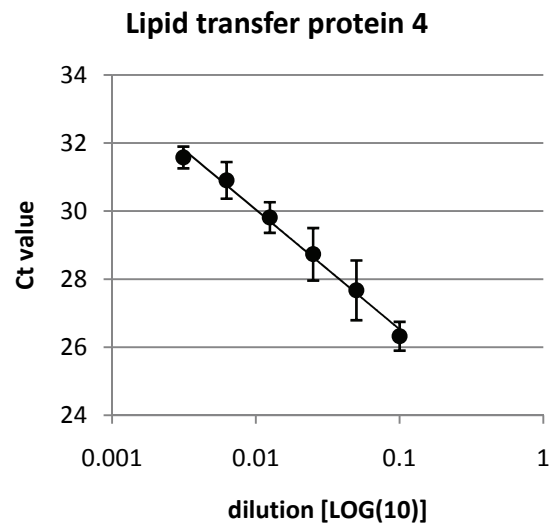
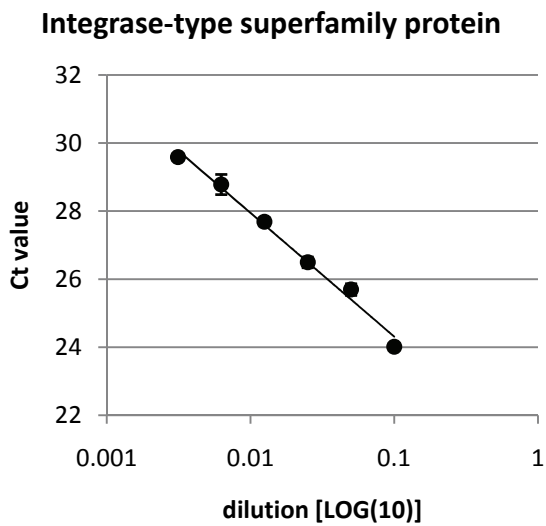
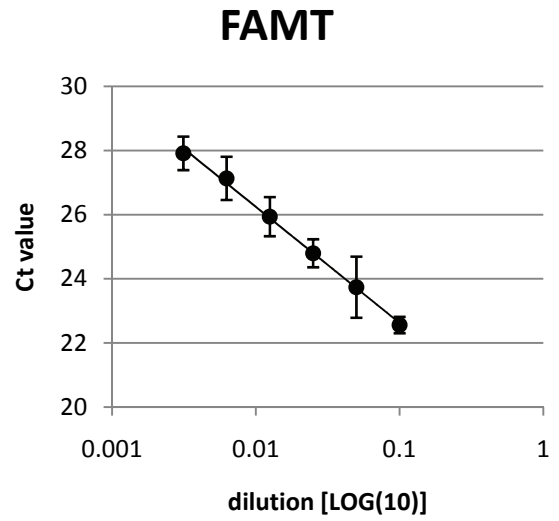
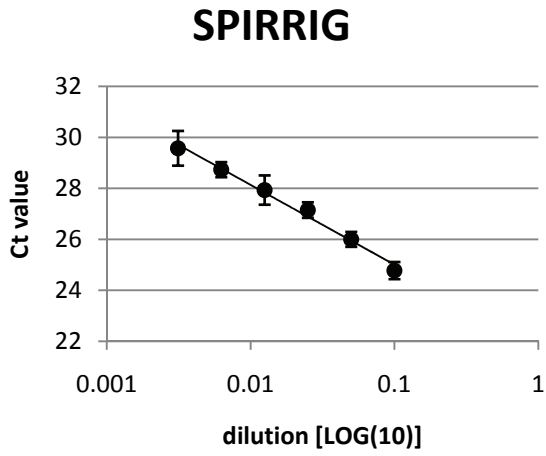


Figure 57: Graphs of qPCR primer efficiency tests.

References

- Alberts, B., Johnson, A., Lewis, J., Raff, M., Roberts, K., and Walter, P. (2002). *Molecular Biology of the Cell*.
- Andersen, C.L., Jensen, J.L., and Ørntoft, T.F. (2004). Normalization of real-time quantitative reverse transcription-PCR data: a model-based variance estimation approach to identify genes suited for normalization, applied to bladder and colon cancer data sets. *Cancer Res.* **64**, 5245–5250.
- Andrei, M.A., Ingelfinger, D., Heintzmann, R., Achsel, T., Rivera-Pomar, R., and Lührmann, R. (2005). A role for eIF4E and eIF4E-transporter in targeting mRNPs to mammalian processing bodies. *RNA* **11**, 717–727.
- Avisar, D., Prokhnevsky, A.I., Makarova, K.S., Koonin, E. V, and Dolja, V. V (2008). Myosin XI-K Is required for rapid trafficking of Golgi stacks, peroxisomes, and mitochondria in leaf cells of *Nicotiana benthamiana*. *Plant Physiol.* **146**, 1098–1108.
- Avisar, D., Abu-Abied, M., Belausov, E., and Sadot, E. (2012). Myosin XIK is a major player in cytoplasm dynamics and is regulated by two amino acids in its tail. *J. Exp. Bot.* **63**, 241–249.
- Basu, D., Le, J., El-Essal, S.E.-D., Huang, S., Zhang, C., Mallery, E.L., Koliantz, G., Staiger, C.J., and Szymanski, D.B. (2005). DISTORTED3/SCAR2 is a putative arabidopsis WAVE complex subunit that activates the Arp2/3 complex and is required for epidermal morphogenesis. *Plant Cell* **17**, 502–524.
- Beilstein, M.A., Nagalingum, N.S., Clements, M.D., Manchester, S.R., and Mathews, S. (2010). Dated molecular phylogenies indicate a Miocene origin for *Arabidopsis thaliana*. *Proc. Natl. Acad. Sci. U. S. A.* **107**, 18724–18728.
- Berardini, T.Z., Reiser, L., Li, D., Mezheritsky, Y., Muller, R., Strait, E., and Huala, E. (2015a). The arabidopsis information resource: Making and mining the “gold standard” annotated reference plant genome. *Genesis* **53**, 474–485.
- Berardini, T.Z., Reiser, L., Li, D., Mezheritsky, Y., Muller, R., Strait, E., and Huala, E. (2015b). The arabidopsis information resource: Making and mining the “gold standard” annotated reference plant genome. *Genesis* **53**, 474–485.
- Bögre, L., Magyar, Z., López-Juez, E., Busov, V., Brunner, A., Strauss, S., Fleming, A., Tsukaya, H., Reddy, G., Heisler, M., et al. (2008). New clues to organ size control in plants. *Genome Biol.* **9**, 226.
- Burgess, A., Mornon, J.-P., de Saint-Basile, G., and Callebaut, I. (2009). A concanavalin A-like lectin domain in the CHS1/LYST protein, shared by members of the BEACH family. *Bioinformatics* **25**, 1219–1222.
- Bustin, S.A., Benes, V., Garson, J.A., Hellems, J., Huggett, J., Kubista, M., Mueller, R., Nolan, T., Pfaffl, M.W., Shipley, G.L., et al. (2009). The MIQE Guidelines: Minimum Information for Publication of Quantitative Real-Time PCR Experiments. *Clin. Chem.* **55**.
- Chang, W., Zaarour, R.F., Reck-Peterson, S., Rinn, J., Singer, R.H., Snyder, M., Novick, P., and Mooseker, M.S. (2008). Myo2p, a class V myosin in budding yeast, associates with a large ribonucleic acid-protein complex that contains mRNAs and subunits of the RNA-processing body. *RNA* **14**, 491–502.

References

- Coates, J.C. (2003). Armadillo repeat proteins: beyond the animal kingdom. *Trends Cell Biol.* *13*, 463–471.
- Cougot, N., Babajko, S., and Séraphin, B. (2004). Cytoplasmic foci are sites of mRNA decay in human cells. *J. Cell Biol.* *165*, 31–40.
- Cullinane, A.R., Schäffer, A.A., and Huizing, M. (2013). The BEACH is hot: a LYST of emerging roles for BEACH-domain containing proteins in human disease. *Traffic* *14*, 749–766.
- Duan, Z., and Tominaga, M. (2018). Actin–myosin XI: An intracellular control network in plants. *Biochem. Biophys. Res. Commun.*
- Esseling-Ozdoba, A., Houtman, D., Van Lammeren, A.A.M., Eiser, E., and Emons, A.M.C. (2008). Hydrodynamic flow in the cytoplasm of plant cells. *J. Microsc.* *231*, 274–283.
- Eulalio, A., Behm-Ansmant, I., and Izaurralde, E. (2007). P bodies: at the crossroads of post-transcriptional pathways. *Nat. Rev. Mol. Cell Biol.* *8*, 9–22.
- Fagarasanu, A., and Rachubinski, R.A. (2007). Orchestrating organelle inheritance in *Saccharomyces cerevisiae*. *Curr. Opin. Microbiol.* *10*, 528–538.
- Fagarasanu, A., Fagarasanu, M., Eitzen, G.A., Aitchison, J.D., and Rachubinski, R.A. (2006). The Peroxisomal Membrane Protein Inp2p Is the Peroxisome-Specific Receptor for the Myosin V Motor Myo2p of *Saccharomyces cerevisiae*. *Dev. Cell* *10*, 587–600.
- Feys, B.J., Wiermer, M., Bhat, R.A., Moisan, L.J., Medina-Escobar, N., Neu, C., Cabral, A., and Parker, J.E. (2005). Arabidopsis SENESCENCE-ASSOCIATED GENE101 stabilizes and signals within an ENHANCED DISEASE SUSCEPTIBILITY1 complex in plant innate immunity. *Plant Cell* *17*, 2601–2613.
- Fridy, P.C., Li, Y., Keegan, S., Thompson, M.K., Nudelman, I., Scheid, J.F., Oeffinger, M., Nussenzweig, M.C., Fenyö, D., Chait, B.T., et al. (2014). A robust pipeline for rapid production of versatile nanobody repertoires. *Nat. Methods* *11*, 1253–1260.
- Gerald, N.J., Siano, M., and De Lozanne, A. (2002). The Dictyostelium LvsA protein is localized on the contractile vacuole and is required for osmoregulation. *Traffic* *3*, 50–60.
- Guimil, S., and Dunand, C. (2007). Cell growth and differentiation in Arabidopsis epidermal cells. *J. Exp. Bot.* *58*, 3829–3840.
- Hammer, J.A., and Sellers, J.R. (2011). Walking to work: roles for class V myosins as cargo transporters. *Nat. Rev. Mol. Cell Biol.* *13*, 13.
- Hardham, A.R., Takemoto, D., and White, R.G. (2008). Rapid and dynamic subcellular reorganization following mechanical stimulation of Arabidopsis epidermal cells mimics responses to fungal and oomycete attack. *BMC Plant Biol.* *8*, 63.
- Hashimoto, K., Igarashi, H., Mano, S., Nishimura, M., Shimmen, T., and Yokota, E. (2005). Peroxisomal localization of a myosin XI isoform in Arabidopsis thaliana. *Plant Cell Physiol.* *46*, 782–789.
- Hashimoto, K., Igarashi, H., Mano, S., Takenaka, C., Shiina, T., Yamaguchi, M., Demura, T., Nishimura, M., Shimmen, T., and Yokota, E. (2008). An isoform of Arabidopsis myosin XI interacts with small GTPases in its C-terminal tail region. *J. Exp. Bot.* *59*, 3523–3531.
- Hu, J., Baker, A., Bartel, B., Linka, N., Mullen, R.T., Reumann, S., and Zolman, B.K. (2012). Plant peroxisomes: biogenesis and function. *Plant Cell* *24*, 2279–2303.

References

- Hulo, N., Bairoch, A., Bulliard, V., Cerutti, L., Cuče, B.A., de Castro, E., Lachaize, C., Langendijk-Genevaux, P.S., and Sigrist, C.J.A. (2007). The 20 years of PROSITE. *Nucleic Acids Res.* *36*, D245–D249.
- Hülkamp, M., Misfa, S., and Jürgens, G. (1994). Genetic dissection of trichome cell development in *Arabidopsis*. *Cell* *76*, 555–566.
- Ishikawa, K., Catlett, N.L., Novak, J.L., Tang, F., Nau, J.J., and Weisman, L.S. (2003). Identification of an organelle-specific myosin V receptor. *J. Cell Biol.* *160*, 887–897.
- Jakoby, M.J., Weinl, C., Pusch, S., Kuijt, S.J.H., Merkle, T., Dissmeyer, N., and Schnittger, A. (2006). Analysis of the subcellular localization, function, and proteolytic control of the *Arabidopsis* cyclin-dependent kinase inhibitor ICK1/KRP1. *Plant Physiol.* *141*, 1293–1305.
- Jogl, G., Shen, Y., Gebauer, D., Li, J., Wiegmann, K., Kashkar, H., Krönke, M., and Tong, L. (2002). Crystal structure of the BEACH domain reveals an unusual fold and extensive association with a novel PH domain. *EMBO J.* *21*, 4785–4795.
- Kleinboelting, N., Huet, G., Kloetgen, A., Viehoveer, P., and Weisshaar, B. (2012). GABI-Kat SimpleSearch: new features of the *Arabidopsis thaliana* T-DNA mutant database. *Nucleic Acids Res.* *40*, D1211–D1215.
- Koch, M.A., Kiefer, C., Ehrich, D., Vogel, J., Brochmann, C., and Mummenhoff, K. (2006). Three times out of Asia Minor: the phylogeography of *Arabis alpina* L. (Brassicaceae). *Mol. Ecol.* *15*, 825–839.
- Koncz, C., Martini, N., Mayerhofer, R., Koncz-Kalman, Z., Körber, H., Redei, G.P., and Schell, J. (1989). High-frequency T-DNA-mediated gene tagging in plants. *Proc. Natl. Acad. Sci. U. S. A.* *86*, 8467–8471.
- Kost, B., and Chua, N.-H. (2002). The Plant Cytoskeleton: Vacuoles and Cell Walls Make the Difference. *Cell* *108*, 9–12.
- Lamesch, P., Berardini, T.Z., Li, D., Swarbreck, D., Wilks, C., Sasidharan, R., Muller, R., Dreher, K., Alexander, D.L., Garcia-Hernandez, M., et al. (2012). The *Arabidopsis* Information Resource (TAIR): improved gene annotation and new tools. *Nucleic Acids Res.* *40*, D1202–D1210.
- Li, J.-F., and Nebenführ, A. (2008a). The tail that wags the dog: the globular tail domain defines the function of myosin V/XI. *Traffic* *9*, 290–298.
- Li, J.-F., and Nebenführ, A. (2008b). Inter-dependence of dimerization and organelle binding in myosin XI. *Plant J.* *55*, 478–490.
- De Lozanne, A. (2003). The role of BEACH proteins in *Dictyostelium*. *Traffic* *4*, 6–12.
- Madison, S.L., and Nebenführ, A. (2013). Understanding myosin functions in plants: are we there yet? *Curr. Opin. Plant Biol.* *16*, 710–717.
- Marchler-Bauer, A., and Bryant, S.H. (2004). CD-Search: protein domain annotations on the fly. *Nucleic Acids Res.* *32*, W327–31.
- Marchler-Bauer, A., Lu, S., Anderson, J.B., Chitsaz, F., Derbyshire, M.K., DeWeese-Scott, C., Fong, J.H., Geer, L.Y., Geer, R.C., Gonzales, N.R., et al. (2011). CDD: a Conserved Domain Database for the functional annotation of proteins. *Nucleic Acids Res.* *39*, D225–D229.
- Marchler-Bauer, A., Bo, Y., Han, L., He, J., Lanczycki, C.J., Lu, S., Chitsaz, F., Derbyshire, M.K., Geer, R.C., Gonzales, N.R., et al. (2017). CDD/SPARCLE: functional classification of

References

- proteins via subfamily domain architectures. *Nucleic Acids Res.* **45**, D200–D203.
- Mathur, J., and Hülskamp, M. (2002). Microtubules and Microfilaments in Cell Morphogenesis in Higher Plants. *Curr. Biol.* **12**, R669–R676.
- Muhlrad, D., and Parker, R. (2005). The yeast EDC1 mRNA undergoes deadenylation-independent decapping stimulated by Not2p, Not4p, and Not5p. *EMBO J.* **24**, 1033–1045.
- Murashige, T., and Skoog, F. (1962). A Revised Medium for Rapid Growth and Bio Assays with Tobacco Tissue Cultures. *Physiol. Plant.* **15**, 473–497.
- Nakano, A., and Luini, A. (2010). Passage through the Golgi. *Curr. Opin. Cell Biol.* **22**, 471–478.
- Nelson, B.K., Cai, X., and Nebenführ, A. (2007). A multicolored set of *in vivo* organelle markers for co-localization studies in *Arabidopsis* and other plants. *Plant J.* **51**, 1126–1136.
- Ojangu, E.-L., Järve, K., Paves, H., and Truve, E. (2007). *Arabidopsis thaliana* myosin XIK is involved in root hair as well as trichome morphogenesis on stems and leaves. *Protoplasma* **230**, 193–202.
- Ojangu, E.-L., Tanner, K., Pata, P., Järve, K., Holweg, C.L., Truve, E., and Paves, H. (2012). Myosins XI-K, XI-1, and XI-2 are required for development of pavement cells, trichomes, and stigmatic papillae in *Arabidopsis*. *BMC Plant Biol.* **12**, 81.
- Okamoto, K., Ueda, H., Shimada, T., Tamura, K., Kato, T., Tasaka, M., Morita, M.T., and Hara-Nishimura, I. (2015). Regulation of organ straightening and plant posture by an actin-myosin XI cytoskeleton. *Nat. Plants* **1**, 15031.
- Peremyslov, V. V, Prokhnevsky, A.I., Avisar, D., and Dolja, V. V (2008). Two class XI myosins function in organelle trafficking and root hair development in *Arabidopsis*. *Plant Physiol.* **146**, 1109–1116.
- Peremyslov, V. V, Prokhnevsky, A.I., and Dolja, V. V (2010). Class XI myosins are required for development, cell expansion, and F-Actin organization in *Arabidopsis*. *Plant Cell* **22**, 1883–1897.
- Peremyslov, V. V, Mockler, T.C., Filichkin, S.A., Fox, S.E., Jaiswal, P., Makarova, K.S., Koonin, E. V, and Dolja, V. V (2011). Expression, splicing, and evolution of the myosin gene family in plants. *Plant Physiol.* **155**, 1191–1204.
- Peremyslov, V. V, Klocko, A.L., Fowler, J.E., and Dolja, V. V (2012). *Arabidopsis* Myosin XI-K Localizes to the Motile Endomembrane Vesicles Associated with F-actin. *Front. Plant Sci.* **3**, 184.
- Pfaffl, M.W., Tichopad, A., Prgomet, C., and Neuvians, T.P. (2004). Determination of stable housekeeping genes, differentially regulated target genes and sample integrity: BestKeeper – Excel-based tool using pair-wise correlations. *Biotechnol. Lett.* **26**, 509–515.
- Prokhnevsky, A.I., Peremyslov, V. V, and Dolja, V. V (2008). Overlapping functions of the four class XI myosins in *Arabidopsis* growth, root hair elongation, and organelle motility. *Proc. Natl. Acad. Sci. U. S. A.* **105**, 19744–19749.
- Saedler, R., Jakoby, M., Marin, B., Galiana-Jaime, E., and Hülskamp, M. (2009). The cell morphogenesis gene SPIRRIG in *Arabidopsis* encodes a WD/BEACH domain protein. *Plant J.* **59**, 612–621.
- Schwab, B., Mathur, J., Saedler, R., Schwarz, H., Frey, B., Scheidegger, C., and Hülskamp, M. (2003). Regulation of cell expansion by the DISTORTED genes in *Arabidopsis thaliana*:

References

- Actin controls the spatial organization of microtubules. *Mol. Genet. Genomics* 269, 350–360.
- Sellers, J.R. (2000). Myosins: a diverse superfamily. *Biochim. Biophys. Acta* 1496, 3–22.
- Sessions, A., Burke, E., Presting, G., Aux, G., McElver, J., Patton, D., Dietrich, B., Ho, P., Bacwaden, J., Ko, C., et al. (2002). A high-throughput Arabidopsis reverse genetics system. *Plant Cell* 14, 2985–2994.
- Singh, S., and Bandman, E. (2006). Dimerization specificity of adult and neonatal chicken skeletal muscle myosin heavy chain rods. *Biochemistry* 45, 4927–4935.
- Spudich, J.A. (2001). The myosin swinging cross-bridge model. *Nat. Rev. Mol. Cell Biol.* 2, 387–392.
- Steffens, A., Jaegle, B., Tresch, A., Hülskamp, M., and Jakoby, M. (2014a). Processing-body movement in Arabidopsis depends on an interaction between myosins and DECAPPING PROTEIN1. *Plant Physiol.* 164, 1879–1892.
- Steffens, A., Jaegle, B., Tresch, A., Hülskamp, M., and Jakoby, M. (2014b). Processing-body movement in Arabidopsis depends on an interaction between myosins and DECAPPING PROTEIN1. *Plant Physiol.* 164, 1879–1892.
- Steffens, A., Bräutigam, A., Jakoby, M., Hülskamp, M., and Meyer, S. (2015). The BEACH Domain Protein SPIRRIG Is Essential for Arabidopsis Salt Stress Tolerance and Functions as a Regulator of Transcript Stabilization and Localization. *PLOS Biol.* 13, e1002188.
- Takemoto, D., Jones, D.A., and Hardham, A.R. (2003). GFP-tagging of cell components reveals the dynamics of subcellular re-organization in response to infection of *Arabidopsis* by oomycete pathogens. *Plant J.* 33, 775–792.
- Tamura, K., Iwabuchi, K., Fukao, Y., Kondo, M., Okamoto, K., Ueda, H., Nishimura, M., and Hara-Nishimura, I. (2013). Myosin XI-i links the nuclear membrane to the cytoskeleton to control nuclear movement and shape in Arabidopsis. *Curr. Biol.* 23, 1776–1781.
- Teh, O.-K., Hatsugai, N., Tamura, K., Fuji, K., Tabata, R., Yamaguchi, K., Shingenobu, S., Yamada, M., Hasebe, M., Sawa, S., et al. (2014). BEACH-Domain Proteins Act Together in a Cascade to Mediate Vacuolar Protein Trafficking and Disease Resistance in Arabidopsis. *Mol. Plant.*
- Tominaga, M., and Ito, K. (2015a). The molecular mechanism and physiological role of cytoplasmic streaming. *Curr. Opin. Plant Biol.* 27.
- Tominaga, M., and Ito, K. (2015b). The molecular mechanism and physiological role of cytoplasmic streaming. *Curr. Opin. Plant Biol.* 27, 104–110.
- Tominaga, M., and Nakano, A. (2012). Plant-Specific Myosin XI, a Molecular Perspective. *Front. Plant Sci.* 3, 211.
- Tominaga, M., Kojima, H., Yokota, E., Orii, H., Nakamori, R., Katayama, E., Anson, M., Shimmen, T., and Oiwa, K. (2003). Higher plant myosin XI moves processively on actin with 35 nm steps at high velocity. *EMBO J.* 22, 1263–1272.
- Tominaga, M., Kimura, A., Yokota, E., Haraguchi, T., Shimmen, T., Yamamoto, K., Nakano, A., and Ito, K. (2013). Cytoplasmic streaming velocity as a plant size determinant. *Dev. Cell* 27, 345–352.
- Ueda, H., Yokota, E., Kutsuna, N., Shimada, T., Tamura, K., Shimmen, T., Hasezawa, S., Dolja, V. V., and Hara-Nishimura, I. (2010). Myosin-dependent endoplasmic reticulum motility and F-actin organization in plant cells. *Proc. Natl. Acad. Sci. U. S. A.* 107, 6894–6899.

References

- Vandesompele, J., De Preter, K., Pattyn, F., Poppe, B., Van Roy, N., De Paepe, A., and Speleman, F. (2002). Accurate normalization of real-time quantitative RT-PCR data by geometric averaging of multiple internal control genes. *Genome Biol.* **3**, research0034.1.
- Vick, J.K., and Nebenführ, A. (2012). Putting the Breaks On: Regulating Organelle Movements in Plant Cells. *J. Integr. Plant Biol.* **54**, no-no.
- Wang, R., Farrona, S., Vincent, C., Joecker, A., Schoof, H., Turck, F., Alonso-Blanco, C., Coupland, G., and Albani, M.C. (2009). PEP1 regulates perennial flowering in *Arabidopsis thaliana*. *Nature* **459**, 423–427.
- Weber, C., Nover, L., and Fauth, M. (2008). Plant stress granules and mRNA processing bodies are distinct from heat stress granules. *Plant J.* **56**, 517–530.
- Xu, J., and Chua, N.-H. (2009). Arabidopsis decapping 5 is required for mRNA decapping, P-body formation, and translational repression during postembryonic development. *Plant Cell* **21**, 3270–3279.
- Xu, J., Yang, J.-Y., Niu, Q.-W., and Chua, N.-H. (2006). Arabidopsis DCP2, DCP1, and VARICOSE form a decapping complex required for postembryonic development. *Plant Cell* **18**, 3386–3398.
- Yang, L., Qin, L., Liu, G., Peremyslov, V. V., Dolja, V. V., and Wei, Y. (2014). Myosins XI modulate host cellular responses and penetration resistance to fungal pathogens. *Proc. Natl. Acad. Sci. U. S. A.* **111**, 13996–14001.
- Yang, Y., Yuan, J.S., Ross, J., Noel, J.P., Pichersky, E., and Chen, F. (2006). An *Arabidopsis thaliana* methyltransferase capable of methylating farnesoic acid. *Arch. Biochem. Biophys.* **448**, 123–132.
- Zheng, M., Beck, M., Müller, J., Chen, T., Wang, X., Wang, F., Wang, Q., Wang, Y., Baluska, F., Logan, D.C., et al. (2009). Actin turnover is required for myosin-dependent mitochondrial movements in *Arabidopsis* root hairs. *PLoS One* **4**, e5961.

Declaration of academic integrity

Ich versichere, dass ich die von mir vorgelegte Dissertation selbständig angefertigt, die benutzten Quellen und Hilfsmittel vollständig angegeben und die Stellen der Arbeit - einschließlich Tabellen, Karten und Abbildungen -, die anderen Werken im Wortlaut oder dem Sinn nach entnommen sind, in jedem Einzelfall als Entlehnung kenntlich gemacht habe; dass diese Dissertation noch keiner anderen Fakultät oder Universität zur Prüfung vorgelegen hat; dass sie - abgesehen von unten angegebenen Teilpublikationen - noch nicht veröffentlicht worden ist sowie, dass ich eine solche Veröffentlichung vor Abschluss des Promotionsverfahrens nicht vornehmen werde.

Die Bestimmungen der Promotionsordnung sind mir bekannt. Die von mir vorgelegte Dissertation ist von Prof. Dr. Martin Hülskamp betreut worden.

Datum

Unterschrift

Teilpublikationen

“Selection and validation of reference genes for quantitative Real-Time PCR in *Arabis alpina*.”

PLoS One. 2019 Mar 4;14(3):e0211172. doi: 10.1371/journal.pone.0211172. eCollection 2019.

Lisa Stephan, Vicky Tilmes, Martin Hülskamp

Lebenslauf

Persönliche Angaben

Name Lisa Marie Stephan
Geburtsdatum 28. Dezember 1986
Adresse Kämmergasse 12
50676 Köln
Kontakt lisastephan@gmx.net

Ausbildung

1993-1997 Gemeinschaftsgrundschule Sülztal, Steinenbrück
1997-2003 Paul-Klee-Gymnasium, Overath
Abschluss: mittlere Reife
2003-2006 Dietrich-Bonhoeffer-Gymnasium, Bergisch-Gladbach
Abschluss: Abitur
2007-2011 Universität zu Köln
Abschluss: Bachelor of Science in Biology
2011-2013 Universität zu Köln
Abschluss: Master of Science in Biological Science
seit 2013 Universität zu Köln
Angestrebter Abschluss: Dr.rer.nat

Beruflicher Werdegang

2002 zweiwöchiges Praktikum bei Bayer Industry Services
SUAPUA 1, Wasserlabor
2007 dreiwöchiges Praktikum bei RWE Power Technical Services
Chemical Engineering

Lebenslauf

- 2010 sechswöchiges Praktikum beim Max Planck Institut für Pflanzenzüchtungsforschung, Gruppe Turck
- 2002-2012 Nachhilfe in Mathe, Biologie, Chemie und Englisch
- 2008-2012 SHK an der Universität zu Köln
- WS 08 Modul Zellbiologie
- SS 09 Modul Botanik
- WS 09 – SS 12 Assistentin für eine Doktor-Arbeit zum Thema Osmoregulation in *Chlamydomonas reinhardtii*, Institut für Botanik, Gruppe Becker
- WS 10 Modul Zellbiologie
- seit 2013 Mitglied der Max-Planck Research School und Doktorand an der Universität zu Köln, III. Lehrstuhl, Institut für Botanik, Arbeitsgruppe Hülskamp

Publikationen

The SEC6 protein is required for function of the contractile vacuole in *Chlamydomonas reinhardtii*. Karin Komsic-Buchmann, Lisa Marie Stephan, and Burkhard Becker. Journal of Cell Science (2012)

Ehrenamtliche Tätigkeit

- Seit 2008 Mitglied der Fachschafts-Vertretung Biologie und Biochemie
- 2008-2011 Mitglied des Bachelor-Prüfungsausschusses
- 2009 Gewähltes Mitglied der engeren Fakultät der Biologie
- 2011-2013 Mitglied des Master-Prüfungsausschusses

Fremdsprachen-Kenntnisse

Schulkenntnisse in Französisch ab Klasse 7

Sehr gute Beherrschung von Englisch in Sprache und Schrift